Scaling up the production of protein nanofibres

A thesis submitted in partial

fulfilment of the requirements for the degree of

Master of Engineering in Chemical and Process Engineering

at the

University of Canterbury

By

Kang Yuon Wong

2011

This page intentionally left blank

ABSTRACT

Protein nanofibres, commonly known as amyloid fibrils, are emerging as potential biological nanomaterials in a number of applications. Protein nanofibres are a highly ordered insoluble form of protein, which results when a normally soluble protein aggregates via a self-association process. However, researchers are currently faced with several challenges such as finding a cheap source of proteins that can be obtained without expensive purification and optimizing a scalable method of the manufacturing of protein nanofibres. This thesis has identified crude mixtures of fish lens crystallins as a cheap protein source and has optimized methods for large scale production of protein nanofibres of varying morphologies. Results show that by varying the conditions of fibre formation, individual protein fibres can be used as building blocks to form higher order structures. This ability to control the morphology and form higher ordered structures is a crucial step in bottom up assembly of bionanomaterials and opens possibilities for applications of protein nanofibres.

The method of formation of protein nanofibres was optimized on a bench scale (1.5 mL Eppendorf tubes) and successfully scaled-up to 1 L volume. For larger scale-up volume (i.e. greater than 10 ml), internal surface area was important for the formation of protein nanofibres. The crude crystallin mixture prepared at 10 mg/mL was heated at 80^{o}C in the presence of 10% v/v TFE at pH 3.8 for 24 hours and stored for an additional of 24 hours at room temperature for storage process. Aggregation and precipitation of proteins were observed as the protein solution was added to the pre-heated TFE. The resulting protein nanofibres were characterised using ThT dye binding, TEM and SEM. The TEM images show a network of long and criss-crossing protein nanofibres with individual fibres of approximately 10 to 20 nm in diameter and 0.5 to 1 μm long. These protein nanofibres were prepared in 1 mL centrifuge tubes and were left on the laboratory bench at room temperature.

After 5 months, fresh TEM grids of the sample were prepared and visualized using TEM. Interestingly, TEM images show that a number of individual fibres had self-assembled in an intertwining fashion to form large bundles and higher order structures containing bundles of nanofibres up to 200 nm thick.

This page intentionally left blank

ACKNOWLEDGEMENTS

First of all, I would like to give a big thank you to my research project supervisors Professor Conan Fee, Professor Juliet Gerrard and Dr. Madhusudan Vasudevamurthy. Their knowledge and guidance throughout my project has been invaluable and I would not have been able to complete this thesis without them. I would also like to give special thanks to Madhu who I have worked with very closely on the project for his support and knowledge.

Secondly, I would like to extend my appreciations to Jackie Healy from Biological Sciences for obtaining the transmission electron microscopy images, experimental advices and work preparations. I would also like to say thank you to Laura Domigan and Clement Roux for X-ray diffraction and SEM images.

Finally, I would like to acknowledge all the biochemistry postgraduate students for all their help, technical support and advice on how to approach the problem in the most systematic way.

This page intentionally left blank

TABLE OF CONTENTS

ABBREVIATIONS

AFM	Atomic force microscope
$CaCl_2$	Calcium chloride
CNTs	Carbon nanotubes
Cryo-EM	Cryo-electron microscopy
DMSO	Dimethylsulfoxide
DSP	Deep sea perch
DTT	Dithithreitol
FTIR	Fourier transforms infrared spectroscopy
ISA	Internal surface area
NaCl	Sodium chloride
NaOH	Sodium hydroxide
PNTs	Protein nanotubes
sHSP	Small heat shock protein
SDS-PAGE	Sodium dodecyl sulfate-polyacrylamide gel electrophoresis
SEM	Scanning electron microscope
TEM	Transmission electron microscope
TFE	2,2,2-Trifluoroethanol
ThT	Thioflavin T

LIST OF FIGURES

This page intentionally left blank

LIST OF TABLES

1 INTRODUCTION

1.1 Background

Protein nanofibres are a highly ordered form of aggregated protein usually referred to in the biochemical literature as amyloid fibrils (Fandrich 2007). These nanofibres are formed when soluble proteins are exposed to specific conditions that cause them to misfold, leading to self assembly and reconstruction into alternative β-sheets rich structures (Gras 2007; Pearce *et al.,* 2007; Ecroyd and Carver 2009; Garvey *et al.,* 2009; Maji *et al.,* 2009). Protein nanofibres are defined as fibrillar aggregates of proteins with cross-β conformation, where β-sheets are aligned perpendicular to the long axis of the fibrils. The main features of these self-assembled nanofibrillar structures such as stability, strength and functionality are helping them emerge as potential bionanomaterials in nanotechnology applications (Waterhouse and Gerrard 2004; Gras 2007; Hamedi *et al.,* 2008; Gazit 2010). In recent years, protein nanofibres have been shown to act as nanoscaffolds for enzyme immobilization (Gras 2007; Pilkington *et al.,* 2010) and have found applications as nanowires (Hamedi *et al.,* 2008). In addition, protein fibril elastomer composites (Oppenheim *et al.,* 2009) have been fabricated and characterised and have been proven to be stronger than steel by weight (Arnold 2008). The increasing interest and potential of using these nanofibres poses new challenges to researchers: finding a cheap source of proteins and an optimised method for a large scale manufacturing.

This chapter will provide a review of the literature available on amyloid fibrils and protein nanofibres. The chapter will list the factors that influence the formation of protein nanofibres and important aspects of applications using protein nanofibres in nanotechnology and

bionanomaterials. Finally, the structural details of protein nanofibres will be addressed and followed with the thesis objectives.

1.2 Common characteristics of amyloid fibrils

The term amyloid was first introduced by a German scientist Rudolf Virchow in 1854 when he discovered the abnormal macroscopic appearance found in the brain and spinal cord of humans (Virchow 1854). Amyloid fibrils are usually defined as fibrillar aggregates of proteins with cross-β structures and polymerize into very stable filaments with remarkably high internal order as illustrated in **Figure 1-1** (Jime´nez *et al.*, 2002; Fandrich 2007). A more general term, protein nanofibres, has also been used in the past to refer to amyloid-like fibrils of less defined structure (Garvey *et al.*, 2009).

Normally, each protein folds into a single, energetically favourable conformation that is specified by its amino acid sequence. Researchers began to study amyloid fibrils due to their association with protein misfolding diseases such as Alzheimer's and Parknson's (Dobson 2003; Chiti and Dobson 2006). Dobson and co-workers have shown that even proteins that are not relevant to amyloid diseases are able to form amyloid fibrils under certain conditions *in vitro* (Dumoulin *et al.*, 2003). Another investigation concluded that almost every peptide and protein has the intrinsic potential to adopt an amyloid structure under certain conditions (Chiti and Dobson 2006). Under *in vitro* conditions, the native state of the proteins are destabilized, proteins present an abnormal structure associated with a strong tendency to self-aggregate into an amyloid fibril structure (Taboada *et al.*, 2006). This general ability of every protein and peptide to form amyloid fibrils has made them potential novel biomaterials for bio-nanotechnology applications. In recent years a large amount of focus has also been

placed on the functional use of amyloid fibrils (Waterhouse and Gerrard 2004; Hamedi *et al.*, 2008; Maji *et al.*, 2008; Otzena and Nielsen 2008).

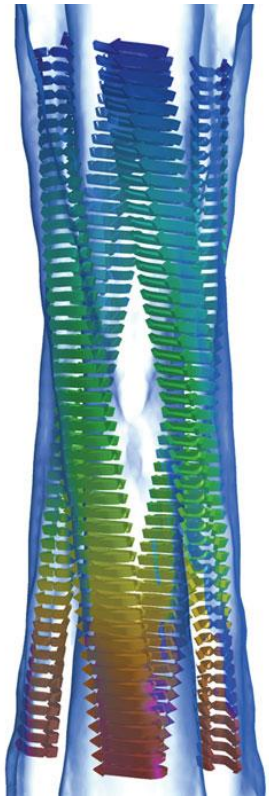

Figure 1-1: Structure of insulin amyloid fibrils obtained by cryo-electron microscopy with a cross-β structure modelled into the electron density map (Jime´nez *et al.,* 2002).

It has become clear that many different protein sequences can form misfolded insoluble aggregates such as amyloid fibrils with common structural elements (Gras 2007). More studies have suggested that the formation of amyloid fibrils can be used in bionanotechnology using a low cost process (Garvey *et al.*, 2009). The ongoing research shows fibrils can potentially provide unique nanotopography and many unique mechanical properties that can be applied to bio-nanotechnology applications. A remarkable example is to use fibrils as a form of nanotubular scaffolding with additional functional groups

incorporated onto the surface of the fibrils *in vitro* (Waterhouse and Gerrard 2004; Gras 2007; Pilkington *et al.,* 2010).

1.3 Protein folding and misfolding

Biophysical methods, theory and computer simulation can determine some of the key questions in the protein folding energy landscapes (Dobson 2003). Under different conditions, the folding process can give proteins with access to several conformational states. A model has been proposed with energy landscapes that describe protein folding as an entropic ally driven process, which is schematically illustrated in **Figure 1-2** (Jahn and Radford 2005). This illustrates the search of an unfolded polypeptide down a funnel-like energy profile towards the native structure. Both thermodynamic and kinetic properties of the polypeptide chain determine the folding funnel for a specific polypeptide sequence under a particular set of conditions. The transition states between the partially folded and aggregate nucleation still remain unclear. However, the partially folded states may be inherently prone to aggregation with favourable intermolecular interaction which lead to their association and ultimately to protein misfolding diseases **Figure 1-2**.

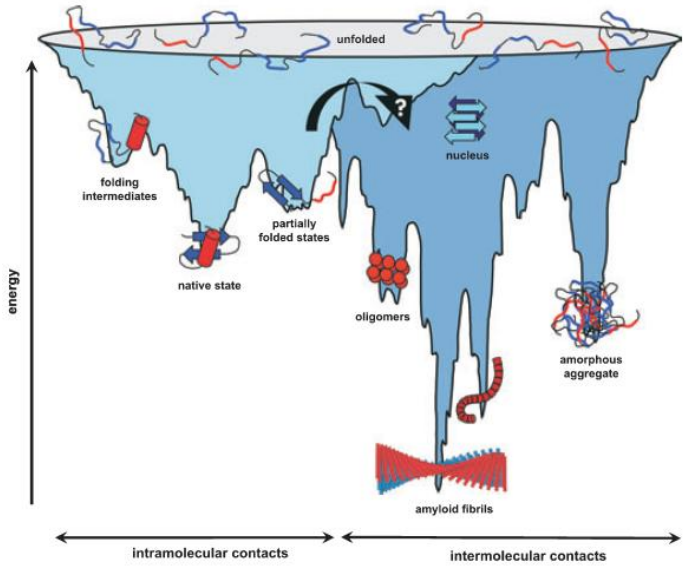

Figure 1-2: Schematic of energy landscape for protein folding and aggregation (Jahn and Radford 2005).

The unfolded proteins show a multitude of conformational states available to a polypeptide chain. The simple folding funnels for unfolded polypeptides (light blue) and intermolecular protein association dramatically increases ruggedness (dark blue).

1.4 Formation of protein nanofibres

The formation of an amyloid fibril is an extremely complex process where a protein can assemble into multiple structurally distinct fibrils (Kreplak and Aebi 2006; Kodali and Wetzel 2007). The unfolding of proteins seems to facilitate specific intermolecular interactions, such as hydrophobic and electrostatic interactions which are required to drive the assembly of protein molecules into amyloid fibrils. It has been shown that there is a relationship between the propensity to fibrillate and the stability of the protein (Hurle *et al.*, 1994; Guijarro *et al.*, 1998; Chiti *et al.*, 2000; Ramírez-Alvarado *et al.*, 2000; Jiang *et al.*, 2001; Khurana *et al.*, 2001; Ahmad *et al.*, 2003; Booth *et al.*, 2007). Destabilizing the native fold of a protein can also increase the tendency to form amyloid fibrils and conversely

stabilization of the native fold of a protein can reduce the fibril formation of the protein (Chiti *et al.*, 2001). In general, protein aggregation can be separated into two main pathways: the ordered pathway and the disordered pathway **Figure 1-3**. In the disordered pathway, the amorphous aggregates contain partly folded polypeptide chains clumped together in an overall disordered arrangement. In contrast, amyloid fibril aggregates are highly ordered species and comprise of rich β-sheet structures. However, *in vivo* the cell is very competent at preventing amorphous aggregation via chaperone and proteasome-dependent mechanisms but it is poor at inhibiting amyloid fibril formation.

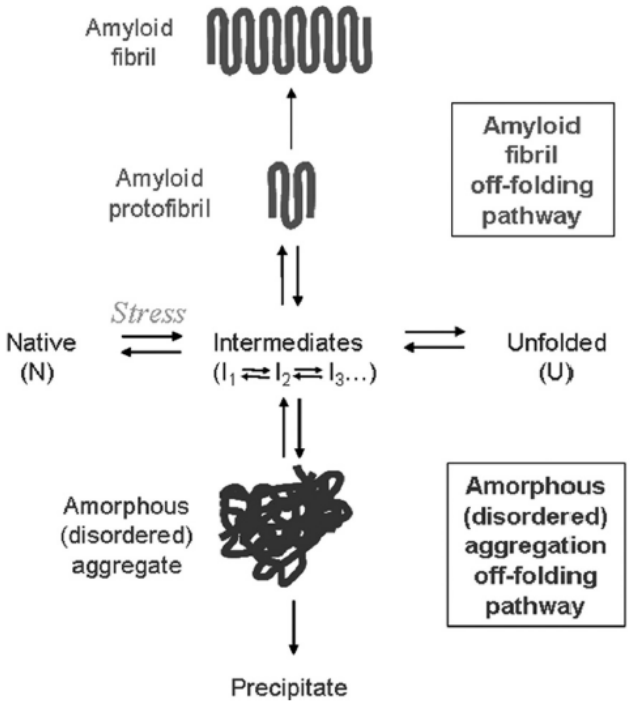

Figure 1-3: Schematic show amyloid fibrils pathways (Ecroyd and Carver 2009).

The native protein (N) unfolds via a variety of intermediate states (I_1, I_2, I_3) which can progress to the unfolded state (U). During intermediate states, they can enter the off-folding pathways comprising either the amorphous (disordered) aggregation or the amyloid fibril-forming pathway which, via the formation of small, soluble protofibril species, leads to insoluble, highly ordered cross β-sheet fibril arrays (Ecroyd and Carver 2009).

The process of nanofibres assembly is achieved by non-covalent interactions and is responsible for the changes in pH level (acidic to basic). The mechanism behind this bottom up synthesis of large bundles of protein nanofibres needs to be explored further. However, the formation of multi fibrillar bundles under changing conditions has been studied by other researchers (Jung and Mezzenga 2010; Loveday *et al.,* 2010). In addition, helical bundles of β-lactoglobulin fibrils have been observed and it has been shown that raising the pH from 2 to 4 increases the number of helices (Jung and Mezzenga 2010). Recently, the properties of nanofibres have also been tuned with NaCl and $CaCl_2$ and the majority of these studies the 'helical bundles' of protein nanofibres observed contained only a few fibrils (Loveday *et al.,* 2010).

Researchers have been able to favour the formation of amyloid fibril using insulin and crystallin proteins *in vitro* (Sluzky *et al.,* 1991; Turnell and Finch 1992; Bouchard *et al.,* 2000; Jime´nez *et al.,* 2002; Meehan *et al.,* 2004; Chanki and Park 2005; Devlin *et al.,* 2006; Groenning *et al.,* 2007; Andersen *et al.,* 2009; Ecroyd and Carver 2009; Garvey *et al.,* 2009; Jung and Mezzenga 2010). Additionally, it has become clear that all α-helix multi-domain protein bovine serum albumin (BSA) aggregates to regular arrays of β-sheet rich filaments at elevated temperatures (Holm *et al.,* 2007). Holm and colleagues were able to observed the formation of stumpy aggregates after 2 hours of heat incubation **Figure 1-4 A**, and sample incubated for 4 days, curly fibrillar structures with a diameter around 10 nm was observed **Figure 1-4 B**. Furthermore, X-ray fiber diffraction show typical diffraction patterns at around 0.45 nm – 0.5 nm (inter-strand distances) and 0.95 nm – 1.1 nm (inter-sheet distances) were detected. Similar results of X-ray diffraction data were represented elsewhere (Makin and Serpell 2005).

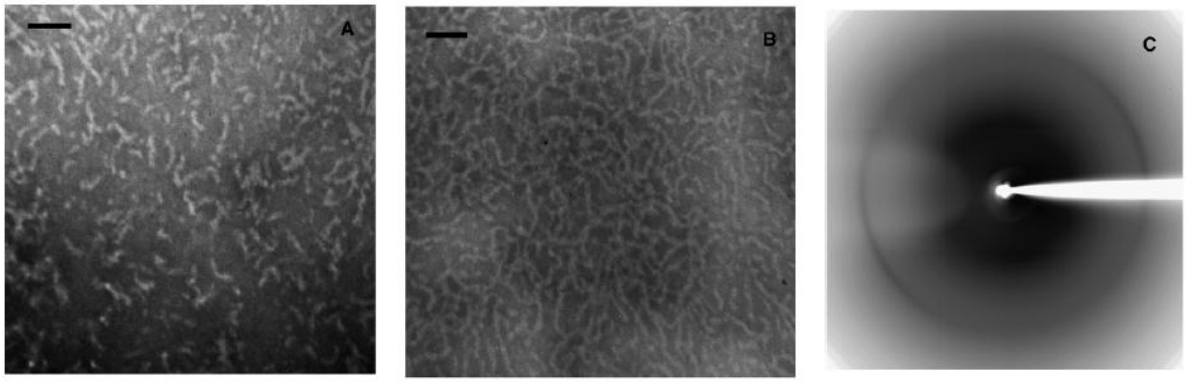

Figure 1-4: Electron microscopy images of 2.5 mg/mL BSA incubated at 70°C (Holm *et al.,* 2007)

A: 2 hours heat incubation at 70°C, B: 96 hours heat incubation at 70°C and C: X-ray diffraction pattern of a BSA fiber.

Traditionally, researchers have used purified proteins to produce protein nanofibres which make them a very expensive product. In a recent study, synthesis of protein nanofibres from crude crystallin protein mixtures have been investigated and can be produced inexpensively using bovine lenses (Garvey *et al.*, 2009). Fish lenses were chosen as the starting materials for this study as they are also a source of crystallin proteins and are readily available as waste materials from the seafood industry. Furthermore, the perceptions of fish waste products are that they are safer than bovine ones because of the BSE outbreaks.

Because there are still many useful applications of using nanofibres in biomaterials and bio-nanotechnology which are yet to be explored, the ability to manufacture amyloid fibrils from an inexpensive source *in vitro* can not only significantly reduce the cost of experiments for scientists but can also help to expedite hitherto unexplored useful applications using nanofibres. Scientists need to find an alternative method to manufacture protein nanofibres in a more economical way and a scalable method for mass production. This approach and the

investigation of a scalable method for mass production lead to the main objective of the thesis which is addressed in Section 1.7.

1.4.1 Protein nanofibres derived from crystallins

The potential of using crystallin proteins as a source to produce protein nanofibres has been investigated (Garvey *et al.,* 2009). The protein nanofibres were manufactured using bovine eye lenses, which is an industrial waste product. In general, these wastes from the meat industry are of little use but they are actually a rich source of well structured β-sheet proteins. Thus, these industrial waste proteins are a readily available source for producing nanofibres and can potentially reduce the operating cost significantly, compared to typical preparations using purified proteins as starting materials, when used as starting materials.

Crystallin proteins are one of the dominant proteins found in the mammalian eye lens (Horwitz 2003). Three different types of crystallin proteins are found in the eye, categorised as α-, β- and γ- crystallins, which are responsible for the eyes stability and transparency. α-Crystallin is a member of the small heat shock protein (sHSP) family and its role is to prevent the aggregation and precipitation of β- and γ- crystallins (Horwitz 1992). The chaperone activity of sHsp against protein aggregation has been well studied but its action against fibril forming proteins has received less attention. It has also been noted that α- subunits are not only found in the lenses. It can also be found in the brain, lungs, skeletal muscles and other tissues. In the same paper by Garvey, the manufacture of protein nanofibres from purified crystallin extracts *in vitro* was reported. The protein nanofibres made from purified α, β and γ-crystallins were described as short and curly **Figure 1-5**. However, using purified α-crystallins seemed to form longer nanofibres **Figure 1-5 A**. In addition, the group was also able to manufacture protein nanofibres using crude extracts of crystallins and the resulted

nanofibres were also short and curly **Figure 1-6**. Furthermore, the group describe how simple changes to buffer conditions altered the morphology of the resulting protein nanofibres. The prepared samples were incubated at 60^{o}C for 18 hours in the presence of 20 mM Tris, 1 mM EDTA and 10% TFE v/v at pH 2. The group placed the focus on using inexpensive proteins to form nanofibres in a more economical way in comparison to nanofibre formation using pure preparations of peptides or proteins (Chiti and Dobson 2006). This was essential and highly desirable characteristic for large scale production in bio-nanotechnology.

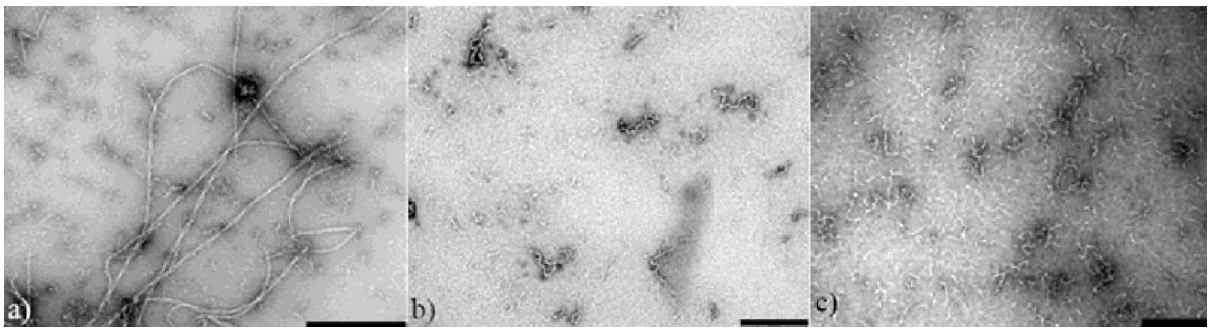

Figure 1-5: Transmission electron of protein nanofibres formed from purified crystallin proteins (Garvey *et al.,* 2009).

(a) α-crystallin; (b) β_L-crystallin; and (c) γ_H-crystallin. The scale bars are 200 nm in length.

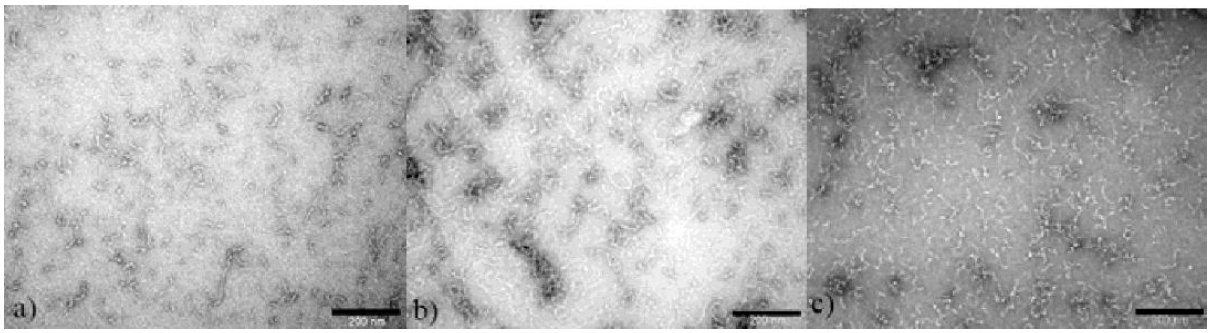

Figure 1-6: Transmission electron of protein nanofibres formed from semi purified mixtures of crystallin proteins (Garvey *et al.,* 2009).

(a) α-crystallin; (b) β_L-crystallin; and (c) γ_H-crystallin. The scale bars are 200 nm in length.

1.4.2 The processes

The in-house method used to manufacture protein nanofibres using crude crystallins mixture was developed by Jackie Healy with modifications from Garvey's paper (Garvey *et al.*, 2009). Crude mixtures of crystallin proteins were obtained by homogenizing fish eye lens in buffer and removing insoluble material by centrifugation. A final protein concentration of 5.8 mg/mL was heated at 60^{o}C in the presence of 10% TFE at pH 2 overnight and up to a period of one week. After heat incubation, the samples were removed from the heat block and leave to cool for a few hours before prepare the TEM grids and visualise under the TEM for protein nanofibres.

Details of the equipment used, with reference to the section of work undertaken, are briefly explained below in a process flow chart. The layout of the experimental apparatus used for laboratory scale production is illustrated in **Figure 1-7**.

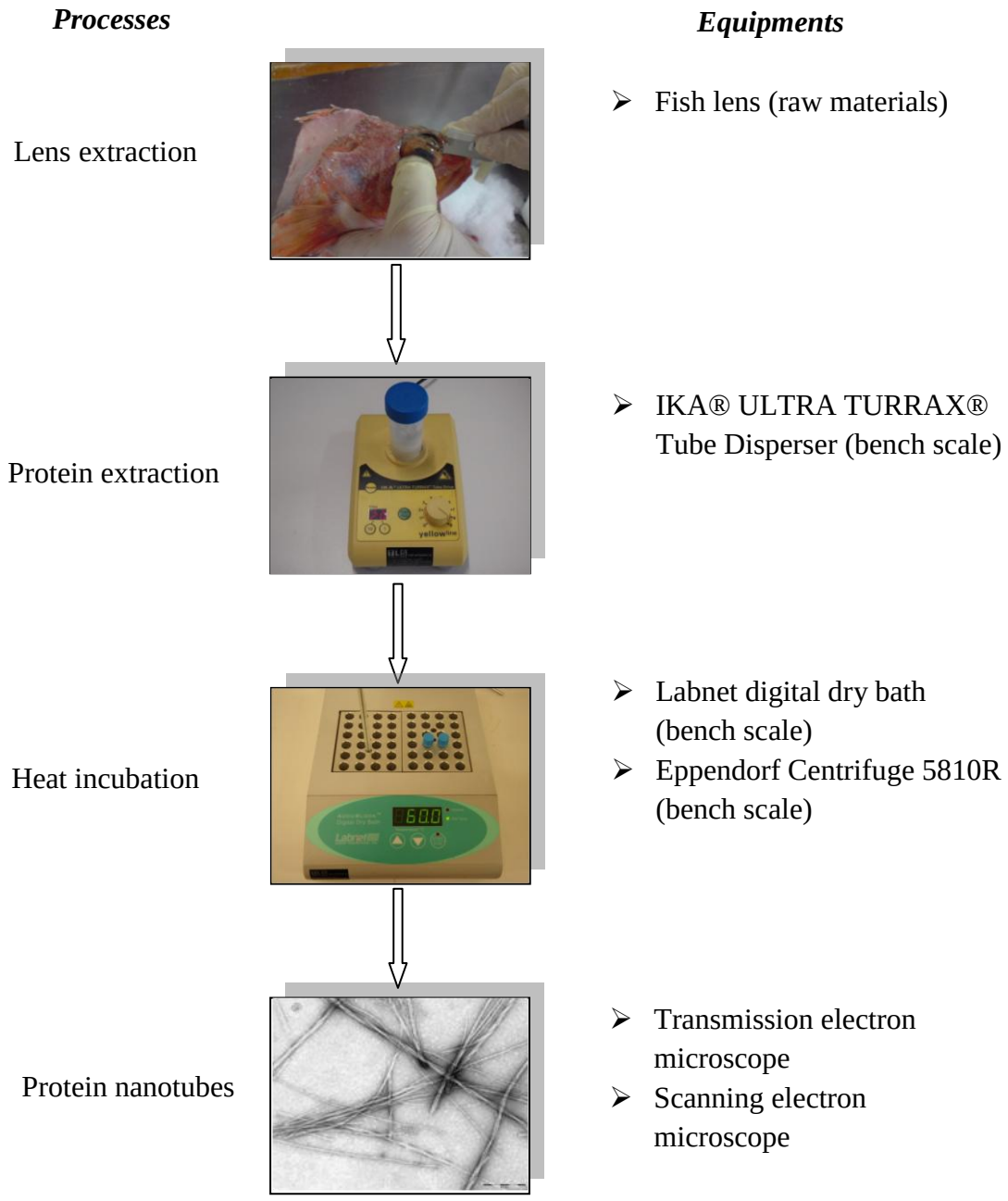

Figure 1-7: The in-house method of making protein nanofibres in laboratory scale (1 mL volume) with modifications (Garvey *et al.,* 2009).

pH effect on fibril formation

The fibril formation from the in-house method was introduced using a low pH of TFE (i.e. pH 2). Similar results were presented elsewhere by incubating the recombinant proteins at various pHs for 24 hours at 37^{o}C (Grothe *et al.,* 2009). Thioflavin T (ThT) is a dye that can enhance fluorescence upon binding to amyloid fibrils present in tissue sections and detailed mechanism of ThT binding will be addressed in Section 1.6.3.2. Based on **Figure 1-8**, there are significant increases in fibril formation measured by ThT fluorescence assay that were detected at pH 6 and below and reached a plateau at pH 3. It was suggested that low pH conditions can also accelerate the chemical cleavage on aspartate and glutamate residues' peptide bonds (Xie and Schowen 1999) and such an effect on peptide fragmentation can be further enhanced with high temperatures (i.e. 60^{o}C) (Konno 2001; Srisailam *et al.,* 2002).

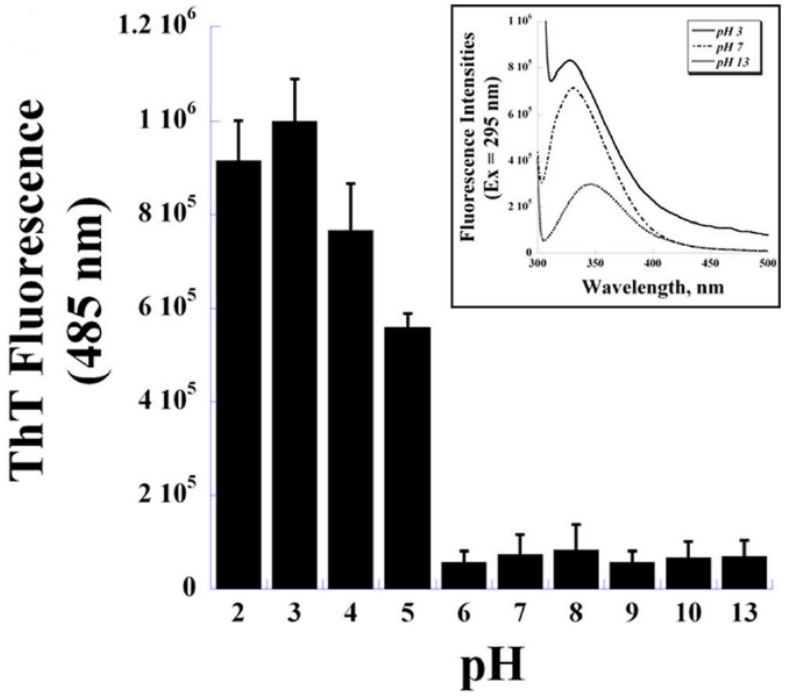

Figure 1-8: Thioflavin T (ThT) fluorescence intensity at 485 nm used to determine the fibril formation of recombinant protein (TGFBIp) at various pH conditions (Grothe *et al.,* 2009).

Trifluoroethanol promotes the unfolding and fibril formation

The in-house method used 10% TFE concentration in fibril formation. It has been suggested that TFE has been used widely to investigate the solvent effects on amyloidogenic peptides and proteins (Ecroyd and Carver 2009; Garvey *et al.*, 2009; Grothe *et al.*, 2009). In the same paper by Grothe, different solvent concentrations of TFE were investigated on fibril formation. The solvent effects on the fibril formation were studied by incubating TGFBIp with TFE at 37^{o}C for 24 hours and then ThT fluorescence was measured. With a low dielectric constant and mildly more acidic than water, this promotes the unfolding and increases the intramolecular hydrogen bonds in proteins (Schönbrunner *et al.*, 1996). During denaturing process, TFE often promotes significant β-sheet formation and leads to fibril formation (Yamaguchi *et al.*, 2006).

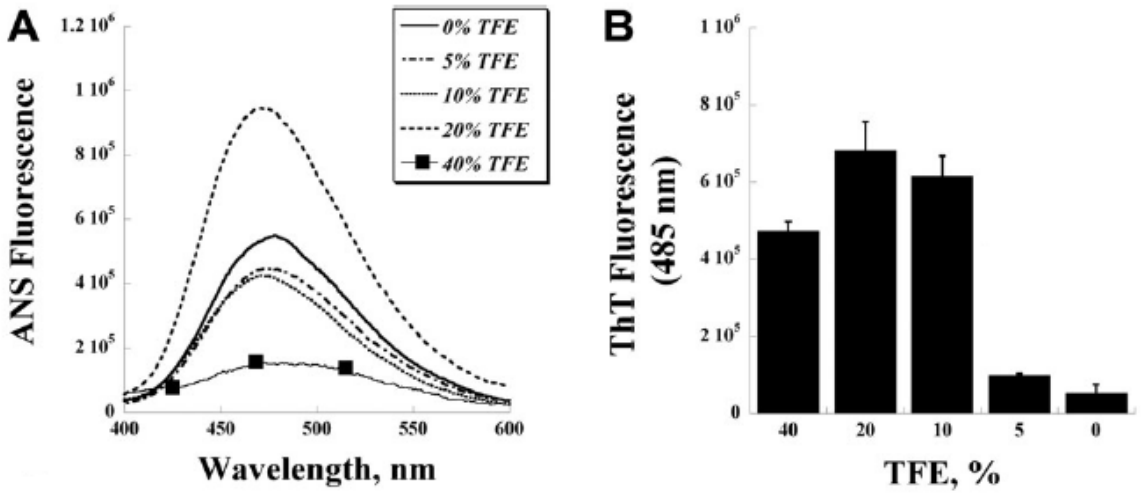

Figure 1-9: The trifluoethanol (TFE) effects on the protein conformations of transforming growth factor beta-induced protein (TGFBIp) (Grothe *et al.,* 2009).

A: The 1 anilionobatgakebe-8-sulfonic acid (ANS) fluorescence spectra and B: Thioflavin T (ThT) intensity used to determine the fibril formation of TGFBIp at various TFE concentrations.

Based on the results presented by Grothe, ANS fluoresces has been used as an indicator for protein unfolding. ANS fluoresces binds to exposed hydrophobic patches and it was used to probe the unfolding of recombinant proteins at various TFE concentrations. Based on **Figure 1-9**, ANS fluorescence experiments showed that TFE exerted its solvent effect by initially unfolding and transforming into rich β-sheet conformer from pre-fibrillar materials at 20% (Grothe *et al.,* 2009). As the concentration of the TFE increased to 40%, non-native α-helix conformer was detected and the ANS fluorescence was significantly reduced.

1.5 Applications of protein nanofibres

The ability to control the morphology of protein nanofibres and to use individual protein fibrils as building blocks to form highly order structures opens many possibilities for applications of protein nanofibres as biological nanomaterials. In addition, the higher order structures themselves have the potential to impart superior properties to bionanomaterials.

The size and structure of amyloid fibrils is comparable with carbon nanotubes and bucky balls (Katz and Willner 2004; Guirado-Lopez and Rincon 2006). Carbon nanotubes (CNTs) are a popular class of nanomaterials with excellent mechanical properties. Protein nanofibres on the other hand offer complementary properties to carbon nanotubes which may offer advantages for many applications, due to their readily functionalisable surface and compatibility with aqueous environments. In recent years, protein nanofibres have continued to emerge, particularly in the fields of bioelectronics and drug delivery (Garvey *et al.,* 2009). Additionally, protein nanofibres are a much more environmentally and economically viable option over traditional plastics and carbon nanotubes which are a high cost nanomaterial that has a very energy intensive fabrication process and potentially high toxicity (Şengül *et al.,*

2008). The diversity of potential applications includes the areas of medicine, health and nutrition, catalysis, electronics, plastic and structural materials (MacPhee and Dobson 2000).

One of the unique features of amyloid-based nanomaterials arises from their ability to self-assemble from protein or peptide solutions, which provides a bottom-up approach to manufacturing. The process of nanofibre assembly is driven by non-covalent interactions and is responsive to changes in pH, temperatures, co-solvents, and ionic concentration (Aggeli *et al.,* 2001; Gast *et al.,* 2003; Smith *et al.,* 2003; Calamai *et al.,* 2005). This process of nanofibre assembly can be very rapid. Proteins with a high tendency to aggregate such as insulin can complete the process within hours (Devlin *et al.,* 2006). A variety of triggers have been developed to initiate nanofibre formation under specific circumstances. The most common approach is to induce change of pH levels for the interactions of charged side chains which potentially exposed the hydrophobic groups and encouraged nanofibre formation (Arnold 2008).

1.5.1 Strength and stability

Due to the size and morphology of amyloid fibrils, these structures are desirable nanomaterials (Nomura *et al.,* 2005; Knowles *et al.,* 2006). Amyloid fibrils are stable at both high and low pH levels, high temperatures and pressures (Nomura *et al.,* 2005). These structures can also be preserved in both aqueous and organic solvents to prevent decaying or spoiling for long preservation time (Gras 2007). Protein nanofibres are also resistant to proteolysis (Zurdo *et al.,* 2001) and dehydration (Squires *et al.,* 2006). The remarkable mechanical property of fibrils' is their strength, which is estimated to be equivalent to that of steel based on the stiffness measured by Young's modulus (Smith *et al.,* 2006).

Furthermore, the strength of fibrils under a tensile axial load (Fukuma *et al.,* 2006) has led to the suggestion that fibrils contribute to the strength of natural adhesives including those used by terrestrial algae (Mostaert and Jarvis 2007). Researchers have compared protein nanofibres to spider silk which is both remarkably strong and resists not only degradation but also breakage and shearing. The disadvantage of spider silk is that it can only be made from spiders whereas the protein nanofibres can manufactured from various sources of proteins and can be made spontaneously in manufacturing settings. Many researchers have begun to examine the biocompatibility of protein nanomaterials and agree that nanofibres derived from proteins are more biocompatible than other bionanomaterials due to their protein origin. Some also suggest that biomaterials made from proteins can be more stable under physiological conditions due to their biological nature (Gras 2007).

1.5.2 Favourable surface interactions

Nanofibres have many advantageous unique properties and thus, they have great potential for several biologically based applications. Such applications include the use of nanofibres as biomimetic materials that can act as scaffolds for the *in vitro* or *in vivo* support of cells. Other applications are its use in catalysis, templating, enzyme immobilization, and as components for biosensors. Most proteins change their original shape, denature and lose their functionalities when they are in contact with a solid surface. Protein nanofibres on the other hand, are less likely to change their original shapes and are more likely to remain intact when coming into contact with a solid surface (Mesquida *et al.,* 2005). The interaction between an individual nanofibre and a solid surface can be controlled by the covalently immobilized seeds on the surface of the solid to direct nanofibre growth (Chanki and Park 2005). The interactions can also be achieved by coupling the pre-formed fibrils with the solid surface by using biotin linkers (Inoue *et al.,* 2001; Collins *et al.,* 2004). Solid surfaces can

have positive influences on fibril formation as they shape the fibril morphology during self-assembly (Kowalewski and Holtzman 1999) and can enhance the growth rate of the fibril structure (Zhu *et al.*, 2002).

Nanofibres can also be used to promote cell interaction as tools to probe fundamental biological processes which are of importance to biomedical research on stem cells and in applications such as tissue engineering (Gras 2007). For example, cells have been shown to be responsive to surface nanotopographies including columns, gratings, and ridges constructed from polymer or silicon (Teixeira *et al.*, 2003; Dalby *et al.*, 2004; Yim and Leong 2005; Yim *et al.*, 2005). Furthermore, cell growth and functions are influenced by the architecture and orientation of electrospun polymeric nanofibres ranging from 400 nm to 800 nm in diameter using poly (L-lactide-co-epsilon-caprolactone) (Xu *et al.*, 2004; Lee *et al.*, 2005).

Additionally, cell-fibril interactions can promote desired cellular responses and can be extended beyond the density of ligands found in natural proteins (Gras 2007). For example, constructed nanofibres have a diameter of 10-30 nm with several micrometers in length, whereas diameters of eukaryotic cells range from 1 μm to 100 μm (Moreira and Lopez-Garcia 2002). Based on the differences in diameter, nanofibres in the solution will potentially bind to the outer layers of the eukaryotic cells. This can change the morphology of the cell and allow foreign proteins or peptide sequences to be tagged onto the cells. By using this technique, many nanofibres can be bound to the surface of the cell and thus promote the binding affinity to a solid surface or control the cell morphology in a reaction (Gras 2007). Fibrils can also be used to promote cell interactions to enhance chemical reactions and promote binding affinity which can be extended beyond the density of ligands

found in natural proteins. Researchers have successfully accelerated a ligation reaction between two short peptides and have highlighted the potential of catalytic ability of fibrils (Takahashi and Mihara 2004).

Another approach is to use enzymes to induce two small precursor peptides to combine and form a single self-assembling fibril (Arnold 2008). With these control abilities, researchers can choose the building blocks for *de novo* synthesis of protein nanofibres, unlike the naturally occurring amyloids found in biology. Researchers have been able to promote fibril formation by changing the solvent properties including polarity and hydrogen bonding strength (Aggeli *et al.*, 1997). Also, altering the solution conditions can favour one particular self-propagating fibril morphology (Petkova *et al.*, 2005). In addition, changing the peptide chirality can alter the handedness of the fibril twist around the protofilament which clearly demonstrate the potential plasticity of these nanomaterials (Koga *et al.*, 2005).

A research group was able to yield hollow silica nanotubes using sol-gel condensation of tetraethoxysilane (TEOS) in the presence of self-assembled β-sheet peptide fibril templates (Meegan *et al.*, 2004). The size of nanotubes can be hundreds of nanometers long and posses a central pore of ~ 3.5 nm. However, the length of the nanotubes is significantly shorter than the length of the fibrils due to fracture during work-up and sample preparation for TEM imaging. The synthesis conditions were investigated and the resultant silica materials characterized by various techniques. Silica deposition at near neutral pH with NaF as catalyst appears to be the most successful method to obtain single nanotubes. These nanotubes have applications in separations, catalysis, nano-optics, and electronics have been of particular interest.

To date, researchers have successfully used protein nanofibres for production of conducting nanowires. These biotemplated metal wires were produced by multiple step process and will be discussed in the next Section 1.5.3. With additional protein backbone properties from amyloid fibrils, different peptides and protein groups can be designed and incorporated with fibrils to produce fluorophores and metalloporphyrins applications (MacPhee and Dobson 2000; Baxa *et al.,* 2003; Baldwin *et al.,* 2006).

1.5.3 Amyloid-based materials as nanowires

It has been suggested that the next generation of microscopic electronic wiring circuits may be derived from biological elements (Whitesides and Grzybowsk 2002). Multiple research groups believe that in an industrial setting, these protein fibres can be manufactured reliably over and over again (Gras 2007; Arnold 2008; Şengül *et al.,* 2008).

Nanofibres made from proteins have no conductive properties (Gras 2007; Arnold 2008; Hamedi *et al.,* 2008). Therefore, the surface of the nanofibres will need to be coated with a conducting material, such as a thin layer of silver first followed by a layer of gold to produce an unbroken network for conduction activities. Recently, a group of researchers have used prion proteins to produce protein nanofibres due to their natural toughness as they are far more difficult to break down compared nanofibres made from other types of proteins, hence this can enhance the strength of the network (Inoue *et al.,* 2011). Another group of researchers led by Professor Susan Linquist have successfully used the protein nanofibres as conducting wires in nanoscale. The group passed a tiny current through their nanowires and the electrical resistance was recorded to be approximately 80 ohms. Other nanowires such as microtubules made from biopolymers have been recorded to have 1,000 times more than the resistance reading of nanowires made from proteins (Scheibel *et al.,* 2003; Hamedi *et al.,*

2008). Having high resistance in the wires will caused some power loss and if the resistance is too high that is travelling on the wire, the wire can overheat and this may even set fire to adjacent materials in a microscopic electrical device. Hence, based on this finding the protein nanofibres have a better advantage compared to other nanowires due to their low electrical resistance.

In the paper by Hamedi, PEDOT-S and amyloid fibrils made from insulin were mixed in water. A visible bluish gel and a less coloured supernatant were observed when the complex between PEDOT-S and amyloid fibrils reaction was completed. The solution was placed on freshly cleaved mica and blown away the solvent with a nitrogen flow. The electrical nanowire network was constructed using platinum interdigitated microgrid with 5 µm electrode gap with the PEDOT-S and amyloid fibrils complex deposited on top **Figure 1-10A**. As a result, a high source of 5 µA was detected from the transistor I-V curves at on state **Figure 1-10 B**. In addition, repetitions and reversions of switching the transistor with an on/off between 0 and 0.5 V shows that PEDOT-S has not lost any electrical or electrochemical properties (Hamedi *et al.*, 2008).

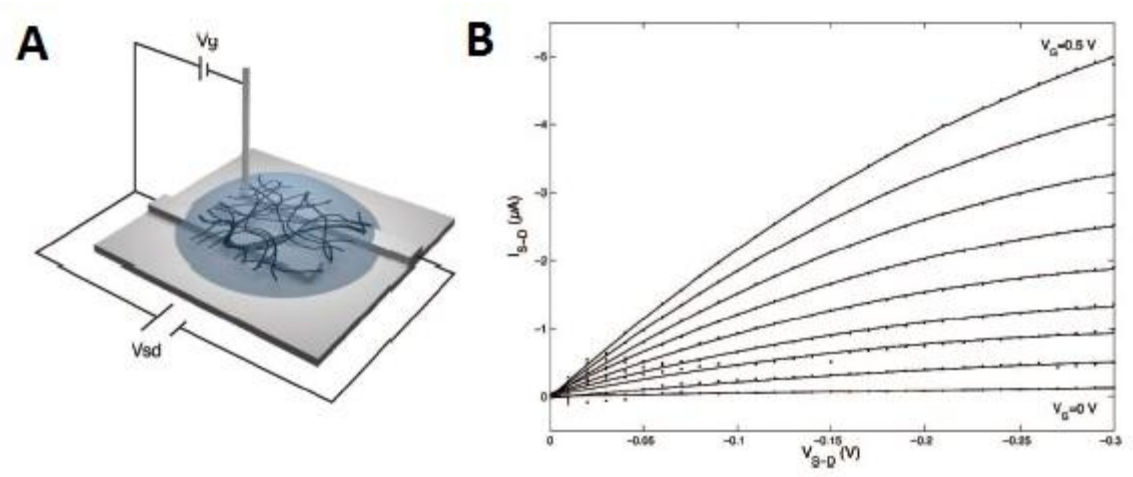

Figure 1-10: Schematic of the experimental setup and I-V curves (Hamedi *et al.,* 2008).

A: is a schematic of the constructed nanowire-decorated grid with nanonetworks deposited on top and immersed in an acetonitrile (0.1 M LiClO4) and B: Measurements of I-V curves were obtained from the constructed electrolyte gated transistor. The voltage is swept from 0 to 0.5 V.

All these remarkable achievements demonstrate not only how protein nanofibres may be used to construct circuit devices on the nanometre scale including diodes, photovoltaics, and transistors but also that they can be manufactured at a low cost. Due to the increasing demand of using these protein nanofibres and the applications of amyloid-based nanomaterials, researchers are currently faced with a number of challenges, including finding a readily available, cheap source of proteins as the initial material for nanofibres synthesis. In addition, ways must be designed to control the morphology of protein nanofibres and to construct individual protein fibrils into building blocks for use in highly ordered structures. Furthermore, researchers are faced with expensive experimental set-up such as purification of the target proteins for nanofibres synthesis and an optimized scalable method of manufacture of protein nanofibres which lead to the goal of this thesis and the objectives will be addressed in Section 1.7.

1.5.4 Seeding using fragmented nanofibres

The formation of fibrils has been simulated using an intermediate-resolution protein model called Protein Intermediate-Resolution Model (PRIME) (Smith and Hall 2001). PRIME is a computational program that allows simulation of multiprotein systems over relatively long timescales. A total of three types of simulations were performed, each highlighting a different aspect of the fibrillization process. They were (i) slow-cooling, (ii) constant-temperature and (iii) seeded constant-temperature. The simulation involved a peptide sequence containing $PH_{14}P$, where H and P are hydrophobic and polar amino acid residues respectively. This peptide sequence mimics another peptide ($Ac\text{-}KA_{14}K\text{-}NH_2$) which will form a stable soluble β-sheet complexes *in vitro* (Forood *et al.*, 1995; Blondelle *et al.*, 1997).

In the simulations of seeded constant-temperature, 48 denatured chains were added randomly to a simulation box containing a fibrillar structure taken from the end of a previous unseed 48-peptide simulation. Based on their findings, fibril formation in the simulations involves a nucleation event which has been suggested in the experimental literature. The results clearly show that the denatured chains exposed to a previously created fibril bypassing the slow fibril nucleation step as illustrated in **Figure 1-11**. With 48 random inserted into the seeded system resulting in fibril growth as a function of the reduced time, t*. In comparison between the two simulations (seeded and unseeded), the lag time for fibril formation in the unseeded simulations is approximately 135 reduced time compared to a lag time of zero for the seeded simulations.

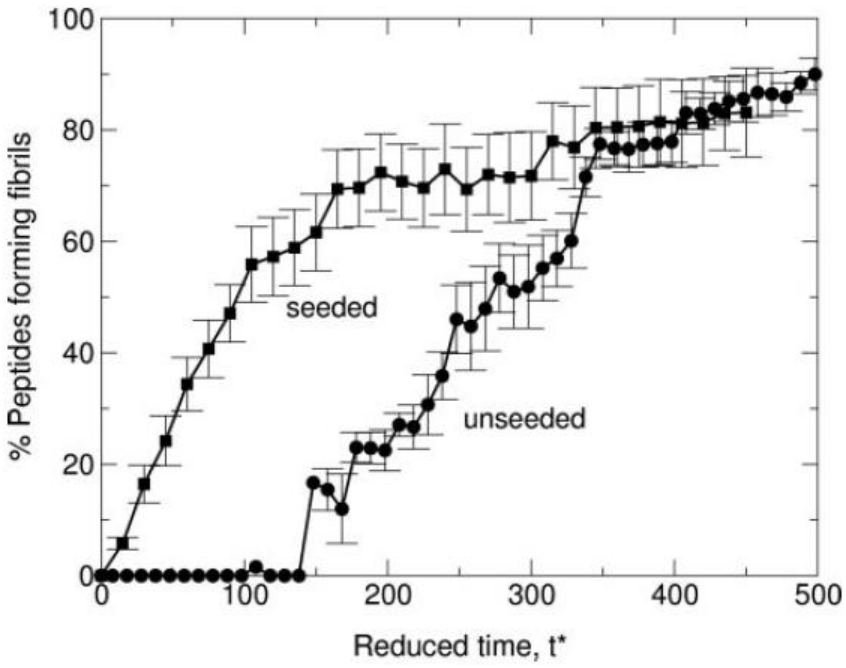

Figure 1-11: Comparison of seeded and unseeded simulations with the percentage of peptides in fibril structures versus reduced time (Hamedi *et al.,* 2008).

1.5.5 Cytotoxicity of amyloid fibrils

Since amyloid fibrils were originally described in the content of disease, there have been suggestions that there could be an issue with toxicity from the development of amyloid-like fibrillar materials (Gras 2007; Arnold 2008; Xue *et al.*, 2009). Xue and colleagues examined how one such physical attribute, length, affects the functional properties of fibrils. They showed how long straight fibrils formed from human β_2-microglobulin could disrupt liposome membranes and reduce cell viability where as prefibrillar oligomers with different structural properties did not **Figure 1-12**. Additionally, they also found that fibril toxicity could be enhanced by reducing the fibril length via breakage and suggested that physical dimensions of fibrils modulate their cytotoxic potential.

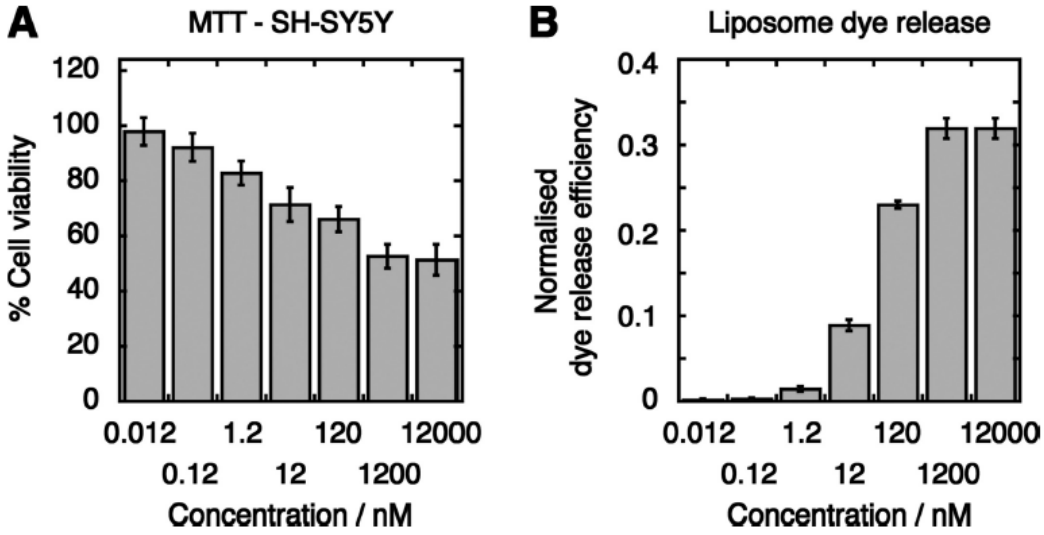

Figure 1-12: The disruption of liposome membranes (Xue *et al.,* 2009).

A: Loss of cell viability and B: both increase as the concentration of fragmented fibrils increases.

Overall, the fragmentation after assembly shortens the average fibril length and enhances the cytotoxic potential as illustrated in **Figure 1-13**. Fragmented fibrils can increases its interaction with cellular membrane and can caused membrane disruption and cytotoxicity but on the other hand long fibrils have limited or no membrane disruption and cytotoxicity. However, by understanding the changes in biological response by fibril fragmentation can become critical in designing therapeutic agents and suggested that targeting amyloid fibril stability against breakage may be a strategy for developing therapies against amyloid disease.

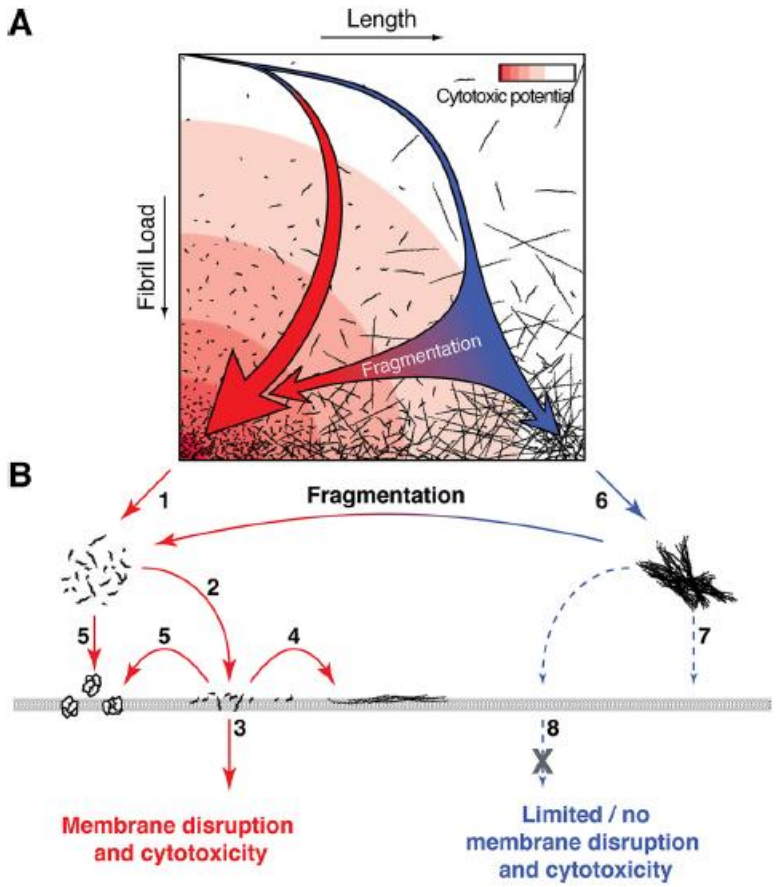

Figure 1-13: Illustration of the landscape of fibril assembly and fragmentation (Xue *et al.,* 2009).

A: The red background colour represents the cytotoxic potential and the red arrow represents the fibril assembly pathway that would occur in the presence of fibril fragmentation. The thin blue arrow represents fibril assembly where little fragmentation occurs. B: *B-1* represents short fibrils could lead to enhanced cytotoxicity and *B-6* is nucleation resulting in a formation of fibrils. *B-2* pathway is the increased fibril-membrane interaction. *B-3* is the interaction between short fibrils and membrane surfaces that could result in membrane damage. *B-4* and *B-5* are the released of cytotoxic species. *B-7* and *B-8* have limited or no membrane disruption and cytotoxicity through the membrane.

It is important to understand how cells respond to their environment, including nano-features present in that environment. This has fundamental importance to biomedical research including stem cells (Chai and Leong 2007) and applications such as tissue engineering (Stevens and George 2005). As mentioned above, although fibrils are typically associated with amyloid materials, the pre-fibrillar aggregates species are thought to be the possible cause of cell toxicity. However, it has become clear that mature fibrils may even serve as rescue mechanism to remove cytotoxic species (Conway *et al.,* 2000). The existence of fibrils with positive functions suggests that controlled interactions between fibrils and cells may be favourable (Fowler *et al.*, 2006).

1.6 Current structural models for protein nanofibres

1.6.1 The macroscopic structure of protein nanofibres

Amyloid fibrils are non-crystalline and insoluble in water, a property which has made detailed structural studies by single X-ray crystallography and multidimensional NMR very difficult (Maji *et al.,* 2009). Hence, only methods with low resolution have provided information for the physical and structural characterization of amyloid fibrils (Maji *et al.,* 2009). A variety of methods of structural analysis have been applied to fibrils from a range of proteins.

The X-ray fibre diffraction method is one of the common ways for definitively characterising amyloid fibrils. The procedures involve filtering the X-ray stream so that only those X-rays travelling parallel to the specified direction are allowed through. As the X-ray stream is exposed to the long axis of the fibrils, reflections on meridional and equatorial will be detected on the screen. Many researchers have proven this structural element using X-ray fibre diffraction pattern with a strong meridional reflection at 0.47 nm and another equatorial

reflection at 0.97 nm (Garvey *et al.*, 2009; Groenning 2009). This set of data indicates that there is a repeating pattern of β-sheets along the fibril axis with a constant distance of 0.47 nm and lamination with a spacing of 1 nm perpendicular to this axis **Figure 1-14**.

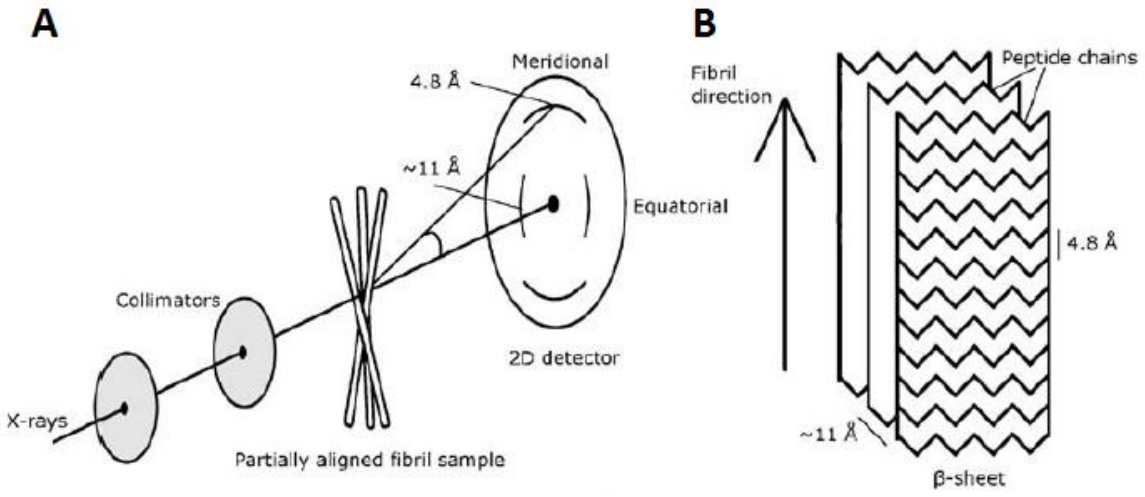

Figure 1-14: Experiment set-up for the detection of cross-β sheet structures of amyloid fibrils (Groenning *et al.,* 2007).

A: Experiment setup for X-ray fibre diffraction and B: The interpretation by X-ray fibre diffraction observation technique showing two distinctive rings at 0.48 nm and 1.1 nm which clearly is an indication of the general structure of cross β sheets.

In addition to the structural information obtained from X-ray fibre diffraction, other experimental techniques such as Fourier transform infrared spectroscopy (FTIR), circular dichroism (CD) and transmission electron microscopy (TEM) have been used simultaneously to monitor the formation of amyloid fibrils from bovine insulin at acidic pH and different heating temperatures (Bouchard *et al.*, 2000). It has been reported that before heat incubation of the samples, structures detected by FTIR and CD were predominantly native-like α-helical. With an increase in temperature, unfolding of the native protein structure was favoured, followed by aggregation. Following this step, changes in FTIR and CD spectra indicated an

extensive conversion of the molecular conformation from α-helical to β-sheet structure. Later stages of TEM show the development of highly ordered fibril structures with well-defined repetitive morphologies of helical twist. Recently, more studies have used cryo-electron microscopy coupled with image processing and reconstruction techniques to gain more detailed molecular structures of the fibrils **Figure 1-1**. These rich β-sheet structures give remarkable strength due to their extensive hydrogen bonding network from the backbone. It has been proposed that the repeating feature of β-strands are aligned either parallel or anti-parallel **Figure 1-15** (Eanes and Glenner 1968; Serpell and Smith 2000).

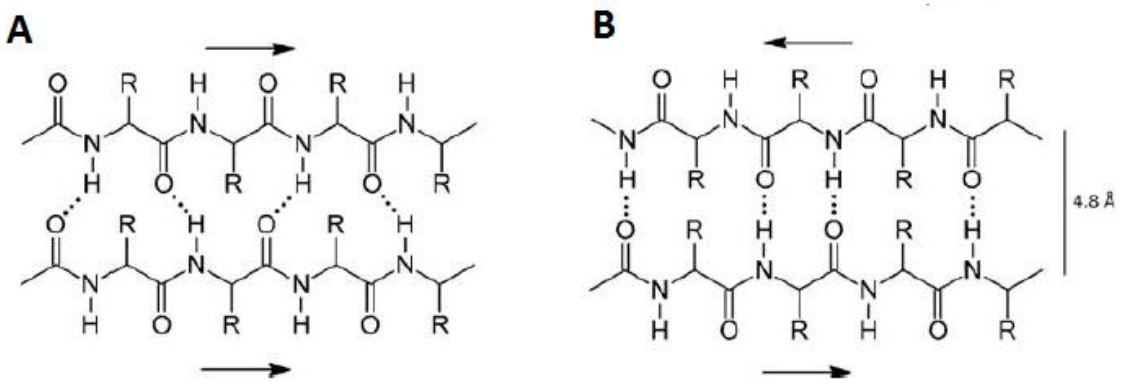

Figure 1-15: Schematic showing the repeating units of secondary structures (Dobson 2003).

The diagram shows the repeating units of secondary structures stabilized primarily by hydrogen bonding between the amino- and carbonyl groups of the main chain with an interstrand distance of 0.48 nm.

One of the unique features of amyloid fibrils is that their general structure does not change, irrespective of the type of proteins used or under different kinds of treatments. However, a subtle change in the dimensions of the nanofibres has been observed (Aggeli *et al.*, 2001; Jime´nez *et al.*, 2002). It has been reported that a typical fibril can have a range of dimensions between 8 nm and 13 nm in diameter and up to several micrometres in length

(Waterhouse and Gerrard 2004). A typical protein nanofibre may consist of up to six single strands protofilaments which are usually wound around each other and form a supercoiled structure **Figure 1-16 A**.

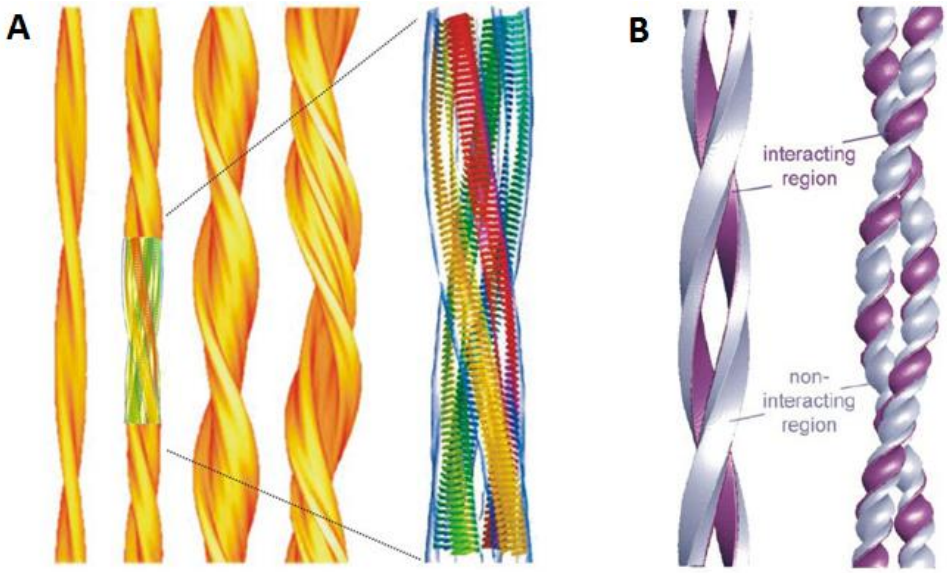

Figure 1-16: A: 3D maps of 4 different insulin fibril morphologies (Jime´nez *et al.,* 2002).

The fibrils are made up of different numbers of component strands (protofilaments; from 2, 4, 6). The individual protofilaments are twisted around each other in either compact or in ribbon-like arrangements and B: Models showing protofilament twist accompanies the filament twist in which an interactive surface is coloured purple.

Dobson and co-workers suggested there are two possibilities on how protofilaments interact (Dobson 2003). One of the possibilities is that there is a consistent interacting interface between the filaments **Figure 1-16 B**. Secondly, if the twist of the β-strands is shorter than the overall twist of the fibril, the region of interactions progressively rotates around the protofibril.

1.6.2 The internal structure of protofilaments

Many researchers have been trying to elucidate the molecular arrangement of amyloid core but there is still no incontrovertible structural model available. The most common features of amyloid that are widely accepted are the cross-β structure based on the results from X-ray diffraction. A group led Eisenberg (Balbirnie *et al.*, 2001) has successfully characterized microcrystals derived from amyloid forming segments GNNQQNY and NNQQNY of the yeast prion Sup35 by X-ray microcrystallography (Nelson *et al.*, 2006). High resolution data of a short peptide was able to provide a very precise view on the cross-β architecture of the inner amyloid core **Figure 1-17**. The extension of GNNQQNY peptide chains is in a conformation with the characteristic hydrogen bonding pattern of parallel β-sheets. The β-strands exhibit the typical strand-strand separation distance of 0.48 nm **Figure 1-17 A**.

It has also been reported that along the axis, a second sheet of β-strands is aligned in an anti-parallel manner with a slight vertical shift relative to the first sheet (Balbirnie *et al.*, 2001). The resulting vertical shift is due to the perfect packing from the side chains within the interface of both sheets **Figure 1-17 B**. Two sheet pairs of GNNQQNY have created the arrangement of dry and wet interface **Figure 1-17 C and D**. Water molecules are completely surrounded in the wet interface which separates the hydrogen bonded side chain residues from the neighbouring sheet (Nelson *et al.*, 2006).

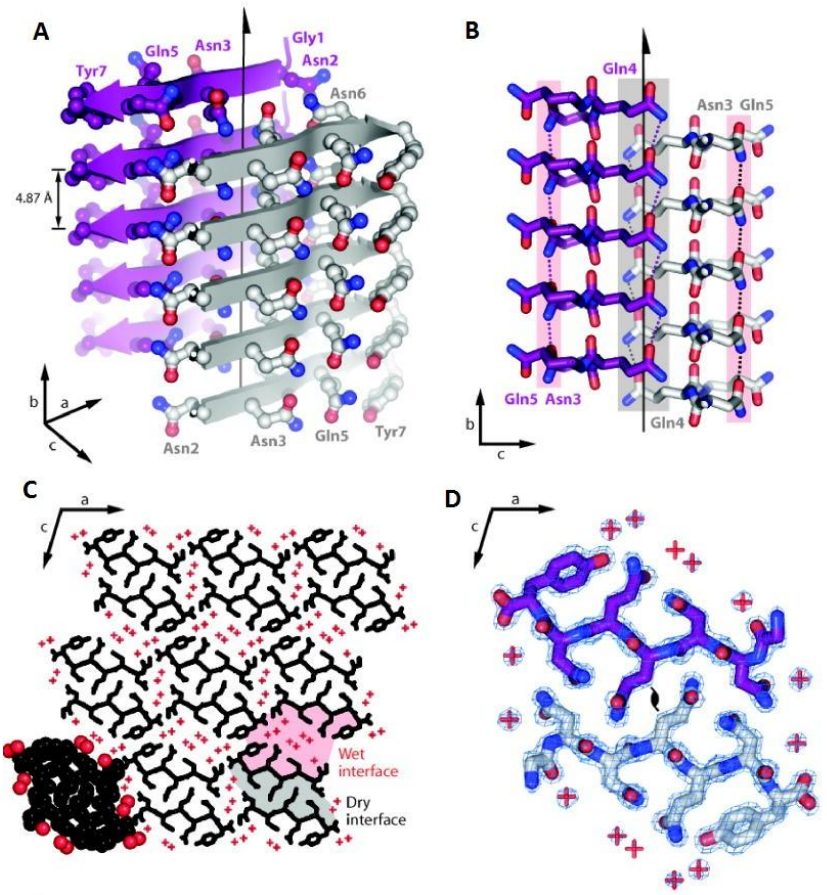

Figure 1-17: Structure of GNNQQNY and NNQQNY of the yeast prion Sup35 (Nelson *et al.*, 2006)

1.6.3 Binding molecular probes to protein nanofibres

It is important to understand the molecular details in amyloid formations to be able to develop strategies to control these amyloid fibril formations in the most efficient way possible. Thioflavin T (ThT) and Congo Red (CR) are the two common classic dyes used for the detection of amyloid fibrils **Table 1**. In general, ThT binds to channels running parallel to the long axis of the fibrils. In the channels, ThT may bind in either a monomeric or dimeric form of which the molecular conformation is likely to be planer. On the other hand, CR binds to grooves formed along the β-sheets as a planar molecule in either a monomeric or

supramolecular form (Groenning 2009). To date, the binding modes of these molecular probes to amyloid fibrils are by no means adequately described or understood.

Molecular probe	Chemical structure	Characteristic signal
Congo Red	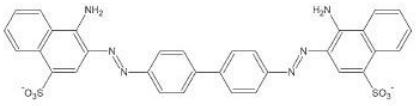	Birefringence Absorbance Fluorescence
Thioflavin T	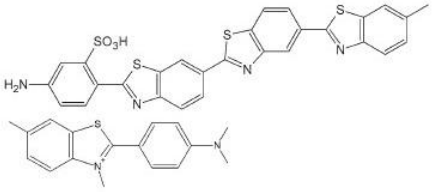	Fluorescence

Table 1: The two common molecular probes applied for amyloid fibril detection (Groenning 2009).

1.6.3.1 Congo red

Staining amyloid fibrils using CR was used for identification of amyloid fibril in the beginning of the 1920s (Howie and Brewer 2009). CR gives a characteristic apple green birefringence when examined between crossed polarized light and analysed using an absorbance maximum from about 490 nm to 540 nm. In the diagnosis of amyloid in *ex vivo* tissue, CR is often used in conjunction with polarization microscopy (Pettersson and Konttinen 2009), light microscopy (Sen and Başdemir 2003) and fluorescence microscopy (Giorgadze *et al.*, 2004). CR staining has been used as one way of quantifying of insulin amyloid fibrils *in vitro* with absorption microscopy (Klunk *et al.*, 1989; Klunk *et al.*, 1999). However, CR lacks sensitivity at low amyloid fibril concentration compared to ThT (Levine 1997). Furthermore, it has been reported that CR may interfere with protein misfolding and aggregation which may either inhibit or enhance amyloid fibril formation for several proteins when monitored using *in situ* detection (Turnell and Finch 1992; Kim *et al.*, 2003; Porat *et al.*, 2006).

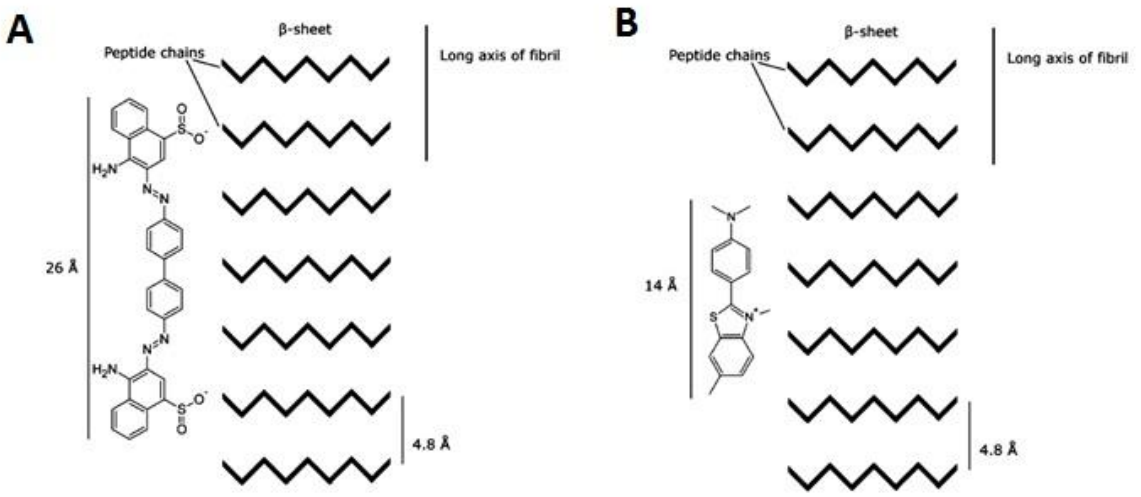

Figure 1-18: Schematic of Congo red and thioflavin t binding on axis of fibril (Groenning 2009).

A: Congo Red oriented with their long axis parallel to the long axis of the fibril and B: Thioflavin T oriented with their long axis parallel to the long axis of the fibril.

1.6.3.2 Thioflavin T

Thioflavin T (ThT) was first introduced in 1959 as a dye that can enhance fluorescence upon binding to amyloid fibrils present in tissue sections (Vassar and Culling 1959). Since then ThT dye has become a standard dye for all amyloid detection. ThT fluorescence upon interaction with amyloid fibrils has excitation and emission maxima at 450 nm and 480 nm respectively (Naiki *et al.*, 1989; LeVine 1993). Besides using ThT for amyloid fibril detection, it also has other useful applications such as diagnosis of amyloid fibrils in tissue sections using fluorescence microscopy (Vassar and Culling 1959; Saeed and Fine 1967), direct observations of amyloid fibril growth (Ban *et al.*, 2003; Andersen *et al.*, 2009), monitoring of the amyloid fibril formation using fluorescence anisotropy (Sabate and Saupe 2007) and monitoring *in vitro* amyloid fibril formation using fluorescence spectroscopy (Naiki *et al.*, 1989; LeVine 1993).

In general, CR binding requires at least six continuous β-strands in a β-sheet, while ThT only needs around three to four binding sites. The kinetics of ThT binding to form fibrils can be completed within 30 seconds (Levine 1997). ThT has been shown to bind with the long axis parallel to the long axis of the fibrils **Figure 1-18 B**. This orientation of ThT is consistent with a recent X-ray crystal structure of ThT bound to a "peptide self-assembly mimic" (PSAM) scaffold (Biancalana *et al.,* 2009). Additionally, a molecular dynamics simulation suggested that ThT bind perpendicular to the β-strands in the β-sheets and also parallel to the β-strand at the end of the β-sheets (Wu *et al.,* 2008). Furthermore, after ThT binding, the interstrand spacing along the fibril axis of 0.48 nm remain unchanged and the reflection at 1.1 nm still remains in insulin fibrils **Figure 1-19 B** (Groenning *et al.,* 2007).

In comparison, the binding kinetics of CR to amyloid fibrils is slower than the binding kinetics of ThT **Figure 1-18**. It has been reported that the binding time of CR to poly-L-lysine fibrils required 60 minutes before reaching its equilibrium (Klunk *et al.,* 1989). This suggested that binding sites may not have easy access for CR to interact due to its larger molecule structure. Although CR has slower binding kinetics compared to ThT, CR has a higher capacity of binding stoichiometry compared to ThT in insulin fibrils. This reveals CR not only bound in central channels of 0.8 – 0.9 nm in diameter but also bind to the β-sheets surface (Groenning 2009). Overall, ThT is considered to be more specific towards amyloid fibrils than CR. Most importantly, the fluorescence upon binding to the precursor proteins or amorphous aggregates of proteins does not occur for ThT (Naiki *et al.,* 1989; Levine 1997; LeVine 1999; Lindgren *et al.,* 2005).

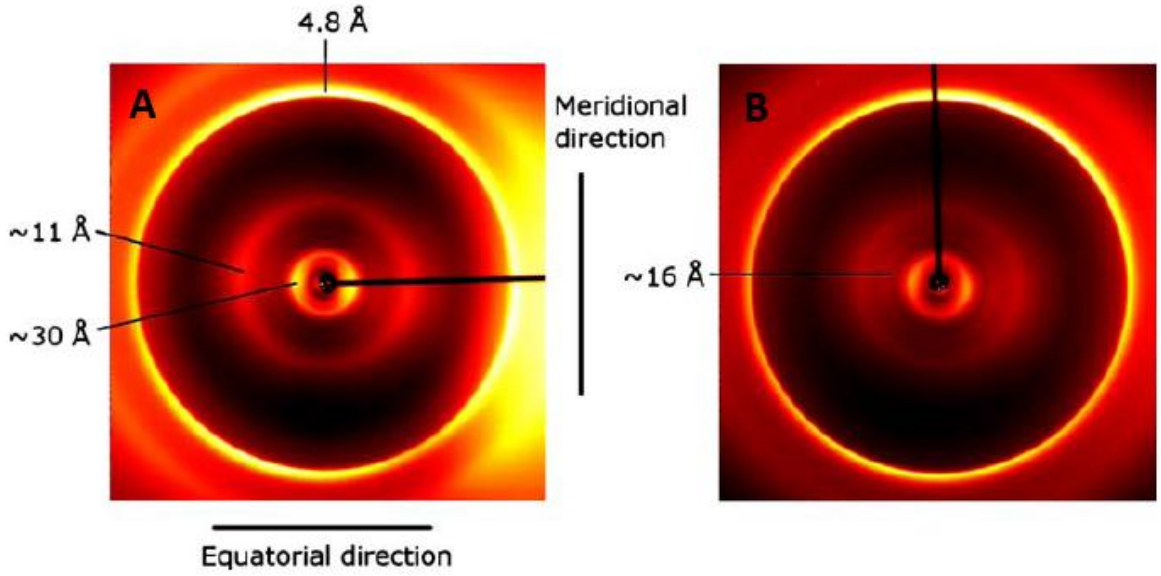

Figure 1-19: X-ray fibre diffraction images of fibrils formed from insulin (Groenning *et al.,* 2007).

A: insulin fibrils formed in 25 mM HCl at pH 1.6 without binding of ThT and B: X-ray fibre diffraction with ThT binding.

1.7 Thesis Objectives

As the applications of amyloid-based nanomaterials and the demand for these protein nanofibres are increasing, a number of challenges are faced, including finding a readily available cheap source of proteins as the initial material for nanofibres synthesis. The overall aim this study was to determine the optimal operating condition to manufacture the highest quality protein nanofibres using deep sea fish lenses as raw materials. The definition of the highest quality of protein nanofibres should contained no protein aggregates and consists of high ordered structures seen in TEM images. The approach to optimizing the method for protein nanofibres synthesis involved altering the heating temperature, heat incubation time, pH levels and protein concentrations. Each of the variables was studied and results were confirmed using TEM and SEM. Thioflavin T fluorescence and Congo red were also used to confirm the presence of protein nanofibres.

The specific objectives of this thesis were:

1. To determine the optimal condition to produce the highest quality of protein nanofibres from a crude protein source at small (~1 mL) scale by varying:
    - pH levels of TFE and starting protein concentrations
    - percentages of TFE (v/v)
    - heating temperatures
    - heating incubation duration
    - storage time

    The presence of fibrils in the solution was to be confirmed using transmission electron microscope and scanning electron microscopy.

2. To scale-up the production of protein nanofibres from bench scale up to commercial scale (1 L).

2 Experimental materials and methodology

This chapter describes the equipment and methods used in the process optimization for laboratory scale and subsequent volume scale-up for production. Most emphasis was placed on development of process optimization for the in-house method for manufacturing protein nanofibres. **Figure 2-1** shows the order of experimental work performed.

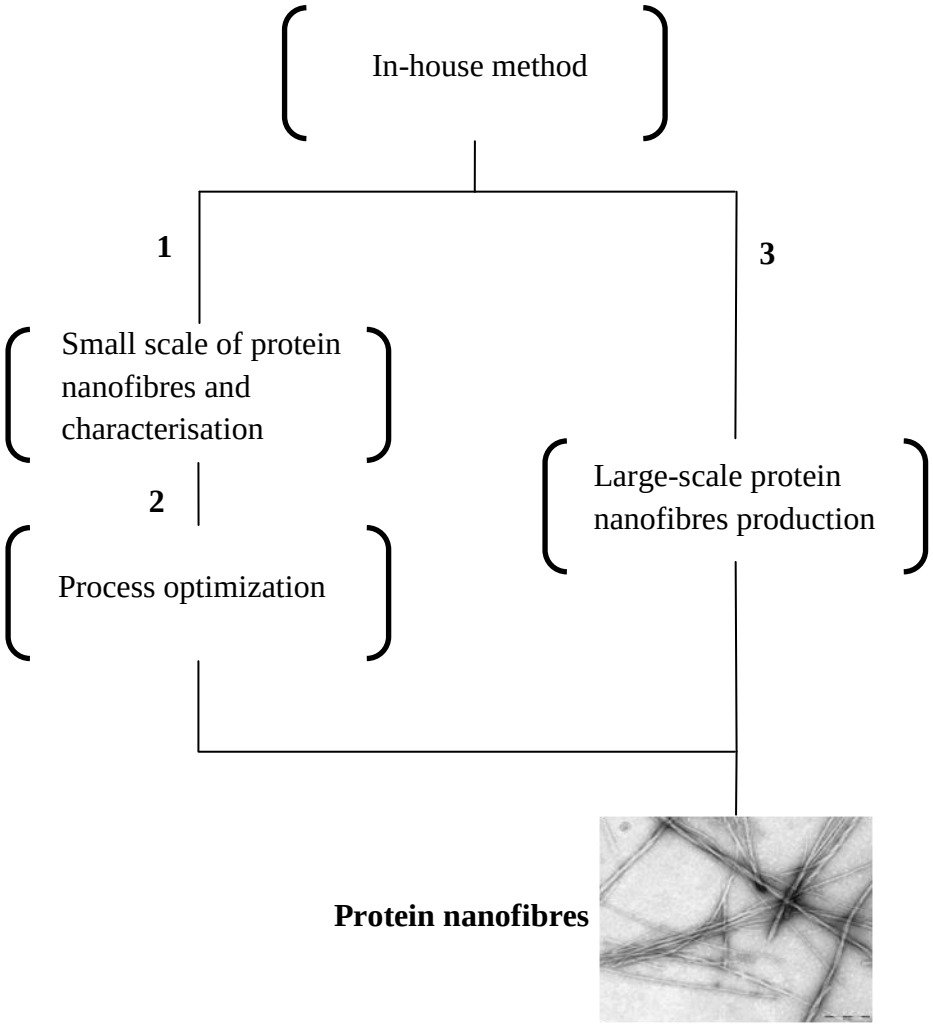

Figure 2-1: Organisation of experimental procedure in laboratory scale and large scale production of protein nanofibres.

2.1 Materials and equipment

Details of reagents used during experiments, including purities and suppliers, are located in **Table 2**.

Table 2: List of chemicals used for experiments including purities and suppliers.

Chemicals	Abbreviation	Purity	Supplier
Calcium Chloride	$CaCl_2$	Analar	BDH Global Sciences
Dimethyl formaldehyde	DMF	99.8%	BDH
Dimethylsulfoxide	DMSO	99.5%	Sigma New Zealand
Dithithreitol	DTT	99.0%	Ajax Finechem New Zealand
Ethanol	EtOH	96%	Anchor, New Zealand
Hydrochloric acid	HCl	37%	BDH
Sodium chloride	NaCl	99.9%	BDH Global Sciences
Sodium hydroxide	NaOH	>98%	Fluka, Germany
2,2,2 - Trifluoroethanol	TFE	99.0%	Sigma New Zealand
Thioflavin T	ThT	Dye Content 65%	Sigma

2.2 The processes

Different types of fish eye lenses from sources such as Salmon, Groper, Hoki and Barracuda were tried during the development and optimization process. The in-house developed method can be separated into four main processes; fish lens extraction, protein extraction, protein nanofibres synthesis and room temperature storage, as illustrated in **Figure 2-2**.

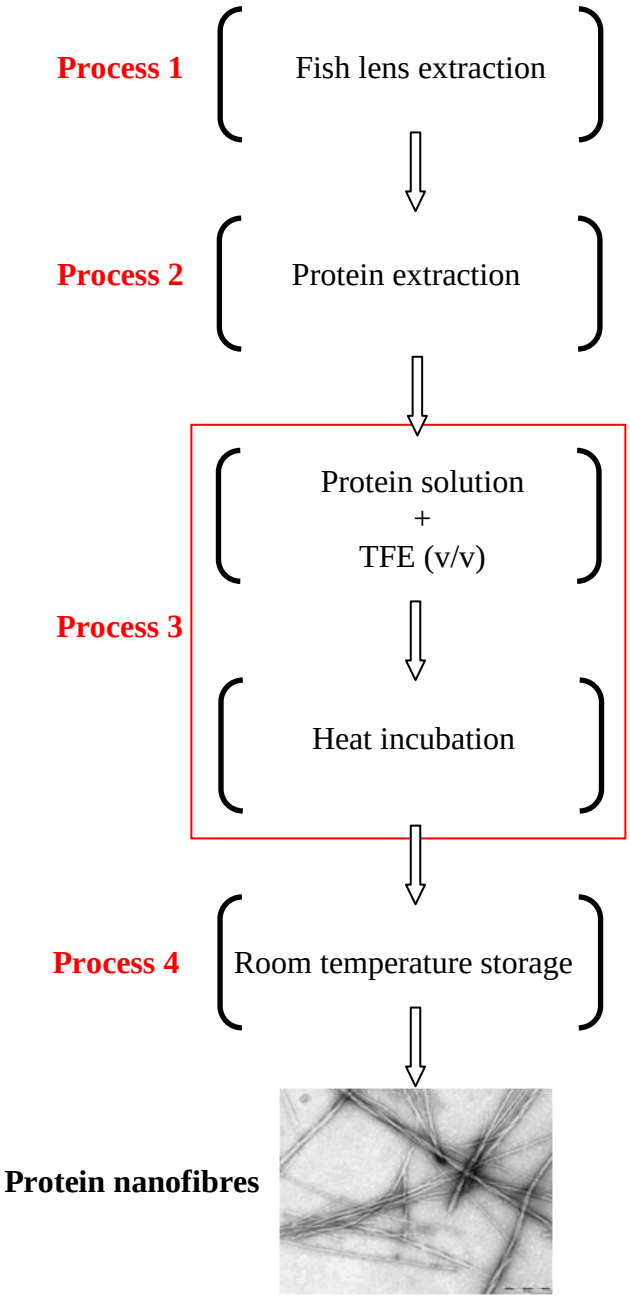

Figure 2-2: Detailed process diagram showing the in-house method for protein nanofibres synthesis developed by our research group.

The process can be divided into four main sections: **process 1**: the fish lens extraction, **process 2**: protein extraction from the fish lens, **process 3**: preparation of 5.8 mg/mL with 10% TFE v/v and incubation in heating block at 60^{o}C and **process 4**: the self-assembly of protein nanofibres at room temperature.

Fish lens extraction

The initial materials for the process were fish lenses. Raw fish lenses were extracted from different types of deep sea fish. Fish heads were supplied by the local fish market. The majority of the fish lenses were from barracuda and deep sea perch. Fish lenses were extracted using sharp razor blades and rinsed with water to remove unwanted membranes and fluids. After the extraction, the lenses were weighed and stored in the freezer until use.

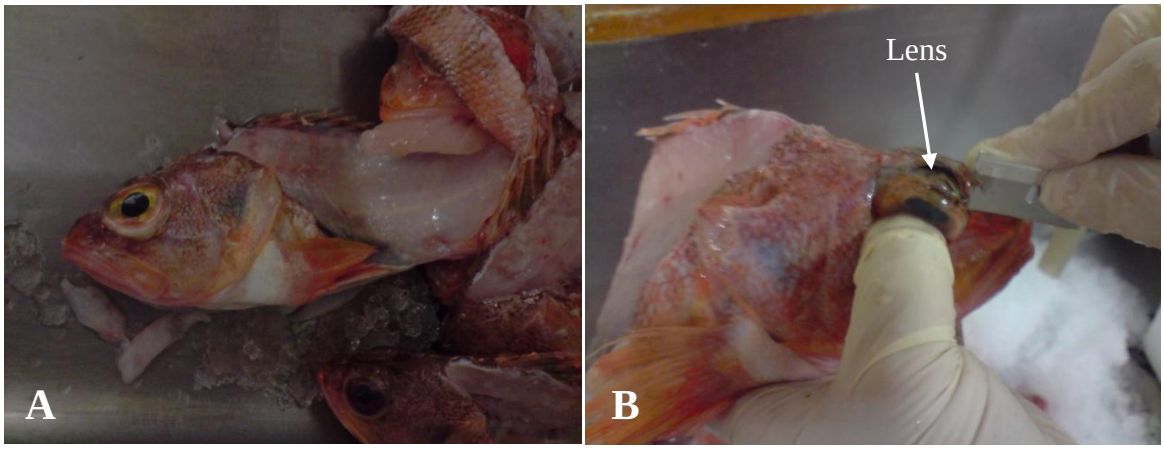

Figure 2-3: Fish lens extraction process in process one.

A: free deep sea perch from local fish market and B: using a sharp razor blade to extract the lens.

Protein extraction from fish lens

The second step was the extraction process of the crude eye lens crystallin proteins from the fish lenses. During the extraction process, an IKA® ULTRA TURRAX® Tube Disperser was used. Extraction buffer (50 mM TRIZMA base, 5 mM EDTA, 1 mM DTT) with a final

pH 7.5 was prepared and added in the ratio of 2 mL per one gram of fish lens. Typically, 5 grams of fish lens was extracted in 10 mL of the extraction buffer. The ULTRA TURRAX was set at maximum speed 9 for 20 minutes at room temperature and the lenses were homogenized in the buffer. After the extraction process is completed, the homogenate was transferred into centrifuge tubes and spun at 12,000 rpm at 18^{o}C for 30 minutes in Eppendorf Centrifuge 5810R. The supernatant containing the soluble proteins was then separated from the insoluble pellet into a new Eppendorf tube. The extracted crude protein solution was diluted 1 in 100 and the protein concentration was determined using the Nanodrop Spectrometer ND-1000 at 280 nm.

Protein nanofibre synthesis

The starting concentration of crystallin proteins used in the initial part of the process was calculated based on the protein concentration reading obtained from the Nanodrop spectrometer. The crude crystallin homogenate was diluted using TFE (i.e. 5% to 20% v/v) at acidic pH to obtain the required final protein concentration (i.e. 5 mg/mL to 50 mg/mL). Detailed calculations for different final protein concentrations can be found in Appendix A1.

Heat incubation process

The mixtures with the final protein concentration (i.e. 5 mg/mL to 50 mg/mL) were incubated at various temperatures (i.e. 60, 75, 80, 85 and 90^{o}C) for up to 24 hours on a heating block, as illustrated in **Figure 1-7**.

Self-assembly process

After the specified time of heat incubation, the sample was removed from the heating block and left on the bench at room temperature for at least a day and in some instances up to a period of a week. This step is known as the self-assembly process of protein nanofibres. In the experimental set-up, this term is also defined as the room temperature storage time. After storage at room temperature, transmission electron microscope (TEM) grids were prepared by depositing 2 microlitres of the final product and staining it with uranyl acetate. TEM analysis was carried out to confirm the presence of protein nanofibres.

2.3 Process optimization

A total of five variables [X_1] to [X_5] of the in-house method were investigated and optimized individually as illustrated in **Figure 2-5**. Process optimization was performed to increase the efficiency of the process and the goal was to manufacture the highest quality of protein nanofibres. The process optimization variables were different pH of TFE, protein concentrations, percentage of TFE, heating temperatures, heat incubation durations and storage durations. Additionally, the goal was also to minimize the capital cost by using crystallin proteins from fish lenses.

Different qualities of protein nanofibres

The optimal conditions for each process optimization variables were evaluated based on the quality of the protein nanofibres, illustrated in **Figure 2-4**. Although both low and high yields protein nanofibres were obtained, the quality of the protein nanofibres produced were significantly different. Based on **Figure 2-4 B**, it was clear that no amorphous aggregates were observed and only bundles of high ordered structures of protein nanofibres were found under the TEM. On the other hand, large amounts of amorphous aggregates were present and

only individual protein nanofibres were detected at low quality **Figure 2-4 A**. Finally, the yield of the product was calculated based on the protein concentrations using a spectrometer. However, the objective of the thesis was to yield the highest quality of protein nanofibres and there were some cases where the quality of the nanofibres was high but the yield of the product was low and vice versa.

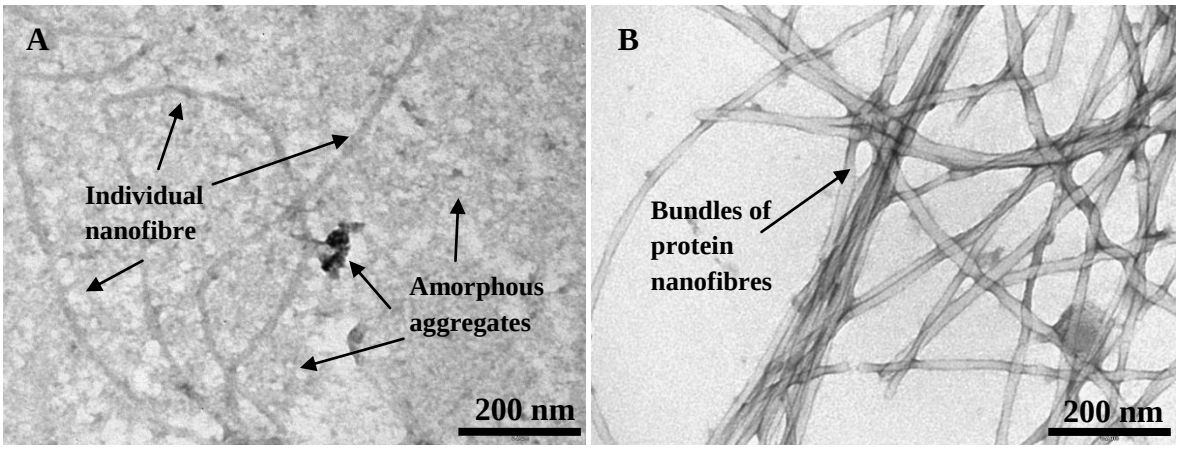

Figure 2-4: The different qualities of protein nanofibres

A: Individual protein nanofibre with amorphous aggregates (low quality) and B: Bundles of high ordered structure of protein nanofibres with no amorphous aggregates (high quality).

2.3.1 Laboratory scale process flow

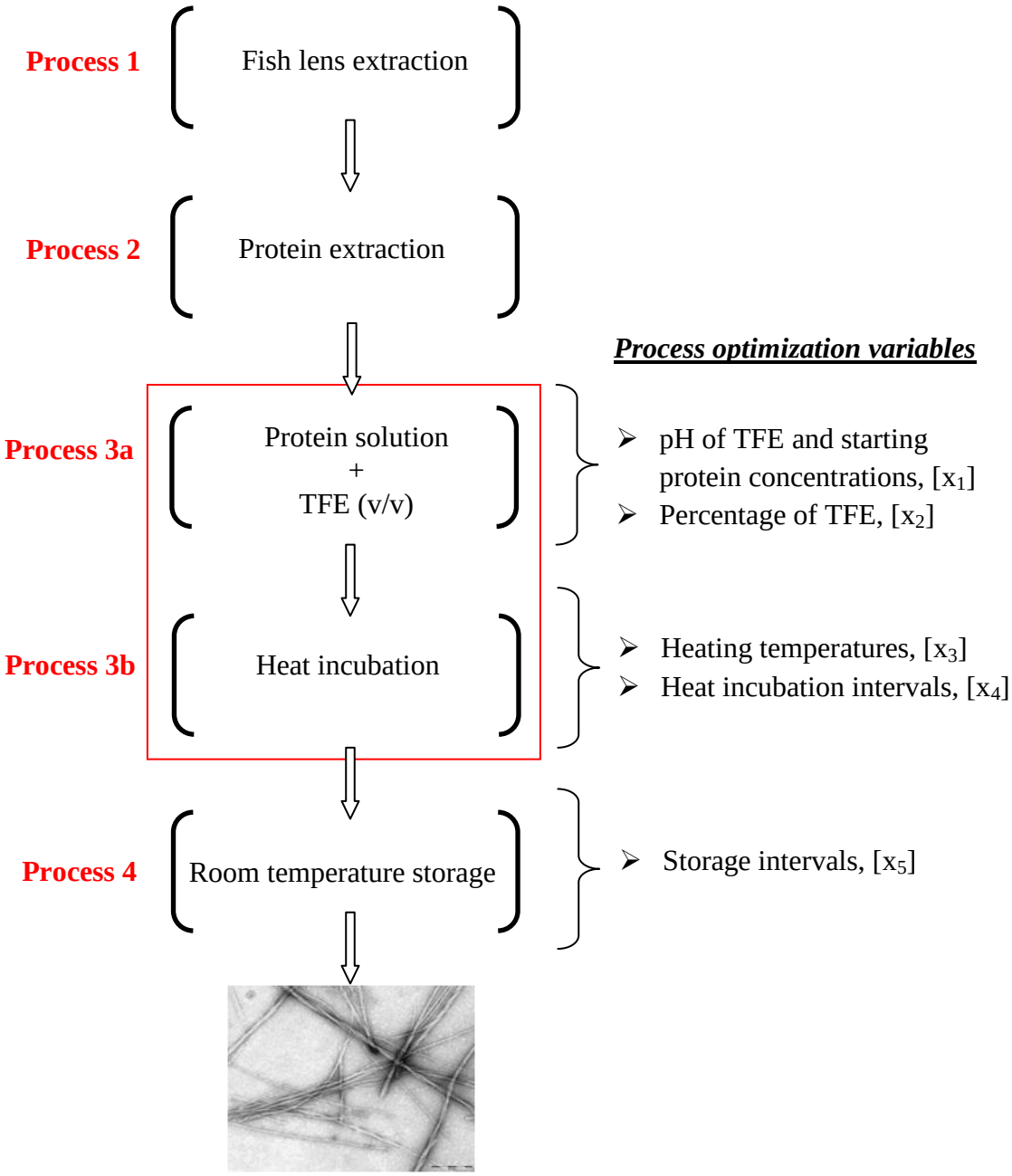

Figure 2-5: Laboratory scale production with process optimization in process 3 and 4.

Table 3: Variables that must be optimized on bench scale volume (1 mL).

Variables	Objective	Process
x_1	Different pH levels of TFE	3a
	Different starting protein concentration	3a
x_2	Different percentage v/v of TFE	3a
x_3	Temperature for incubation	3b
x_4	Incubation interval	3b
x_5	Room temperature storage interval	4

2.3.2 Scale-up process flow

A total of five variables were investigated and optimized (**Table 3**) and the optimized conditions were carried forward for large scale production. The scale-up flow chart is illustrated in **Figure 2-6** and the objective was to scale-up the laboratory scale of 1 mL volume to 1 L volume. Large scale production required a large amount of fish lens from the local seafood industry and the lenses were extracted individually. Due to the volume capacity of the protein extraction, a Silverson L4RT Laboratory mixer (Advanced Packaging Systems Ltd, New Zealand) was used to extract the proteins from fish lenses, instead of the lab bench homogenizer. The mixture of proteins and TFE was heated in a LabServ oven for a period of 24 hours. The protein aggregates formed during heating were spun down using a Sorvall RC6 Plus. The supernatant was collected and left at room temperature for the self-assembly process. Quadruplicate TEM grids were prepared to confirm the formation of protein nanofibres.

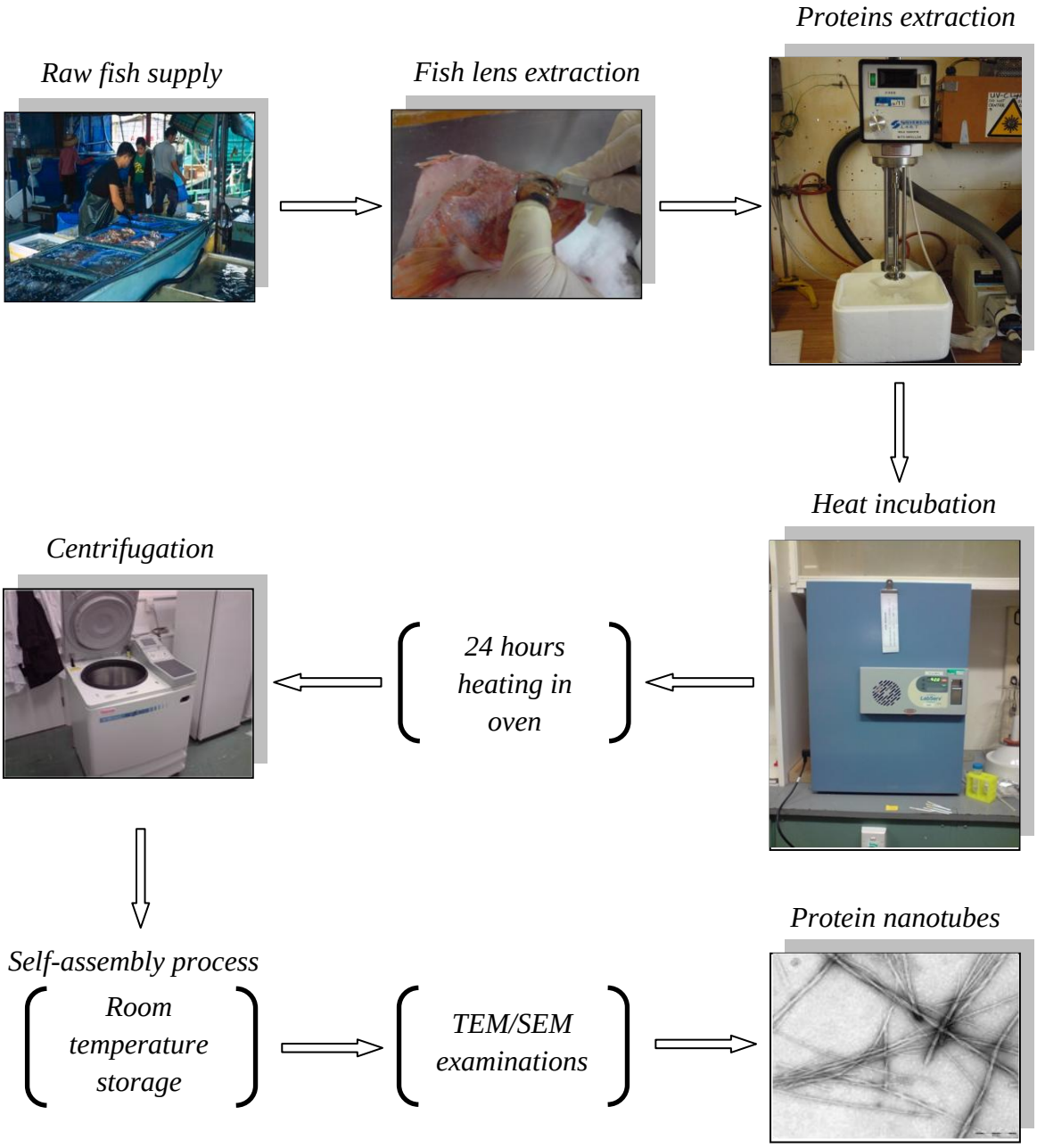

Figure 2-6: Scale-up experiment with maximum capacity of 10 L due to the space limitation in the oven for heating.

2.4 Methods to detect protein nanofibres

2.4.1 Thioflavin T measurements

The formation of protein nanofibres was assessed using the Thioflavin T (ThT) assay. ThT fluorescence measurements were made for each of the trials using a BMG FLUOstar Optima plate reader. The assay was run in a 96-well Greiner microassay plate and the solution in each well comprised of 100 µL of assay buffer (50 mM Tris-HCl and 100 mM NaCl), 4 µL of 5-20 µM ThT, 86 µL of distilled water and 10 µL of the protein aliquot. The samples were excited at 450 nm and the emission was measured at 485 nm with a slit width of 12 nm. The fluorescence measurements were run at 25°C for 6 minutes in the plate reader. Two ThT measurements were made for each aliquot which gives a total of four readings for each sample. Finally, as mentioned in Section 1.6.3, ThT has a higher capacity of binding efficiency to β-sheets compared to Congo red and it has thought to be 20 fold faster based on binding stoichiometry (Groenning 2009), therefore only ThT fluorescence measurement was performed on protein nanofibres.

2.4.2 Transmission electron microscopy (TEM)

The fibril formation and morphology was assessed by TEM (Thorn *et al.,* 2005). In this thesis, TEM was used regularly not only to confirm the protein nanofibres but also as a tool to measure the length and the width of the fibrils to examine the overall structure of the protein nanofibres. While visualizing the structure of nanofibres, the image was magnified up to 89,000 times to examine the ordered structures of the protein nanofibres. However, in some cases the images of nanofibres were only magnified to 14,000 times to examine the overall length and the morphology of the nanofibres. TEM images were captured with an SIS/Olympus Megapixel III digital camera. Quadruplicate TEM grids were prepared for each of the samples to confirm the formation of protein nanofibres.

TEM grid preparation

Samples of protein nanofibres were stained with 1% uranyl acetate for at least 1 minute on formvar-coated copper grids (200 meshes) (Garvey *et al.,* 2009). The grids were examined using a Morgagni 268D transmission electron microscope (FEI Company, Oregon, USA), fitted with a 40 μm objective aperture, working at 80 kV.

2.4.3 Scanning electron microscope

The morphology of higher ordered structures of protein nanofibre were further assessed using SEM. Protein nanofibre formed from crude barracuda lens crystallins were diluted 100x in distilled water and dried overnight on a gold coated cover slip. After drying, the slips were again gold coated for 2 minutes with a sputter coater (Emitech k550x) to get a final coating thickness was about 10 nm. The cover slips were then examined by SEM (Leica S440) at 2 kV and a spot size of 20 mA.

For imaging protein nanofibres on a filter, 300 μL of nanofibre sample was slowly vacuum filtered through a 0.2 μm nitrocellulose filter (Millipore) and air dried over night. The dried filters were gold coated using a sputter coater (Emitech k550x) and examined with a SEM (7000 HRSEM, JEOL, Japan) with accelerating voltage between 5 and 15 kV.

2.4.4 X-ray fibre diffraction of protein nanofibres

X-ray fibre diffraction was used to examine the structure of crude crystallin fibrils (Serpell *et al.,* 1999). X-ray fibre diffraction on protein nanofibres made from crude crystallin proteins were performed by Laura Domigan (PhD student). Protein nanofibres made from crude crystallin were concentrated by centrifuging the sample at 13,500 rpm for a period of 30 minutes. The supernatant was removed and the pellet was suspended in minimal Milli Q

water. Aliquots of crude crystallin fibrils (10-20 μL) were suspended between two waxed-filled capillary ends and the sample was air-dried. The small stalk of protein obtained was aligned in an X-ray beam and diffraction data were obtained using a CuKα Rigaku rotating anode source (wavelength 0.15418 nm) equipped with a MARresearch image plate detector. The sample to detector distance was 175 mm and the exposure time was 20 minutes. Images were examined and reflections were measured using marView.

2.5 Fragmentation on protein nanofibres

Protein nanofibres were sonicated with 20% amplitude at 0.2 second pulse for a period of 10 seconds (total of 50 pulses of 0.2 second) to get fragments of nanofibres that can act as seeds for nanofibres formation. For imaging sonicated protein nanofibres, TEM grids were immediately prepared after the sonication process to visualise the broken pieces of nanofibres.

3 Results and discussion

3.1 Starting materials

Fish lenses were extracted from different types of sea fish where these fish live in the first 50 feet of the water column. The eyes are extremely large because they are primarily sight feeders. Due to the unpredictable nature of the seafood industry supply, different species of fish were trialled and used for the experiments. The varieties considered in this thesis were Great Barracuda (*Sphyraena barracuda*), Deep Sea Perch (*Hoplostethus atlanticus*), Ribaldo Cod (*Mora moro*), Hoki (*Macruronus novaezelandiae*) and Groper (*Achoerodus viridis*) **Figure 3-1**. One of the objectives of the thesis was to perform process optimization for the in-house method to produce the highest quality of protein nanofibres. The variables stated in Chapter 1 Objectives for the in-house method of protein nanofibres synthesis were optimized. In addition, bovine lenses were also investigated by the same methods to assess whether protein nanofibres can be manufactured in the same way because the study by Garvey resulted in formation of both straight and short flexible fibrils **Figure 1-5** and **Figure 1-6**.

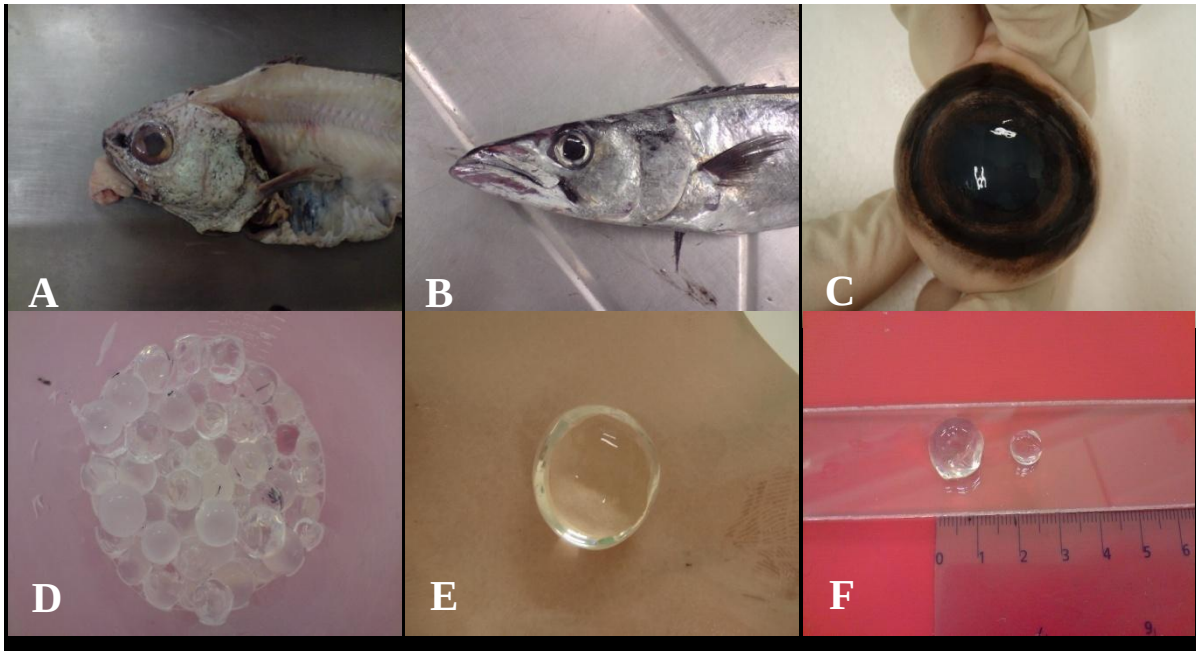

Figure 3-1: A series of photos taken for different types of fish and extracted lenses used for the experiments.

A: Ribaldo fish, B: Barracuda fish, C: Bovine eyeball, D: 200 deep sea perch (DSP) lenses preparation for scale-up experiment, E: Extracted bovine lens (diameter is ranged from 2 to 2.5 cm) and F: Difference sizes of DSP lenses based on the size of the fish (diameter is ranged from 0.6 to 1.2 cm).

3.1.1 Crystallin proteins

One of the objectives of the thesis was to use fish lenses as the starting material to create a substantial opportunity to support environment sustainability but also potentially add value to waste materials from seafood industry. By doing so, the cost of the materials for the process may be significantly reduced.

Crystallins are water soluble (Meehan *et al.*, 2004; Ecroyd and Carver 2009). α-Crystallin is composed of two, closely related subunits, αA and αB. Size exclusion chromatography (SEC) was carried out to compare the content of individual crystallins in fish and bovine lenses, as it is important to distinguish the differences between the two lenses for crystallin

proteins composition comparison. In addition, methods had been developed previously for bovine crystallin but not fish crystallin.

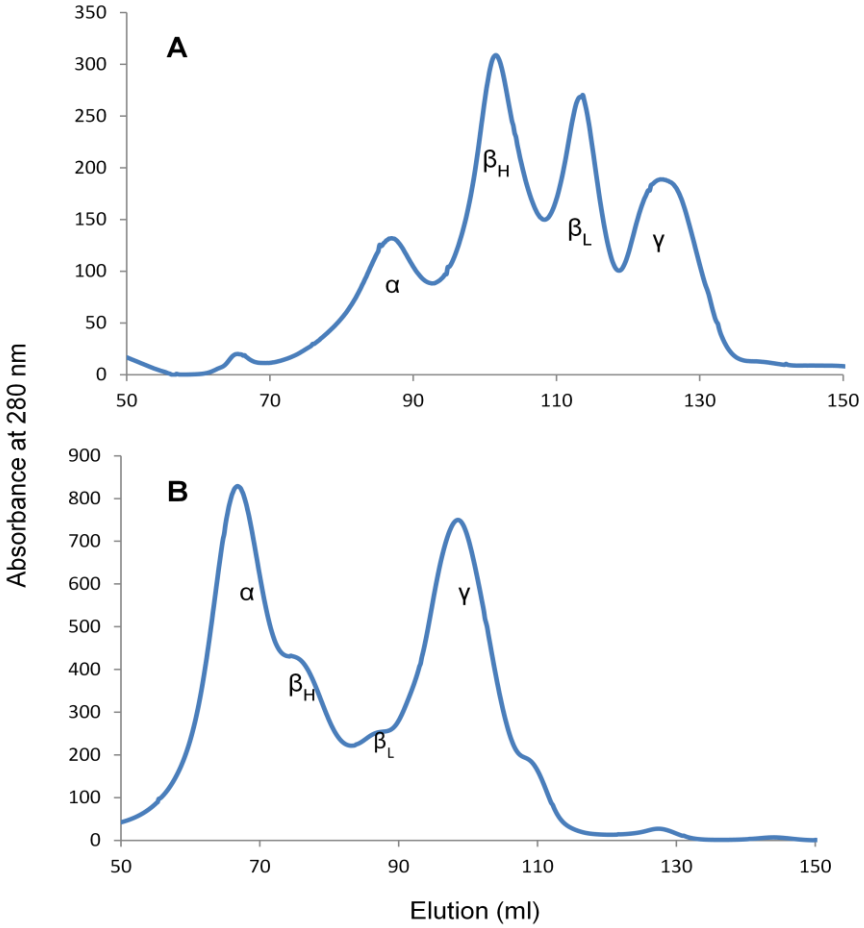

Figure 3-2: The separation of individual crystallins proteins using size exclusion chromatography.

A: Separation of bovine crystallins and B: Separation of barracuda crystallins. Peaks are labelled corresponding to α, β_H, β_L and γ crystallins in both image A and B.

These fractions of various crystallins (α, βH, βL and γ) are similar to those reported in the literature (Devries *et al.*, 2004; Garvey *et al.*, 2009). The SEC elution pattern was similar for fish and bovine crystallins but the relative sizes of α, β and γ peaks were different. The relative amounts of crystallins were estimated and compared. The amount of β crystallins in

fish lens is lower compared to bovine but α and γ are higher in fish. This is in agreement with the results presented elsewhere (Kiss *et al.,* 2004)

3.1.2 Individual proteins

The in-house method can be simplified from **Figure 2-5** to **Figure 3-3**. During the process of protein nanofibre synthesis, waste was generated from the centrifugation process which is classified as C shown in **Figure 3-3**. SDS-PAGE was performed to analyse each individual protein component during from the conversion of crude crystallins mixture into protein nanofibres.

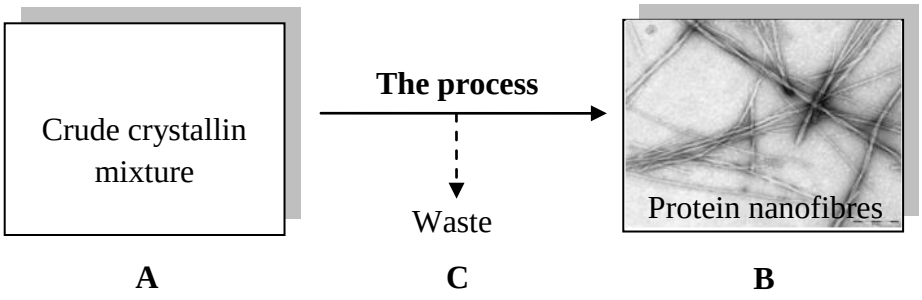

Figure 3-3: Simplified schematic of the entire process.

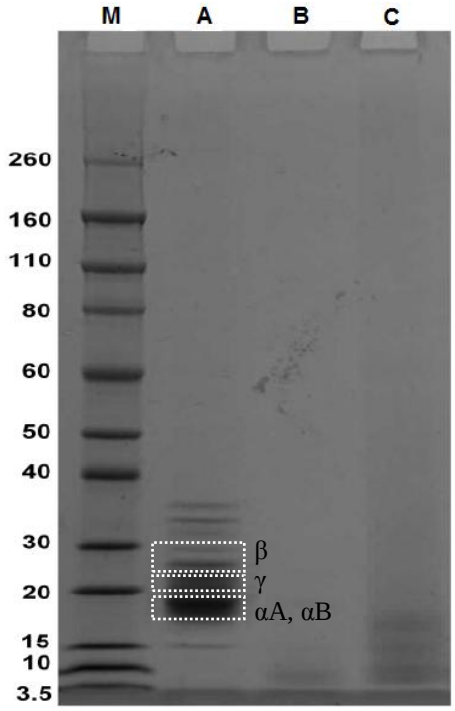

Figure 3-4: SDS-PAGE of crude crystallin mixture from barracuda fish lens.

Lane M: Novex Sharp protein standard (Invitrogen Marker), **Lane A**: Crude mixture of crystallins, **Lane B**: Crystallin in solution after 24 hours heating at 80^{o}C and **Lane C**: Crystallins in precipitate after 24 hours heating at 80^{o}C.

The results of SDS-PAGE were collected from various fractions and analysed to identify the class of crystallins in the crude extract. α-Crystallin is comprised of subunits, αA and αB with a size range of ~18-22 kDa; β-crystallins of ~20-30 kDa subunits; and γ-crystallin monomers of ~20kDa **Figure 3-4**. The results of SDS-PAGE were also similar to those reported in the literature (Garvey *et al.,* 2009). The aggregates from the waste were also analysed using SDS-PAGE. Analysis of the aggregates shows bands for all the crystallins present in the starting crude mixture. However, the gel bands for α and γ-crystallins in the precipitate were reduced relative to the crude mixture, indicating that these crystallins may still be present in the solution, during formation of protein nanofibres.

3.2 Different qualities of protein nanofibres

Protein nanofibres used for nanowires applications (Scheibel *et al.,* 2003; Hamedi *et al.,* 2008) must be purified to some extent. Other applications of protein nanofibres, for example for strengthening a material platform (i.e. films), may not require a high level of product purity. Due to the lack of fluorescence measurements from ThT (which will be addressed in detail in Section 3.5), protein nanfibres were not able to be quantified and the yield of the product was estimated using protein concentrations from spectrometer measurements. In addition, physical observation of the final product were analysed under the TEM to judge the quality of the nanofibres. The optimal operating conditions were determined by the highest quality of the protein nanofibres formed with no amorphous aggregates observed under the TEM. In addition, the length and the clear defined structures with twisting between individual nanofibre were also taken into consideration to determine the optimal operating conditions.

A total of three different nanofibres products, based on their quality, were manufactured from the process: low, medium and high quality **Figure 3-5**. For low quality product, amorphous aggregates were formed during the 24 hours of heat incubation and the centrifugation step was bypassed. These amorphous aggregates were left undisturbed in the samples until the end of the process **Figure 3-5 A**. At medium quality, as the protein solution and the pre-heated TFE were mixed, amorphous aggregates formed instantly. 15 minutes after the addition, the samples were removed from heat and centrifuged to remove all the aggregates that were formed during the first 15 minutes of heating. After centrifugation, the supernatant were collected and the heat incubation process continued for the remaining 24 hours. During the 24 hours heat incubation process, minor protein aggregates were formed again but these were not centrifuged and were left until the end of the process **Figure 3-5 B**. Finally, for the

highest quality, after the addition of protein solution with the pre-heated TFE, the samples were centrifuged only after completing the 24 hours in heat incubation to remove the amorphous aggregates and the supernatant were collected **Figure 3-5 C**.

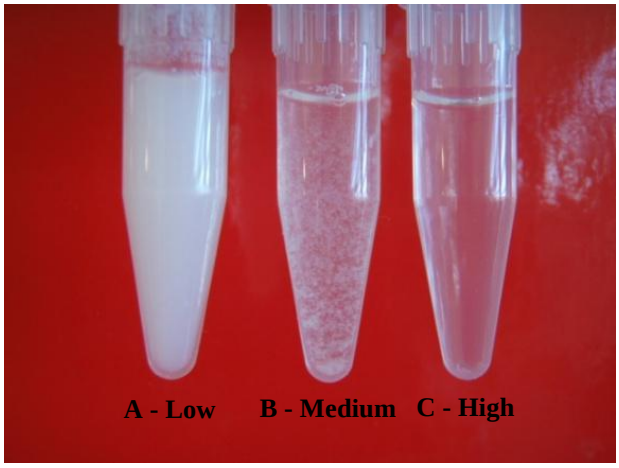

Figure 3-5: Three different qualities of the final product contain protein nanofibres.

A: Low quality with large quantity of white protein aggregates, B: medium quality with some protein aggregates and C: high quality, with no protein aggregates and a clear solution.

TEM images of three different qualities of the final product low, medium and high quality at low magnifications (14,000x)

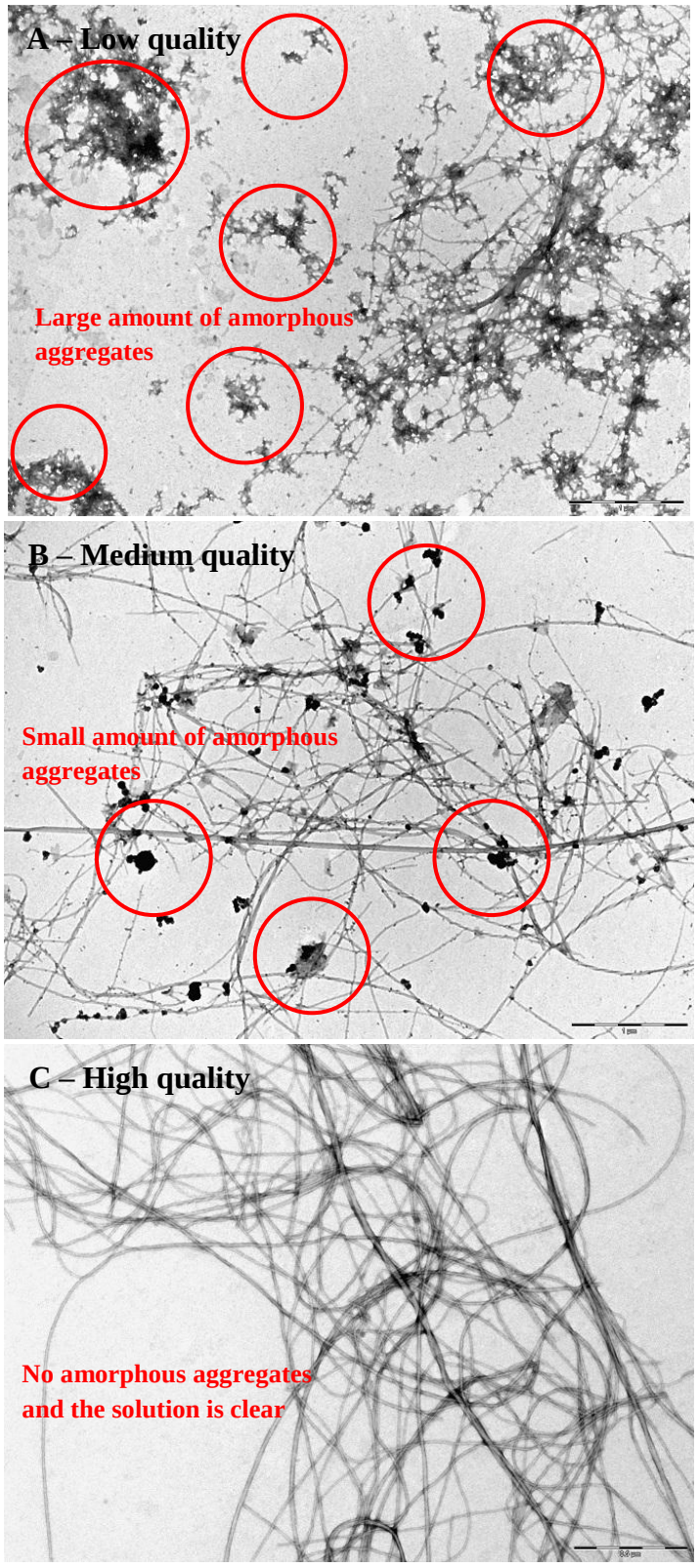

Figure 3-6: TEM images showing three types of qualities of protein nanofibres developed.

Table 4: Estimated yield for all three different qualities of nanofibres developed.

Quality of nanofibres	Yield (%)
Low	25% ~ 35%
Medium	15% ~ 25%
High	7% ~ 12%

The relative amount of amorphous aggregates in the three products were estimated and compared. At low quality, protein nanofibres can be found relatively easily under the TEM to the same extent compared to the medium and the highest of quality nanofibres. In the same sample (low quality), there were many amorphous aggregates found, as highlighted in **Figure 3-6 A** compared to the medium quality sample and none in the highest quality nanofibres sample. For medium quality nanofibres, the amount of amorphous aggregates present were reduced by approximately 60% compared to the lowest quality and the morphology of the nanofibres remained more or less the same as the lowest quality nanofibres **Figure 3-6 B**. Finally, for the highest quality nanofibres, no protein aggregates were found under the TEM, the solution was clear and bundles of nanofibres were found easily **Figure 3-6 C**.

3.3 Process optimization

A total of five variables (i.e. X_1 to X_5) for the in-house method were investigated and optimized individually, as illustrated in **Figure 2-5**. The purpose of the optimization process was to manufacture the highest quality of protein nanofibres, improve the efficiency and minimize the capital cost, creating a final product that meets certain specifications with the associated constraints considered, as mentioned in Section 3.2. For each stage, optimization was intended to yield the highest quality of protein nanofibre.

The first optimization variable investigated was the effect of protein nanofibres formation by altering the pH levels of TFE, followed by different percentages of TFE v/v [X_1]. Different starting protein concentrations [X_2] were also investigated to improve the quality of nanofibres. Different heating temperatures [X_3] to incubate the proteins were also investigated to determine the optimal operating condition. Finding the optimal operating temperature is the most crucial part of the process, as it could be the most expensive variable in the entire process once the volume is scaled-up. Additionally, different heating incubation intervals [X_4] were investigated to determine the optimal operating window. Finally, different durations of room temperature storage times [X_5] were explored and determined. All these five variables were altered systematically and optimized individually to produce the highest quality of nanofibres.

3.3.1 The effect of different TFE pH levels and protein concentrations [X_1]

Different pH levels ranging from acidic to basic were tested to investigate the optimal pH and the impact of various pH conditions on protein nanofibre formation. The tested range of pH was from 2.0 to 7.5. Values of pH greater than 7.5 were not tested as it was suggested the formation of protein nanofibre was not favoured above pH 7.5 (Grothe *et al.,* 2009). The acidic pH was obtained using 0.1 M HCl and more basic pH using 0.1 M NaOH. Apart from the change in pH, the rest of the experimental conditions were maintained constant. These constant conditions were: 1.5 mL Eppendorf tube with sealed screw cap (volume of sample 1 mL) incubated at 60^{o}C temperature for overnight heat incubation (i.e. 16 – 18 hours) and 36 hours at room temperature storage for self-assembly process based on the initial set-up for the in-house method. TEM grids were prepared and examined under TEM to observe the formation of protein nanofibres and their quality.

TEM images for pH 2.0 to pH 7.5

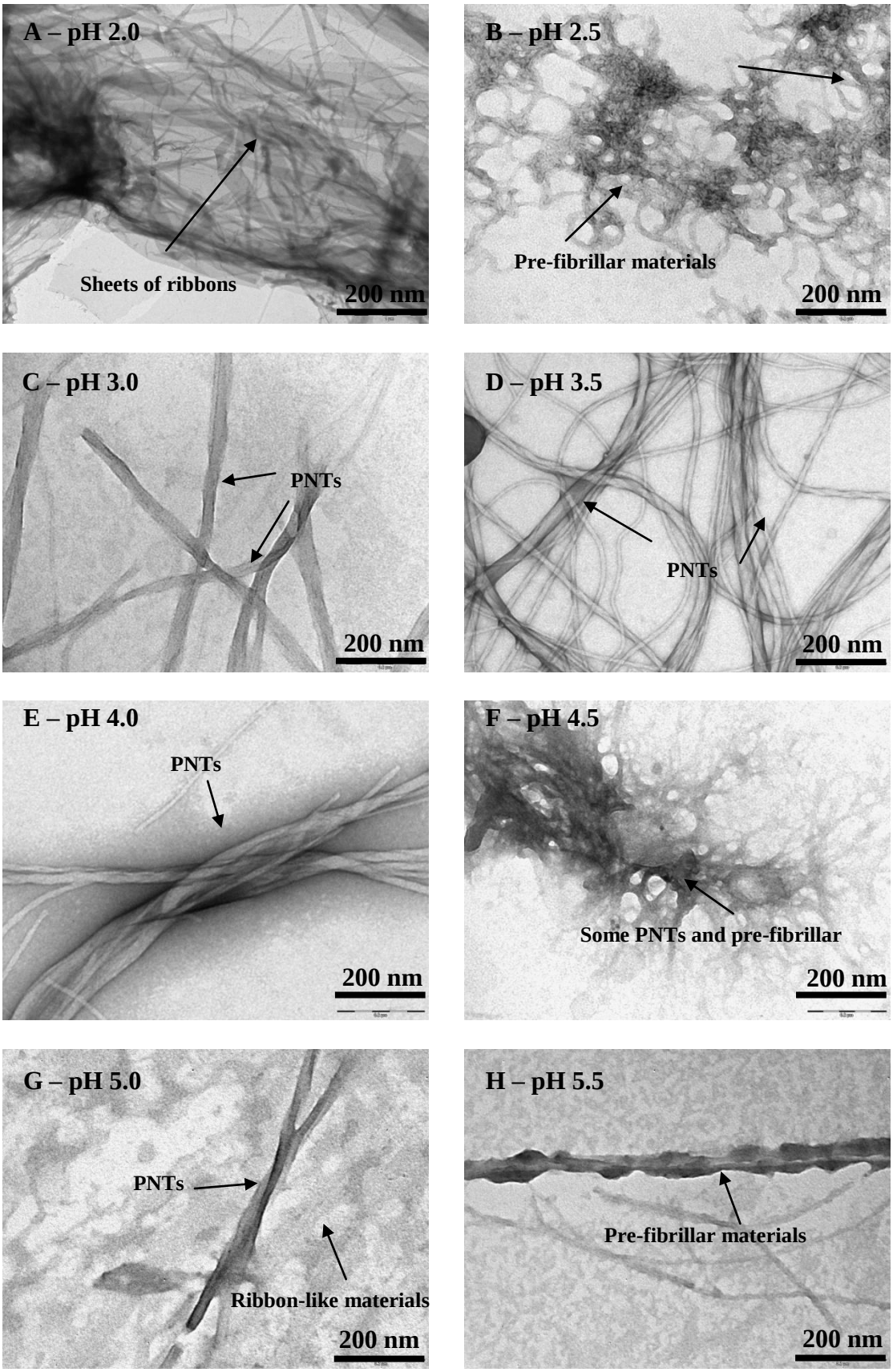

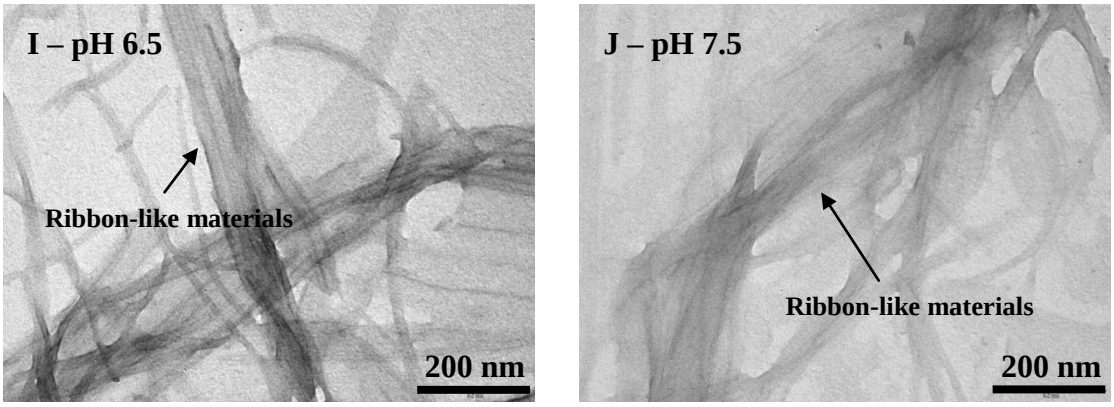

Figure 3-7: TEM images showing the effect of using different pH levels of TFE on protein nanofibres formation.

At very acidic conditions (i.e. pH 2.0 and 2.5), sheets of ribbon and pre-fibrillar materials were observed **Figure 3-7 A, B** and as the pH levels increased to 3.0 and 4.0, bundles of highly ordered structures of nanofibres were found **Figure 3-7 C to E**. Beyond pH 4.5 and above, ribbon-like structures started to reappear, similar to those at pH 2.0 and 2.5. At a higher pH (i.e. pH 5.0 and 6.0), minor individual nanofibres and ribbon-like structures were found together within the same sample. This indicates that pH 5.0 and 6.0 are beyond the operating window for protein nanofibre formation and similar results were observed for pH 2.0 and 2.5. In addition, the majority found in these samples were mostly ribbon-like structures or pre-fibrillar structures with small amounts of protein nanofibres. Finally, at pH levels above 6.0 only ribbon-like structures were present and no protein nanofibres were found. Based on the initial results analysis, the optimal operating pH levels range was found to be between 3.0 and 4.0. Based on these observations, a detailed analysis was performed from pH 3.0 to pH 4.0 with pH increments of 0.2 using the same experimental conditions.

TEM images of detailed pH levels analysis (pH 3.0 – 4.0)

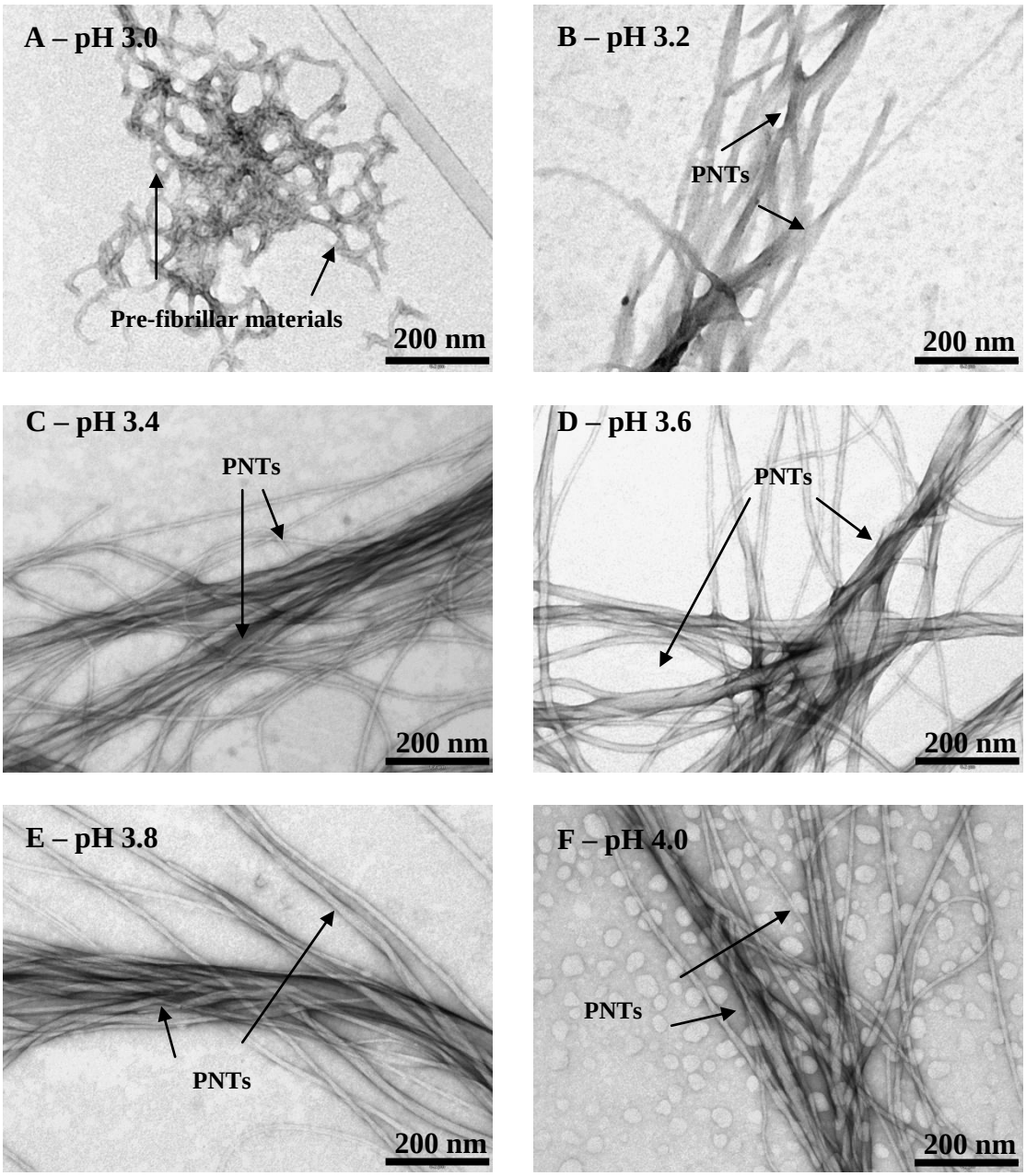

Figure 3-8: TEM images showing the detailed analysis from pH 3.0 to 4.0 of TFE.

Large and long bundles with highly ordered structures were observed under the TEM for pH 3.0 to 4.0 **Figure 3-8**. Based on the detailed analysis of results, repeated experiments were carried out and the optimal operating pH was found to be 3.8 to consistently produce the highest quality of protein nanofibres.

With the TFE pH finalised at 3.8 the optimal starting protein concentration was determined. In the process set up, the proteins were extracted using the extraction buffer prepared at pH 7.5 and the homogenate was diluted to the final starting protein concentration by diluting it in 10% TFE v/v at pH 3.8. Various starting protein concentrations of crude fish lens crystallins were incubated at 60^{o}C and the resulting structures were visualized using TEM to determine the optimal concentration to produce the highest quality of nanofibres. The different protein concentrations were 5, 10, 20, 30, 40 and 50 mg/mL while the rest of the experimental conditions remained constant.

TEM images for different starting protein concentrations at high magnifications (89,000x)

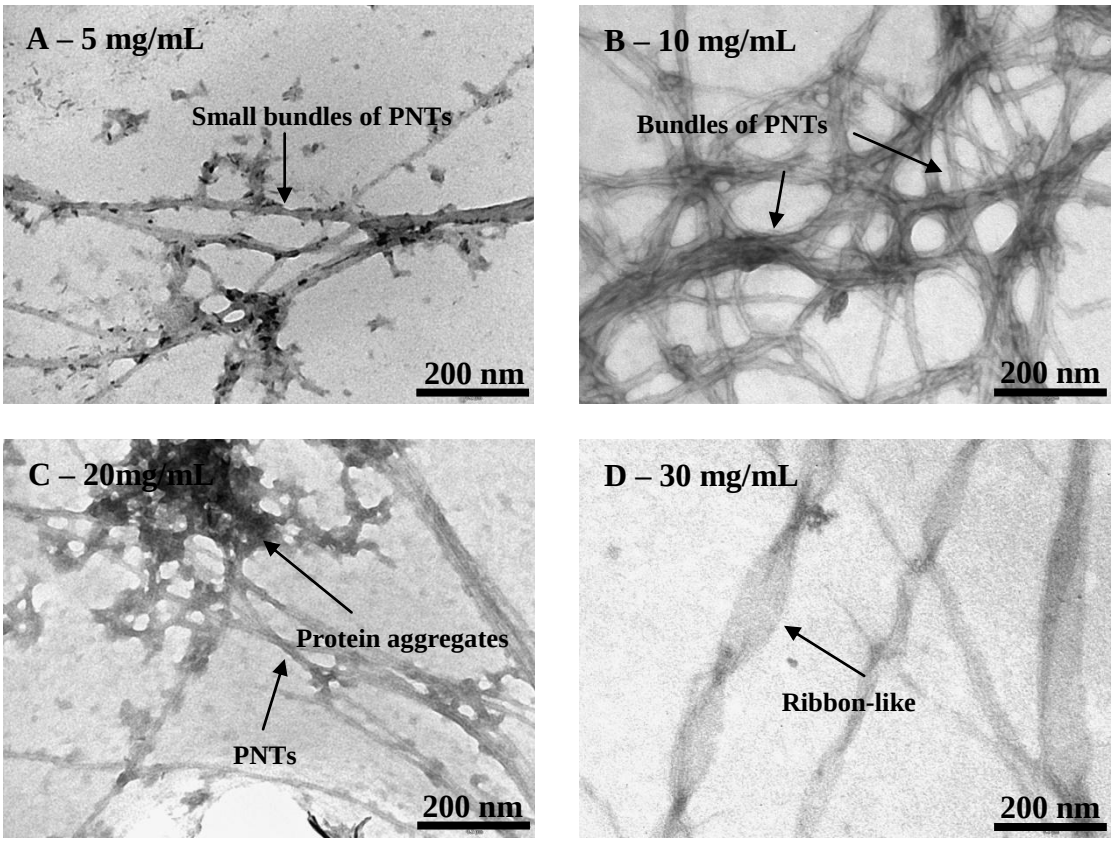

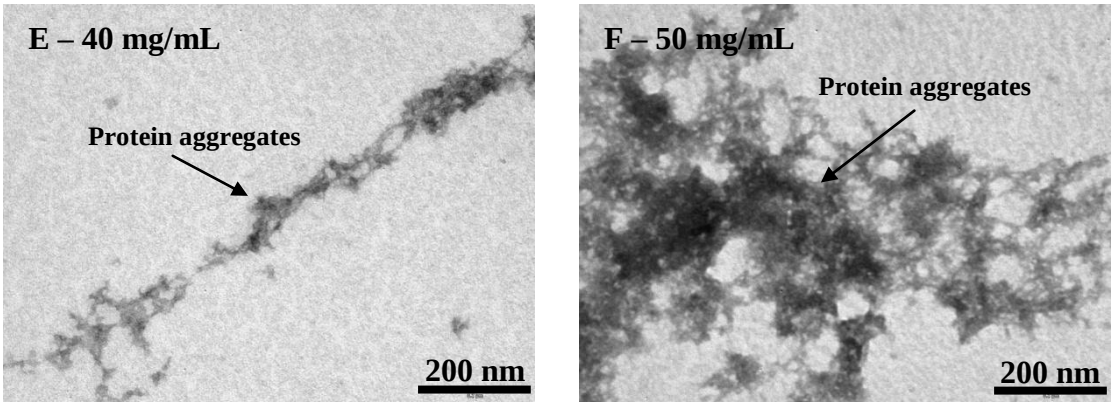

Figure 3-9: TEM images showing the effect of different protein concentrations on protein nanofibres formation.

It was difficult to distinguish the physical appearance of protein nanofibres and protein aggregates as both of these look very similar at low magnifications at 14,000x (TEM images not shown). Based on the observation, as the protein concentrations increased from 5 to 30 mg/mL, bigger bundles of protein nanofibres were formed. Additionally, there was also significant amounts of amorphous protein aggregates found at high protein concentrations. Hence, a higher magnification with 89,000 times was needed to examine and confirm the structure of protein nanofibres.

At high magnifications, large bundles of nanofibres were observed under the TEM for samples prepared using 10 and 20 mg/mL starting protein concentration **Figure 3-9**. Although some protein nanofibres were found at 5 mg/mL, these were very small bundles of nanofibres compared to the bundles of nanofibres found at higher protein concentrations (i.e. 10 and 20 mg/mL). In addition, there were also some small bundles of protein nanofibres found in the 30 mg/mL sample but these were very difficult to find under the TEM. As the starting protein concentration increased from 30 to 50 mg/mL, only individual nanofibres and a majority of protein aggregates were found instead of large bundles of nanofibres at low protein concentrations. After the primary analysis of the data, a 10 mg/mL starting protein

concentration was concluded to be the optimal starting protein concentration to yield the highest quality of protein nanofibres for the process.

The formation of amyloid materials was introduced with a slight pH change in the system that favoured the formation of protein nanofibres (Gras 2007). A similar approach was introduced in our process, as two solutions mixed together to obtain the final protein concentrations (i.e. crude protein solution and TFE), which resulted in a change in pH. During the preparations, the extraction buffer used to extract the proteins from fish lens were homogenised in buffer at pH 7.5. After the extraction of proteins, the protein solution was then diluted with TFE at pH 3.8 to obtain the final protein concentration. Clearly, with this dilution to prepare the final protein concentration, a change of pH would occur as the two solutions were mixed together.

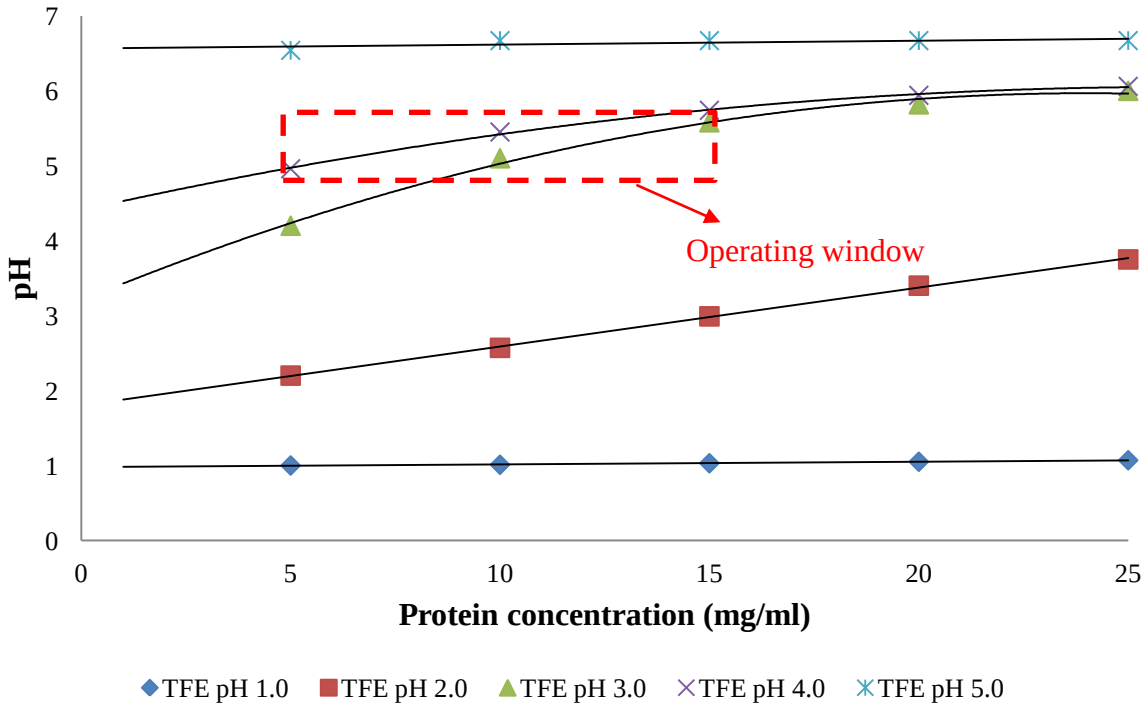

Figure 3-10: The final pH levels after mixing different protein concentrations with different TFE pH.

A plot was produced to record the final pH levels as different protein concentrations were mixed with different pH levels of TFE **Figure 3-10**. Based on the graphical results, it was found that there is a relationship for the pH levels between the protein concentrations and TFE when these two solutions were mixed. It was clear that as long as the pH levels for TFE were prepared between pH 3.0 to 4.0 and the protein concentrations were at 10 to 15 mg/mL, this would yield high quality protein nanofibres, as long the range was still within the operating window, as highlighted in **Figure 3-10**. It was found that if the protein concentrations or the TFE pH levels were prepared outside of these operating ranges, nanofibres and pre-fibrillar materials were formed. Preparation outside of the operating window will create an unfavourable condition for protein nanofibres formation and not yield good quality protein nanofibres. Finally, when the TFE and the protein solutions were mixed together, a final pH between 5.0 and 5.5 yielded the highest quality protein nanofibres. Furthermore, the line of the best fit for the final pH plots have an average of 0.995 R-Squared values, indicating that the measurements of the experiments were consistent and accurate **Table 5**.

Table 5: R-squared values on final pH plot.

TFE pH	R^2
1.0	0.988
2.0	0.999
3.0	0.991
4.0	0.999
5.0	0.998

3.3.2 The effect of different percentage of TFE [X_2]

With pH and the protein concentration finalised at 3.8 and 10% TFE v/v to yield the highest quality of protein nanofibres, the next step was to investigate the effect of different percentages (v/v) of TFE and its impact on the protein nanofibre formation. TFE with 10% v/v is commonly used in the method of preparation for amyloid-fibrils formation (Meehan *et al.,* 2004). Using a low percentage of TFE may produce an insufficient solvent effect for unfolding and refolding and vice versa for high percentage of TFE. Thus, different percentages of TFE were investigated, 5, 10, 15 and 20% v/v, to observe the impact on the protein nanofibres formation. The percentage of TFE is one of the most important components to be evaluated as it will have an impact on the operating cost of the overall process. The optimal operating condition was judged based on the highest quality of nanofibres formed.

TEM images of different percentages of TFE v/v at high magnifications (89,000x)

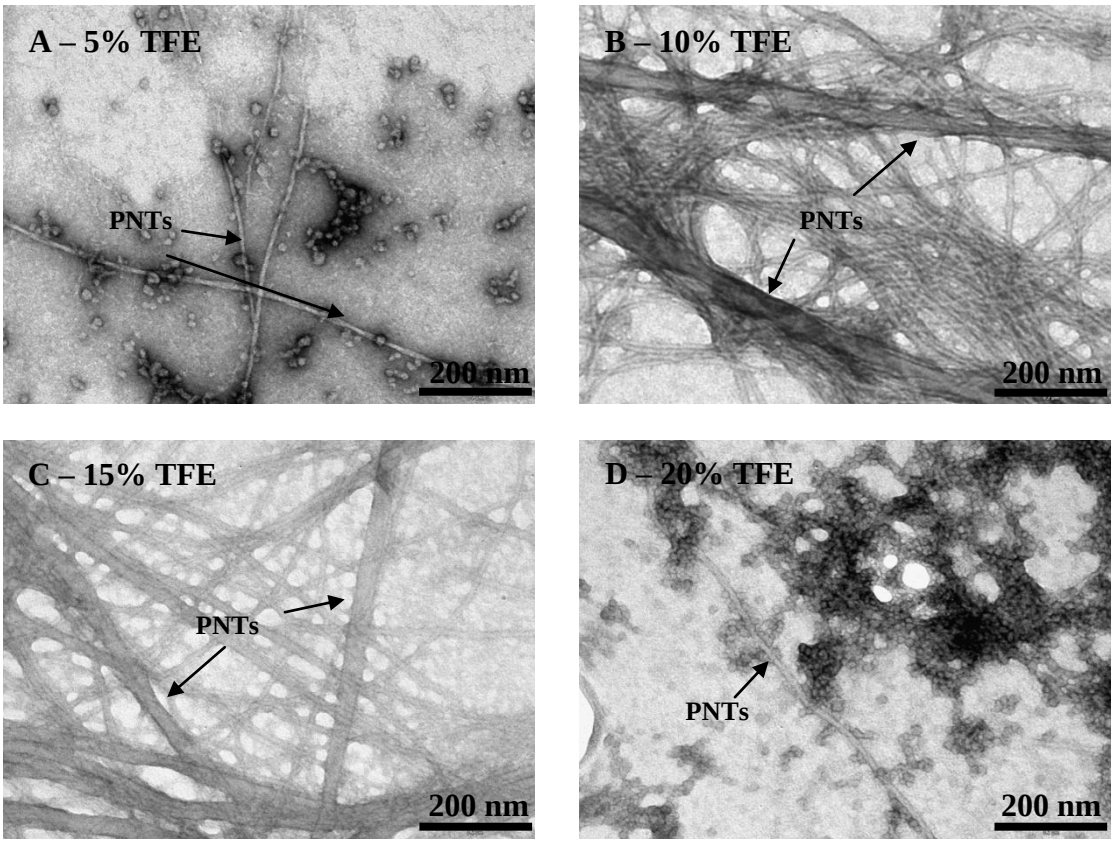

Figure 3-11: TEM images showing the effect of using different percentage of TFE v/v on protein nanofibres formation.

As shown in **Figure 3-11 A to D**, various percentages of TFE appear to have the ability to yield protein nanofibres. After careful analysis, it was clear that at a low percentage of TFE (i.e. 5% v/v), there is insufficient solvent effect to transform all the pre-fibrillar materials into rich β-sheet conformation **Figure 3-11 A**. As the percentage of TFE increased further to 10 and 15%, bundles of nanofibres were observed under the TEM with clear high-order structures. Finally, at 20% TFE v/v the results were similar to 5% TFE, where pre-fibrillar materials start to reappear. The experiment was repeated and the optimal operating TFE percentage was finalised at 10% v/v.

3.3.3 The effect of different heating temperatures [X_3]

Heating at high temperatures can be very costly in large-scale process. Therefore, different heating temperatures were explored to determine the optimal operating temperatures to yield the highest quality of protein nanofibres. Heating temperatures chosen were 37, 50, 60, 75, 80, 85 and 90^{o}C.

TEM images of different heating temperatures at low magnifications (14,000x)

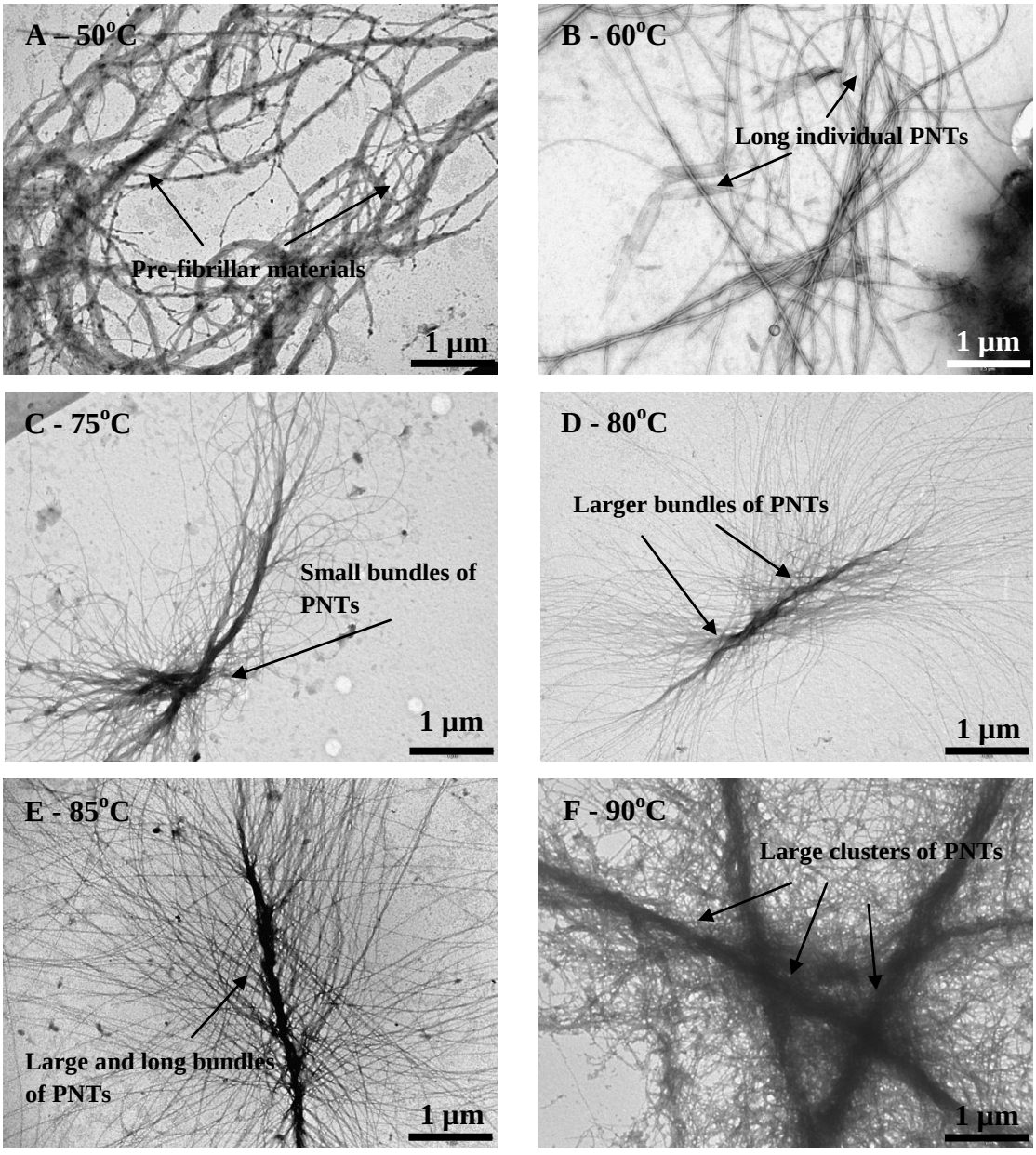

Figure 3-12: TEM images showing the effect of different temperatures on nanofibres formation (sample incubated at 37^{o}C is not included).

Based on **Figure 3-12 A to F**, it was observed all temperatures can yield protein nanofibres. Temperatures greater than 50^{o}C had no difficulty yielding protein nanofibres **Figure 3-12 B, C, D, E**. In addition, as the temperature increased further to 80^{o}C, even larger bundles of protein nanofibres were observed. The lengths of the nanofibres were longer and of larger diameter compared to those at low temperatures **Figure 3-12 B, C**.

Different heating temperatures at high magnifications (89,000x)

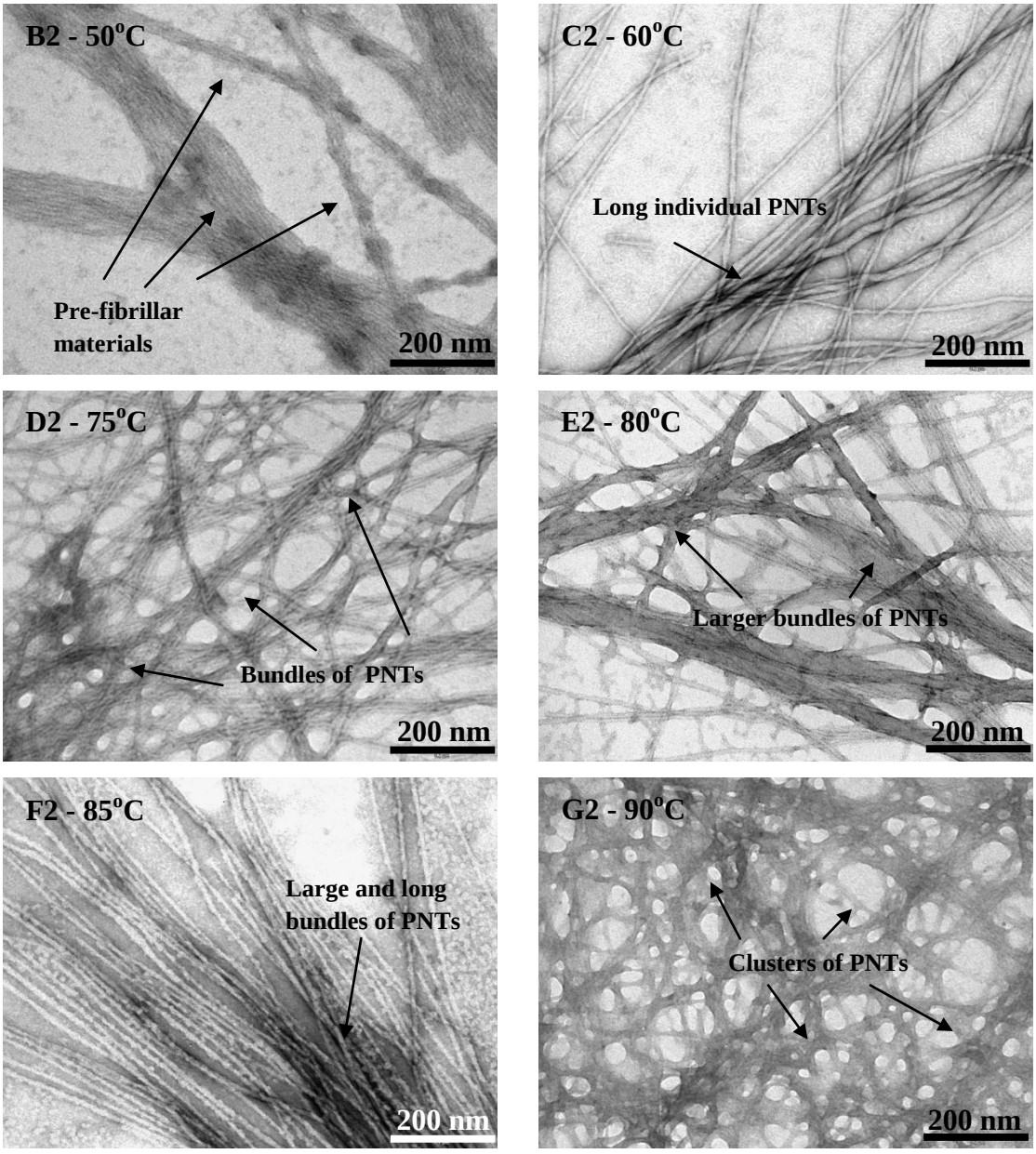

Figure 3-13: TEM showing the effect of different temperatures on nanofibres formation in high magnifications.

Based on **Figure 3-13**, with elevated temperatures from 50 to 90^{o}C for heat incubation, there was a noticeable pattern of different morphologies of nanofibres that were produced. In addition, it was observed that the increase in temperature of incubation resulted in the more rapid formation of higher order structures. At 37 and 50^{o}C, bundle formation was not observed **Figure 3-13 A**. As the temperature increased to 60^{o}C, larger structures of nanofibres started to form and were found very easily under the TEM, with clear structures **Figure 3-13 B**. This is consistent with an earlier study, in which it was shown that fibrils can be made to assemble into bundles by increasing the temperature of fibril synthesis from 37 to 67^{o}C (Carrotta *et al.*, 2007). The elongated fibrils of protein amyloid β-protein packed into large size compact bundles were studied using X-ray scattering experiments and shown to be elongated in shape, consistent with bundles of linear fibrils. At 75^{o}C, the fish crystallin proteins formed small bundles containing 6 to 10 individual fibres. The length of these individual fibres varied from 3 to 5 µm and it appears that these long fibres come together in an intertwining fashion at a point and then extend out of the bundle as individual fibres **Figure 3-13 C**. The resulting formations were higher order structures with larger bundles and longer individual fibres at 75^{o}C. Such a pattern of formation was not observed in the TEM images of the 60^{o}C sample. Based on the results, the TEM images showed that these long fibrils are prerequisites for formation of large bundles and higher ordered structures. As the temperature for incubation increased further to 85^{o}C, more than 20 individual fibres came together to form larger structures, 200 nm thick and more than 2 µm long **Figure 3-13 E**. At 90^{o}C, the diameter of each individual nanofibres remained unchanged but each individual long nanofibres intertwined with more neighbouring fibrils and resulted in even larger bundles of fibres compared to 85^{o}C. The individual fibres started formed bundles that were 500 nm thick and approximately 10 µm in length **Figure 3-13 F**. These structures were densely packed with individual nanofibres, which could be visualized even at 1,800x

magnifications on a TEM. These higher order structures of protein nanofibres observed on multiple TEM grids were prepared using the same sample but with different batches of protein.

It is clear that as the temperature increased to 80^{o}C and above, larger bundles and longer structures of nanofibres can be manufactured. The optimal temperature was set at 80^{o}C as it was sufficient to yield high quality nanofibres. Additionally, due to safety reasons, operating TFE at high temperature (TFE boiling point is 78.5^{o}C) was not advisable. Temperatures above 80^{o}C with 100% TFE would not be possible. However, because only 10% v/v of TFE was prepared and used during the heating process, therefore, the actual boiling point of the 10% TFE was increased as it was prepared with distilled water.

3.3.4 The effect of different heat incubation interval [X_4]

In order to minimise the energy required for a large scale process, different heating incubation times were explored to determine the optimal heating time needed on nanofibres formation. In addition, it was also critical to provide sufficient heating time for all the proteins to be refolded and transformed into β-sheet conformers. Different heat incubation periods were investigated: 0, 6, 12, 24, 36 and 48 hours.

TEM images of different heat incubation time at low magnifications (14,000x)

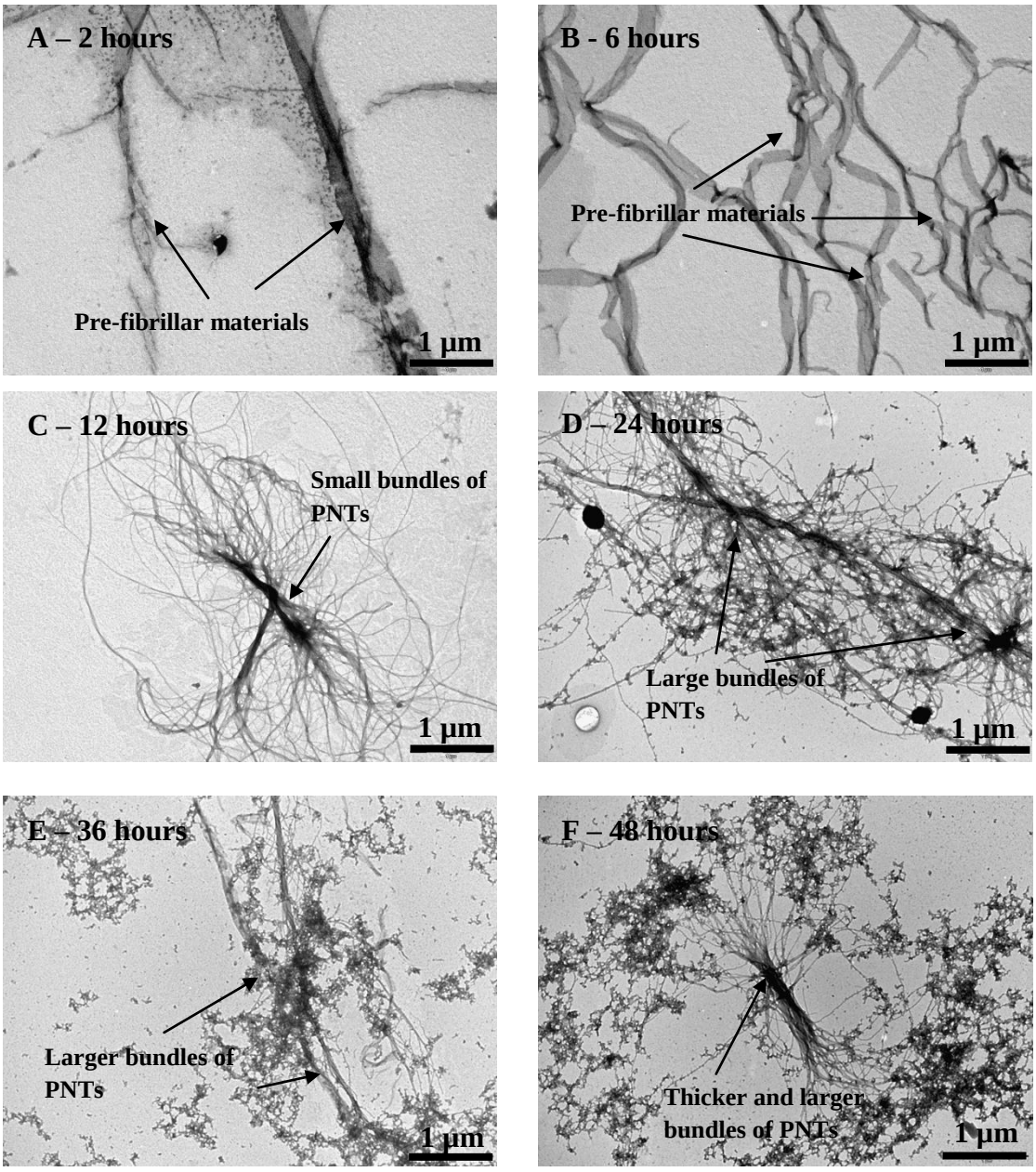

Figure 3-14: TEM images showing the effect of different heat incubation time on protein nanofibres formation.

Based on **Figure 3-14**, sufficient heating time was critical for the formation of protein nanofibres. Elevated temperatures (and the presence of TFE) served to disrupt the bonding interactions of the native proteins and assist with the reconstruction of peptides into nanofibres structures under favourable conditions. The minimum heating time to yield

protein nanofibres was at least 12 hours **Figure 3-14 C** and any heating time less than 12 hours (i.e. 2 and 6 hours) yielded ribbon-like structures **Figure 3-14 A, B.** As the heating time increased to 24, 36 and 48 hours, bundles of protein nanofibres were easily observed under the TEM **Figure 3-14 D, E, F**. The experiment was repeated multiple times and the results confirmed that there were no differences between 24 hours to 48 hours. Based on this finding, the optimal heating time was optimized at 24 hours as it was sufficient to yield the highest quality of nanofibres and heating times greater than 24 hours can be costly when the volume is scaled-up.

3.3.5 The effect of different storage time at room temperature on protein nanofibres self-assembly process [X_5]

In this section, different times intervals of storage at room temperature was explored to determine the optimal duration for protein nanofibres to self-assemble. Different time intervals ranging from 0 hour to 5 months were investigated to determine which of the storage times was sufficient for the self-assembly process to yield the highest quality of nanofibres.

TEM images of different room temperature storage intervals at low and high magnifications (14,000x and 89,000x respectively)

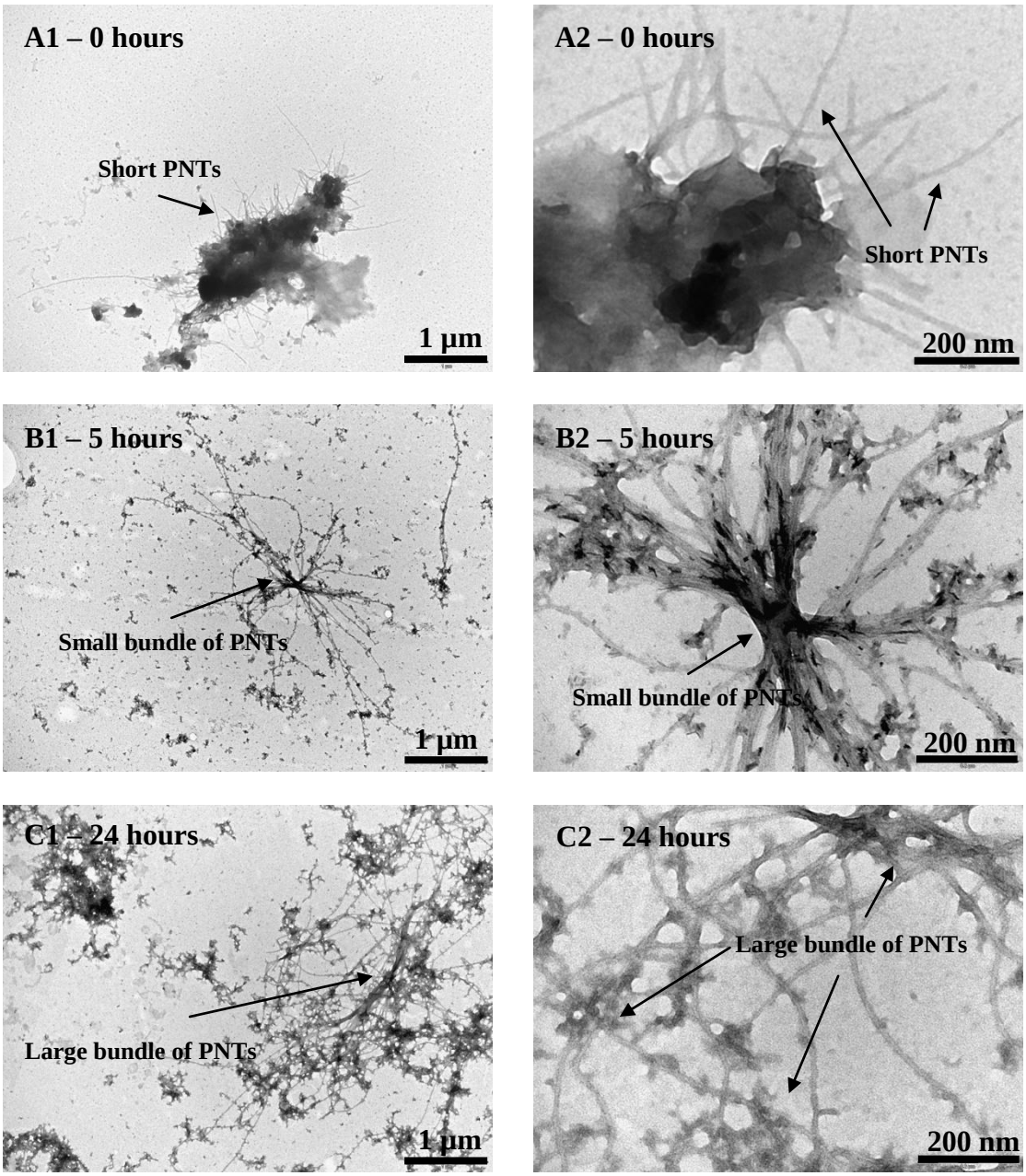

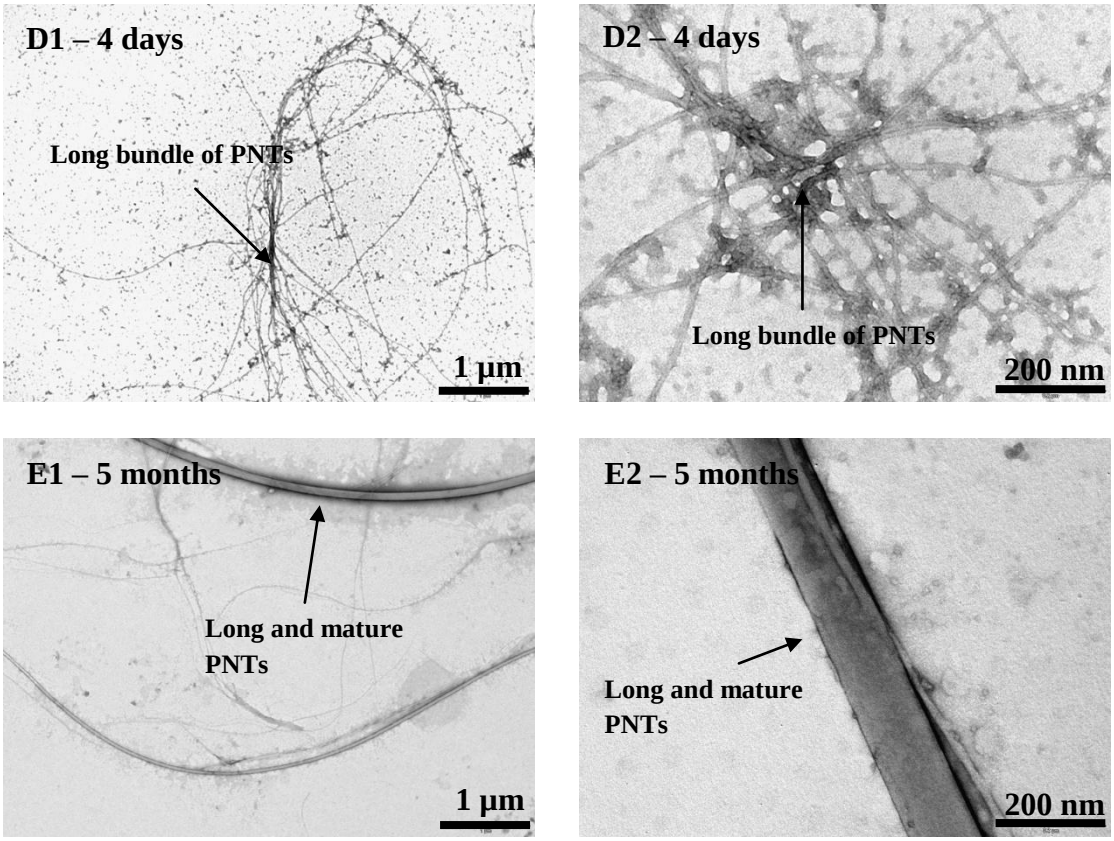

Figure 3-15: TEM showing the effect of different bench storage interval on nanofibres formation.

Based on **Figure 3-15**, it was clear that with no storage at room temperature (i.e. 0 hours), protein nanofibres do not have the sufficient time to assemble and only short nanofibres with an average of 0.5 µm in length were observed **Figure 3-15 A**. However, after 5 hours of storage time longer nanofibres with an average of 4 to 5 µm in length were observed **Figure 3-15 B**. As the interval time increased further to 24 hours, nanofibres longer than 8 µm were observed **Figure 3-15 C**. Similar results were observed after 4 days and in addition, multiple long nanofibres started to twist around each other to form bigger bundles of intertwining nanofibres **Figure 3-15 D**. Finally, after 5 months, mature nanofibres were found with a length of 20 µm and diameter 150 to 200 nm (**Figure 3-15 E**). Thus, for various desired product specifications, different sizes of nanofibres can be manufactured using duration of

storage at room temperature. In this case, 24 hours of storage is sufficient to yield high quality protein nanofibres around 8 µm in length and approximately 0.02 µm in diameter.

3.3.6 Waste from protein nanofibres synthesis

It was observed that the amorphous aggregates formed instantly when the protein solution (10 mg/mL) was added to pre-heated TFE at 80^{o}C. After 24 hours of heat incubation at 80^{o}C in the heating block, the solutions were centrifuged at 12,000 rpm at 18^{o}C for one minute to remove the aggregates (or waste) formed during the process. Protein nanofibres can be found very easily in the clear supernatant solution but not in the amorphous aggregate fraction. The aggregates were dissolved with 1 M NaOH to re-suspend the centrifuged pellets back into the solution and TEM grids were prepared to check for protein nanofibres.

TEM images of the waste generated from the process at low and high magnifications (14,000x and 89,000x respectively)

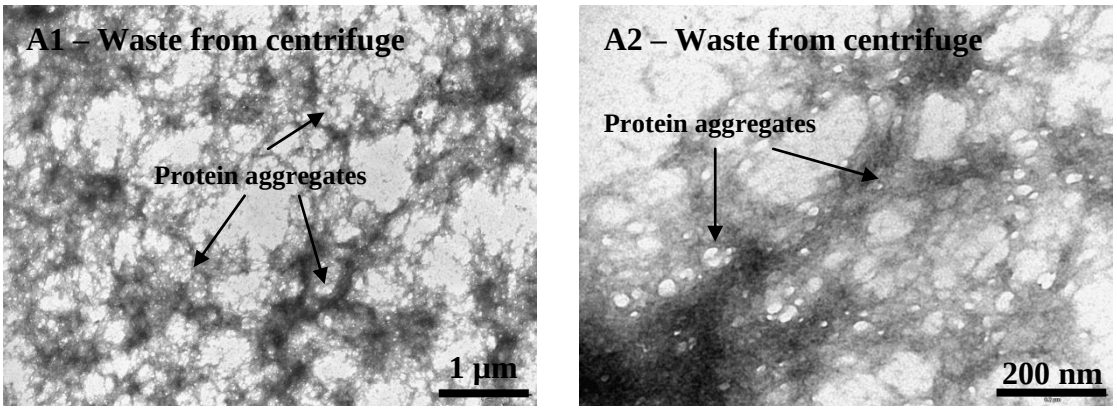

Figure 3-16: TEM images showing the results of the protein aggregates (waste) dissolved in 1M NaOH.

At low magnifications (14,000x), appeared that there were some fibril-like structures of nanofibres present in the resuspended pellet, based on **Figure 3-16 A1**. However, at high

magnifications, it was confirmed that there were no nanofibres or fibril-like structures found under the TEM **Figure 3-16 A2**. This suggested that the centrifugation step harvested the amorphous aggregates and left the nanofibres in the solution.

3.4 The Scale-up

3.4.1 Trial #1 - 5 L volume scale-up

In summary, all five variables were optimized to yield the highest quality of protein nanofibres and the results are tabulated in **Table 6**. The next phase of the objective was to perform scale-up for mass production. The target scale-up volume is from 1.0 mL to 1 L.

Table 6: Optimized variables for protein nanofibres synthesis.

Variables	Objective	Optimized
x_1	Different pH levels of TFE	3.8
	Different starting protein concentration	10 mg/ml
x_2	Different percentage v/v of TFE	10%
x_3	Temperature for incubation	80^{o}C
x_4	Incubation interval	24 hours
x_5	Room temperature storage interval	24 hours

The first scale up trial was performed in 5 L volume using all the optimised variables found from bench scale (i.e. 1 mL) **Table 6**. At small scale, the fish lenses were extracted using IKA® ULTRA TURRAX® tube disperser; however, due to its volume limitation (maximum capacity of 30 mL) a Silverson L4RT machine was used for the homogenization during scale-up. The Silverson L4RT has a range of volume capacity from 1 mL up to 12 L. The speed of the motor can be controlled with an infinitely variable electronic speed control with an integral on/off switch. The speed range of the motor can be tuned from as low as 50 rpm and up to a maximum of 8000 rpm.

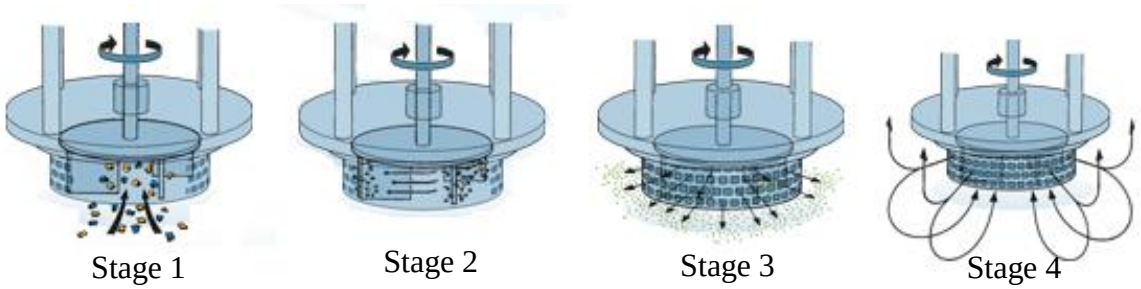

Figure 3-17: A schematic showing different stages of the Silverson L4RT mixing.

At stage 1, the rotor blades create a powerful suction by drawing liquid from the bottom of the vessel upwards into the centre of the working head. At stage 2, the rotor blades and the inner wall of the stator creates a milling action within the work head. At stage 3, this creates an intense hydraulic shear as the materials are forced at high velocity suction and out through the perforations in the stator. Finally at stage 4, fresh materials are continually drawn into the work head from the bottom of the vessel maintaining the mixing cycle throughout the main body of the mix. The shearing and mixing of water at different rpm is illustrated in **Figure 3-18**.

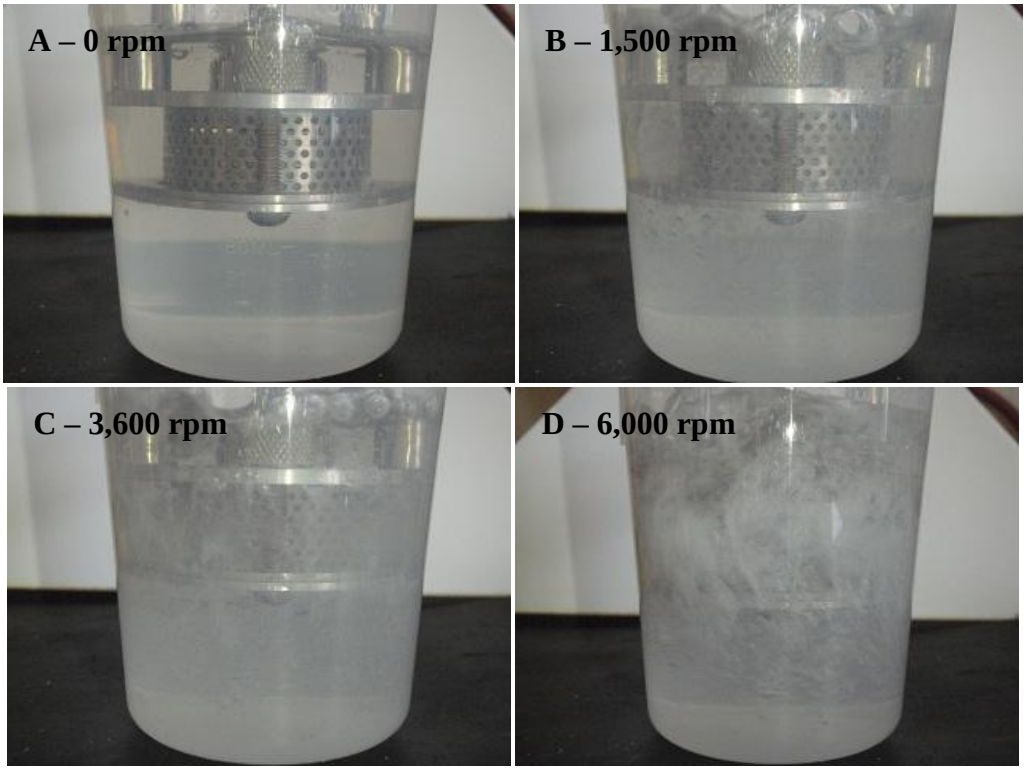

Figure 3-18: Different rotor speed setting tested with water to illustrate the shearing and mixing.

Trial and error was used to determine the optimal rpm setting for the large scale fish lenses extraction. It was very important not to over shear the proteins solution to avoid heating the solution. The optimal shearing rpm was determined by measuring the temperature using a thermometer while shearing the fish lenses and maintaining the temperature at 0^{o}C in an ice bucket. The duration of shearing was determined as when all the fish lenses were sheared thoroughly until the solid lens inside the fish lens were observed **Figure 3-20**. Before the extraction process took place, the work head was rinsed with ethanol to sterilize and kill bacteria, followed by rinsing with distilled water at 3,600 rpm for 5 minutes. The total number of fish lenses needed for the 5 L scale-up was pre-calculated and the detailed calculations can be found in Appendix A2.

Based on the pre-calculations in Appendix A2, at least 176 of DSP lenses were required for 5 L scale-up. To include the uncertainties and the accuracy of the results, a total of 200 fish lenses were used for the scale-up experiments. All the lenses were thawed and kept in a 400 mL plastic container before the extraction process.

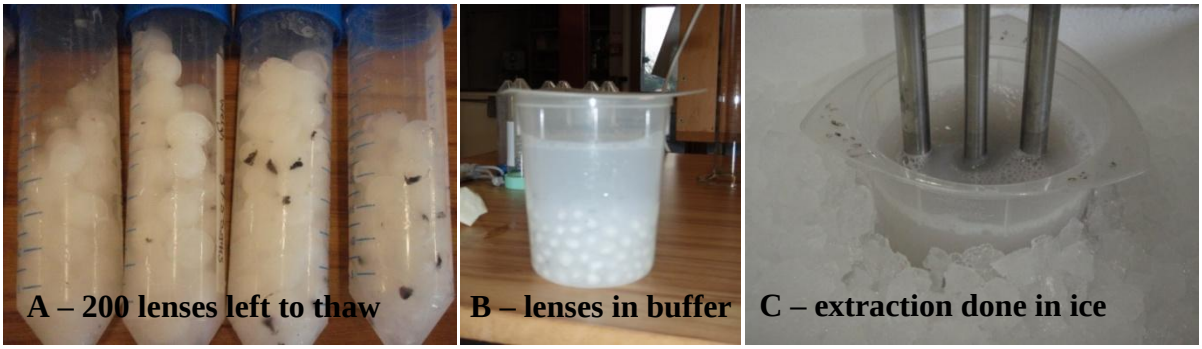

Figure 3-19: 200 DSP lenses extraction using Silverson.

A: Thawing 200 fish lenses for the 5 L scale-up, B: Thawed fish lenses mixed with the extraction buffer ready for the protein extraction process and C: Extraction of the fish lenses inside an ice bucket using Silverson.

During the extraction process, the temperature of the liquid was gradually heated due to the high shear mixing inside the work head at 3,600 rpm. An ice bucket was used to keep the extracted solution cool for the entire extraction process to prevent proteins denaturing before the process started. The rotor speed was set at 3,600 rpm and left for 25 minutes on ice **Figure 3-19 C**. Once the extraction process was completed, the extracted protein solution was transferred into centrifuge tubes for centrifugation. The protein solution was centrifuged in a Sorvall PC 6 PLUS Superspeed Centrifuge at 18^{o}C, 12,000 rpm for 30 minutes. The final recorded volume from the extraction process was approximately 200 mL.

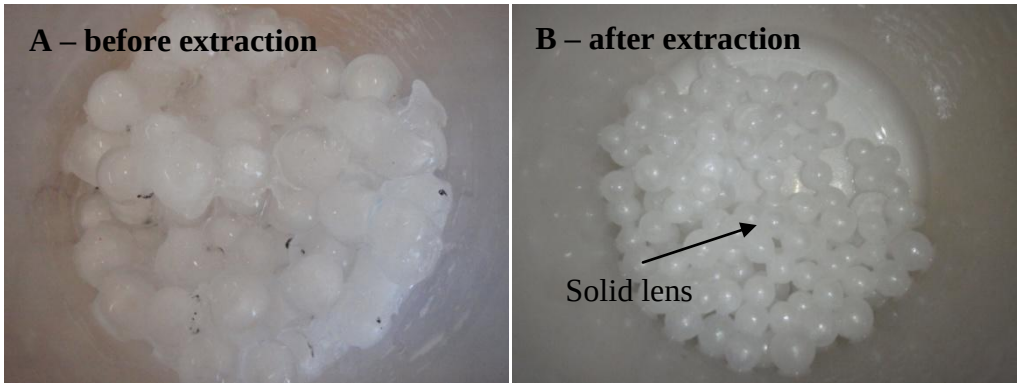

Figure 3-20: Before and after extraction of DSP fish lenses.

A: Before the extraction using Silverson and B: after the extraction using Silverson.

The protein concentration was recorded at 300 mg/mL using the Nanodrop measurement, therefore, for a 5 L volume, a total of 166.7 mL extracted protein solution was required to prepare 10 mg/mL of protein solution for the scale-up volume. 10% TFE v/v at pH 3.8 was prepared in five 1 L Schott bottles and pre-heated in the LabServ oven at 80^{o}C for at least 2 to 3 hours to reach the target temperature of 80^{o}C.

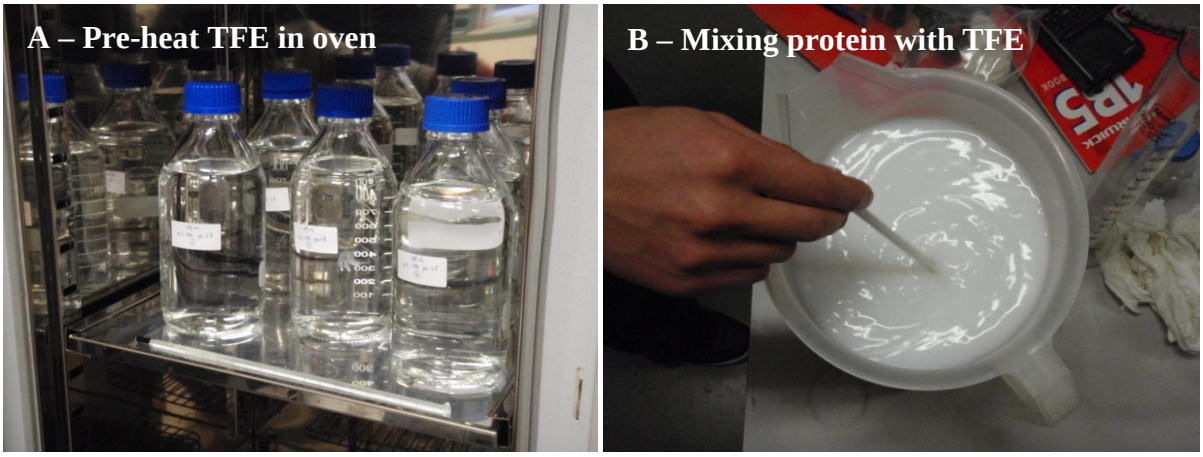

Figure 3-21: 5 l scale-up preparations.

A: Pre-heat the TFE solution inside the oven to 80^{o}C before mix with the protein solutions and B: Mixing the protein solution with the 80^{o}C TFE.

The temperature of TFE was checked using a thermometer and once the target temperature was reached, the pre-heated TFE solutions were pooled into a 5 L polypropylene measuring jug. 166.7 mL of protein solution was measured using a measuring cylinder and poured slowly into the 5 L jug with TFE and stirred for consistent mixing. It was observed the mixed solution (protein solution and TFE) turned milky in colour and the final temperature after mixing was recorded at 75^{o}C. The solution was then put back into the 80^{o}C oven for 24 hours of heat incubation. After 24 hours of 80^{o}C heat incubation in the oven, the milky solution was transferred for centrifugation. Due to the limitation of the centrifuge volume (max volume is 120 mL), the 5 L solution were separated into six equal volumes and spun at 18^{o}C, 10,000 rpm for 5 minutes. After centrifugation, the supernatants were pooled into the 5 L polypropylene jug and left on the bench for 24 hours to promote the self assembly process. In addition, two control samples of 1 mL volume were placed inside the oven and in the heat block for comparison.

TEM images of 5 L scale-up and controls at low and high magnifications (14,000x and 89,000x respectively)

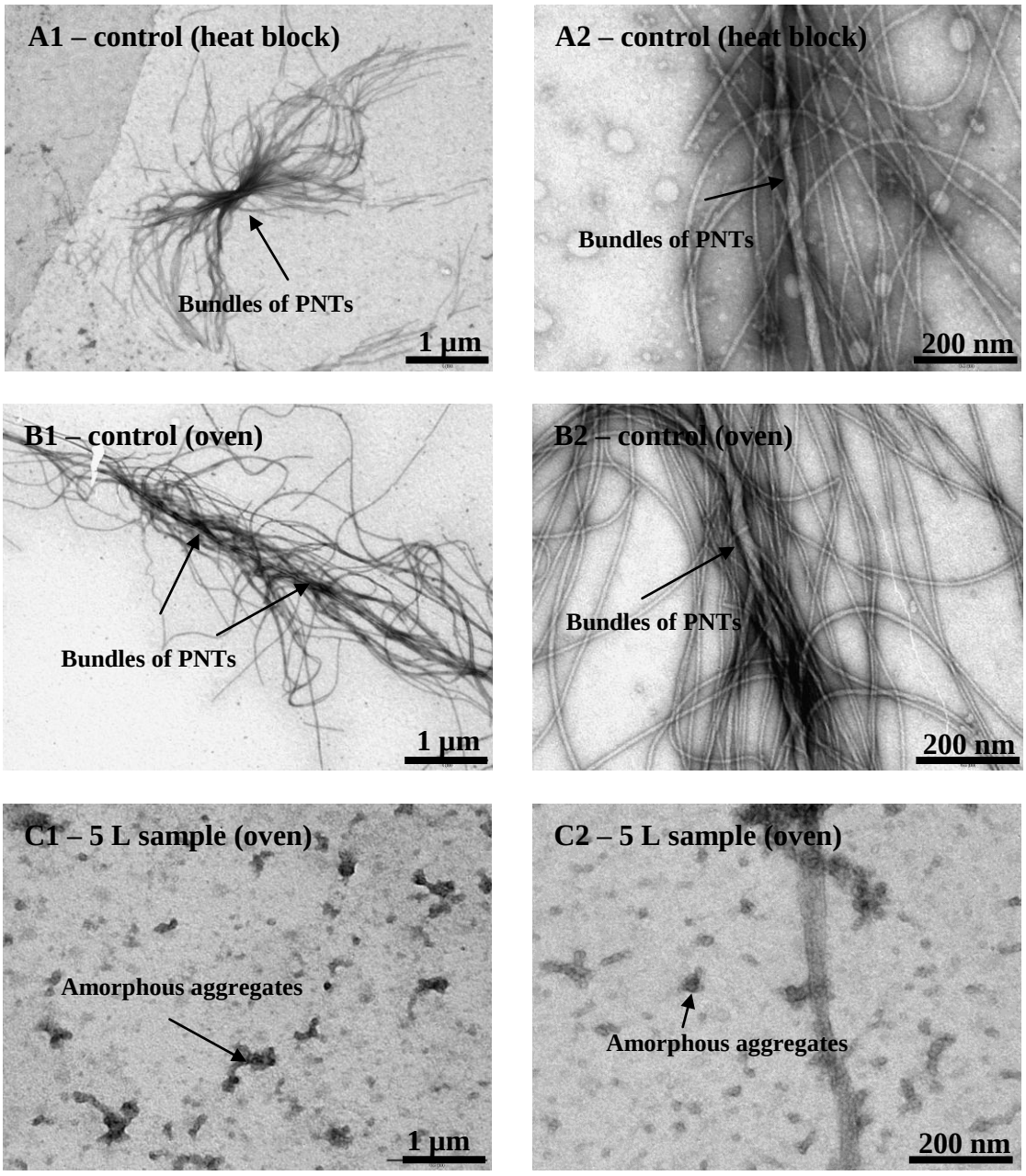

Figure 3-22: TEM images showing the results for 5 l scale-up and two controls for heat block and oven.

Based on the results from 5 L scale-up above, the majority on the TEM grids were protein aggregates, pre-fibrillar materials and no protein nanofibres were found **Figure 3-22 C2**. However, in both the control samples of 1 mL volume incubated in the heat block and in the

oven, protein nanofibres were found **Figure 3-22 A2, B2**. Multiple TEM grids were prepared and the results confirmed that the 5 L scale up volume failed to produce protein nanofibres. The suspected reason why the 5 L scale-up failed to yield protein nanofibres and only found in the 1 mL control samples was because of the poor sealing of the polypropylene measuring jug. The result of poor sealing could lead to TFE evaporation during pre-heating inside the oven, which may influence the solvent effect on protein nanofibres formation.

3.4.2 Trial #2 - Different containers

Trial #2 was set up to test different volume containers and the containers, made of polypropylene materials were 10, 40, 100, 200 mL, and 1 L volume. These different volume containers had excellent sealing and could prevent TFE evaporation during the pre-heating process in the oven.

TEM images of different volume containers and controls at high magnifications (89,000x)

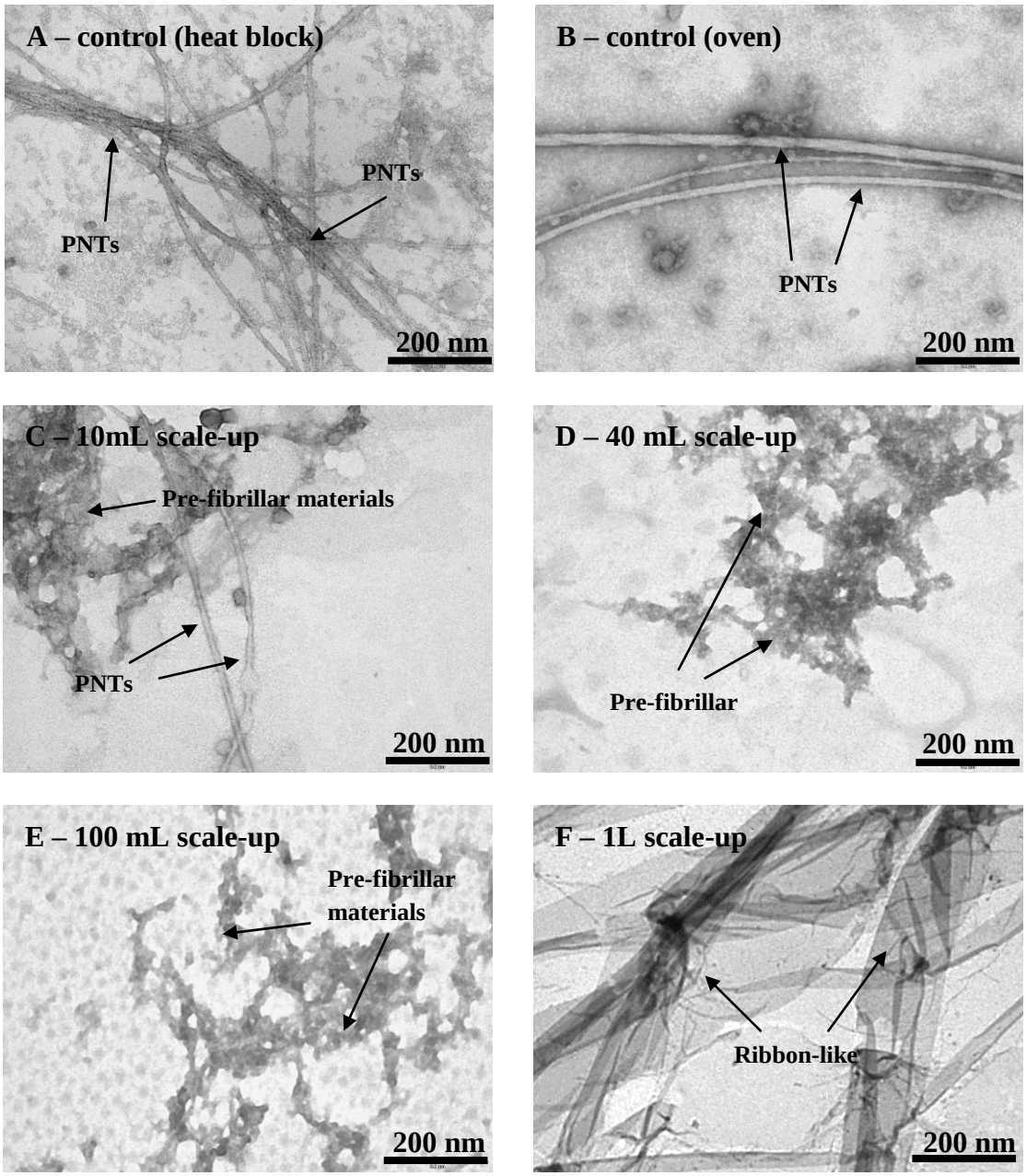

Figure 3-23: TEM images showing protein nanofibres for different volume scale-up.

Based on the results for using different scale-up volume containers, protein nanofibres were found only in both the control samples (heat block and oven heating) and only minor nanofibres were found in the 40 mL volume **Figure 3-23 A, B, C**. As the scale-up volume increased further to 100 mL and 1 L, virtually no protein nanofibres were found in these volumes. The majority of material found under the TEM was amorphous aggregate and pre-

fibrillar structures **Figure 3-12 D, E, F**. Based on these results, a number of observations were made and it was concluded that as the scale-up volume increased from 1 mL (control) to 1 L, the formation of protein nanofibres becomes progressively more difficult. As the scale-up volume increased to 40 mL and above, no protein nanofibres were observed under the TEM.

3.4.3 Trial #3 - Internal surface area

TFE evaporation was not the primary issue for lack of protein nanofibres formation, based on the results obtained from trial #2. Evaporation of TFE could be a secondary issue but this was not tested. It was hypothesised that internal surface area was key to promote the self assembly process produce protein nanofibres. Dr Kevin Sutton from Plant and Food Research Institute suggested that different containers have different internal surface areas and this may impact on the yield of protein nanofibres produced for large volumes. Based on this suggestion, the internal surface areas (ISA) for all the different volume containers were calculated and compared. The internal diameter and height of different containers/tubes were measured, and the internal surface area was calculated based on the height when filled with the particular volume. The 1.5, 10 and 40 mL tubes were simplified as cylinders although these tubes have a conical bottom. The ratios of internal surface area over volume were calculated and tabulated in the table below.

Table 7: The ratio of internal surface area to volume for all the different volume scale-up.

Sample	Ratio ISA/V	Fold
1 ml	5.82	1.0
10 ml	2.16	2.7
40 ml	1.52	3.8
100 ml	0.6	9.7
200 ml	0.49	11.9
1000 ml (1L)	0.36	16.2

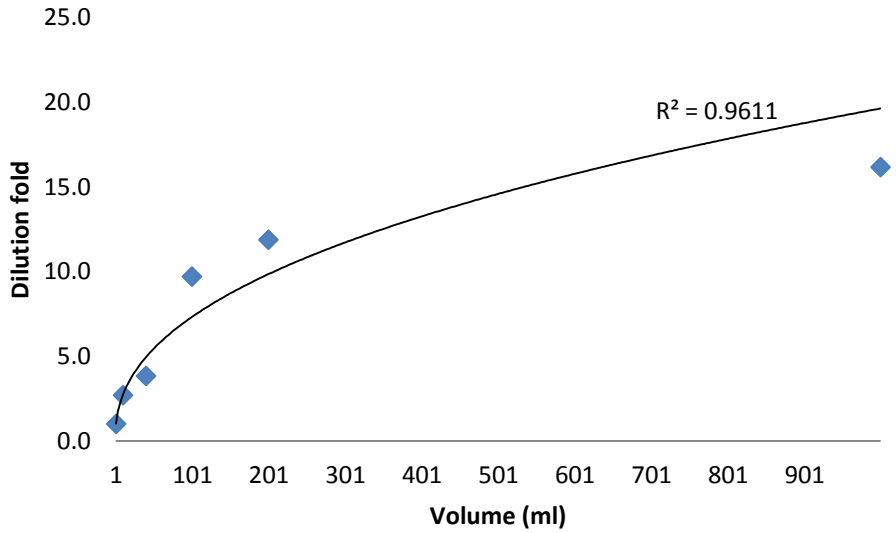

Figure 3-24: Fold reduction in ISA for different scale-up volume.

Based on the table above, clearly the ratio between the ISA and the volume were significantly different as the scale-up volume increases. In comparison, as the volume increased from 1 to 40 mL, the original ISA for 1 mL volume was reduced by nearly 4 times. As the volume of the containers increased further to 1,000 mL, the total ISA was reduced 16 times and this relationship follows a power law relationship **Figure 3-24**. This finding, may explain why a few protein nanofibres can be found in 10 mL volume and even some in 40 mL but none at larger volumes (i.e. 100 mL and more) because the relationship follows a mathematical

equation $y = x^k$, where k is a scaling exponent. The equation for the power law relationship is defined as

$$y = x^{0.47}$$

Because there are significant differences in the ratio of ISA to volume for large volumes, trial #3 was to determine if the ISA of the tube create any impact on protein nanofibres formation. In this section, 40 1 mL Eppendorf tubes were prepared for the experiment **Figure 3-25 A**, Duplicates of 40 mL Falcon tubes with 40 mL solution **Figure 3-25 B** and quadruplicate 1 mL controls **Figure 3-25 C** were prepared to confirm the effect of ISA for these different volumes. After the protein nanofibres synthesis process, the solution from 40 of 1 mL Eppendorf tubes were pooled into one 40 mL Falcon tube and TEM grids were prepared to check for nanofibres. In addition, the 40 mL Falcon tube and the 1 mL control sample were also analyzed under the TEM. The set up of the experiment is shown in **Figure 3-25**.

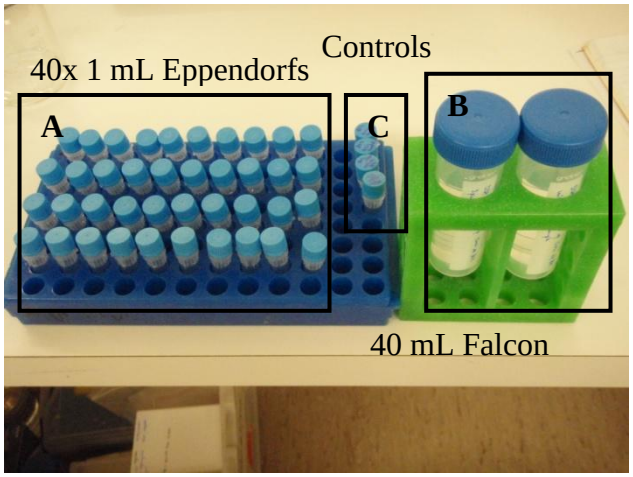

Figure 3-25: Procedure for testing effect of internal surface area on the protein nanofibres formation for larger volumes.

A: The 40 samples (total volume of 40 mL if pooled together), B: 40 mL volume in one Falcon tube and C: 1 mL control samples.

TEM images of 40 mL volume pooled scale-up with ISA at low and high magnifications (14,000x and 89,000x respectively)

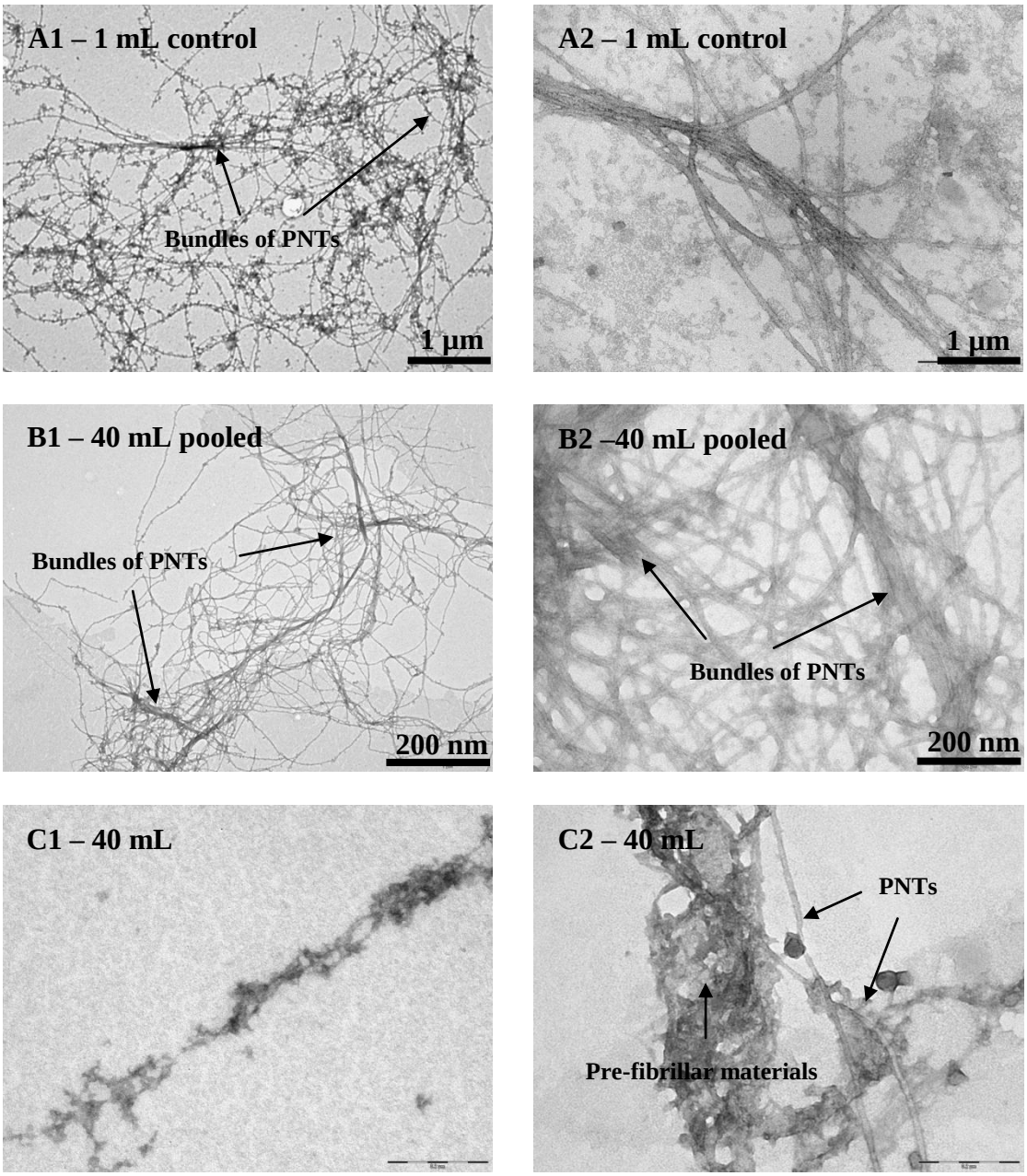

Figure 3-26: The impact of internal surface area on protein nanofibres formation.

Based on **Figure 3-26 A1, A2**, protein nanofibres can be found relatively easy in the control samples. Furthermore, protein nanofibres were also found relatively easily in the pooled solution from 40 x 1 mL Eppendorf tubes **Figure 3-26 B1, B2**. However, in the 40 mL

volume there were only a few protein nanofibres found and the majority were protein aggregates or pre-fibrillar materials **Figure 3-26 C1, C2**. Based on this finding, internal surface area is a key component for large volume scale-up and is critical to yield protein nanofibres.

Previous research indicates that there is likelihood for these protein nanofibres to form under these conditions (Sluzky *et al.*, 1991). However, it is reasonable to say that the ISA within the tube in which the nanofibres form has a large part to play in its production. This may be due to nanofibres needing some kind of hydrophobic scaffolding to form the oligomers, which are the starting point for the protein nanofibre. In the same research, scientists used UV absorption spectroscopy and quasi-elastic light scattering to look at the development of the structure of insulin aggregates in the presence of hydrophobic surfaces. It was clear that the aggregates formed in the presence of polytetrafluoroethylene (PTFE) surfaces were found to be larger than those found in the solutions without any surface. It also shows that the rate of aggregation can be increased by increasing the surface area of the chemically inert PTFE in contact with the solution. These studies provide strong evidence that ISA is important in controlling both the rates and extent of unfolding and aggregation in protein nanofibres formation.

3.4.3.1 Trial #4 - 100 mL volume with ISA scale-up

Trial #4 was to scale-up the volume to 100 mL with ISA taken into account. The calculated ideal ISA for 1 mL is 5.46 cm^2, and the detailed calculations can be found in Appendix A3. Based on **Table 8**, the total ISA needed for 100 mL scale-up will be 546 cm^2 (5.46 × 100). The 1 mL Eppendorf tubes are made out of polypropylene, which appears to have an impact on protein nanofibres formation. Therefore, polypropylene materials were used for 100 mL

scale-up. It was calculated that approximately six 10 mL Falcon tubes were required to be cut into small pieces and packed into a 100 mL container to achieve a total ISA of 546 cm^2. These small pellets were cut with the same individual dimensions **Figure 3-27**. The surface areas for the cut edges were neglected and only those surface areas for the outside and inside were used for calculation.

Table 8: Internal surface area required for scale-up volume.

Sample	ISA (cm^2)
1 ml	5.46
10 ml	54.6
100 ml	546
500 ml	2730
1000 ml (1L)	5460

Figure 3-27: 15 mL Falcon tube fabricated into smaller pieces as pellets to increase the ISA for large volume production.

TEM images of 100 mL volume scale-up with ISA at low and high magnifications (14,000x and 89,000x respectively)

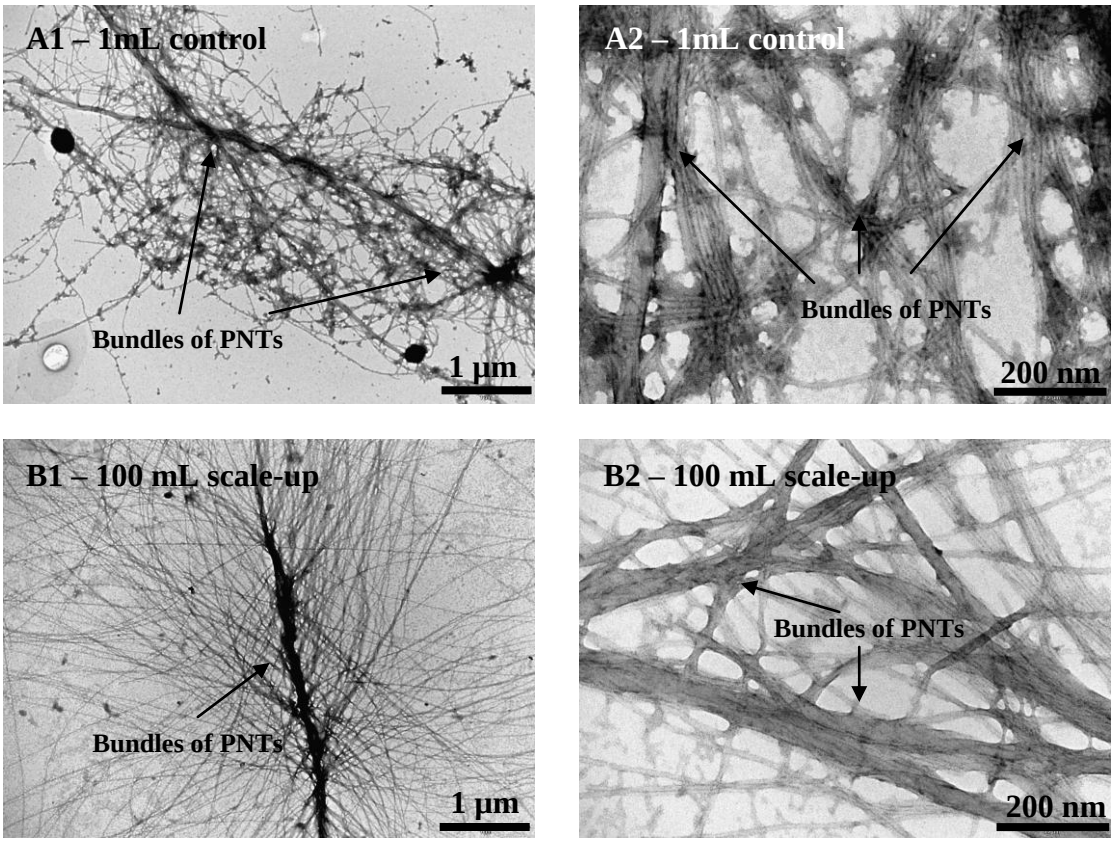

Figure 3-28: Scale-up of 100 mL volume with ISA using polypropylene pellets.

Based on **Figure 3-28**, by taking the internal surface area into consideration for the scale-up, the formation of protein nanofibres was successful in 100 mL volume. In addition, bundles of protein nanofibres were observed in both the control samples (1 mL) and 100 mL volume scale-up. Additionally, protein nanofibres have been confirmed to stick to the surface of polypropylene pellets under the SEM. The SEM images show a blank polypropylene pellets where a rough surface was observed **Figure 3-29 A**. Another SEM analysis was performed on the polypropylene pellets after a scale-up experiment, where bundles of protein nanofibres were found attached to the surface of the pellets **Figure 3-29 B**. It is become clear that ISA is a key factor that plays an important role for protein nanofibres formation for large volume production.

SEM images of a blank polypropylene pellets and a used polypropylene pellets at 1,300x and 10,000 magnifications respectively

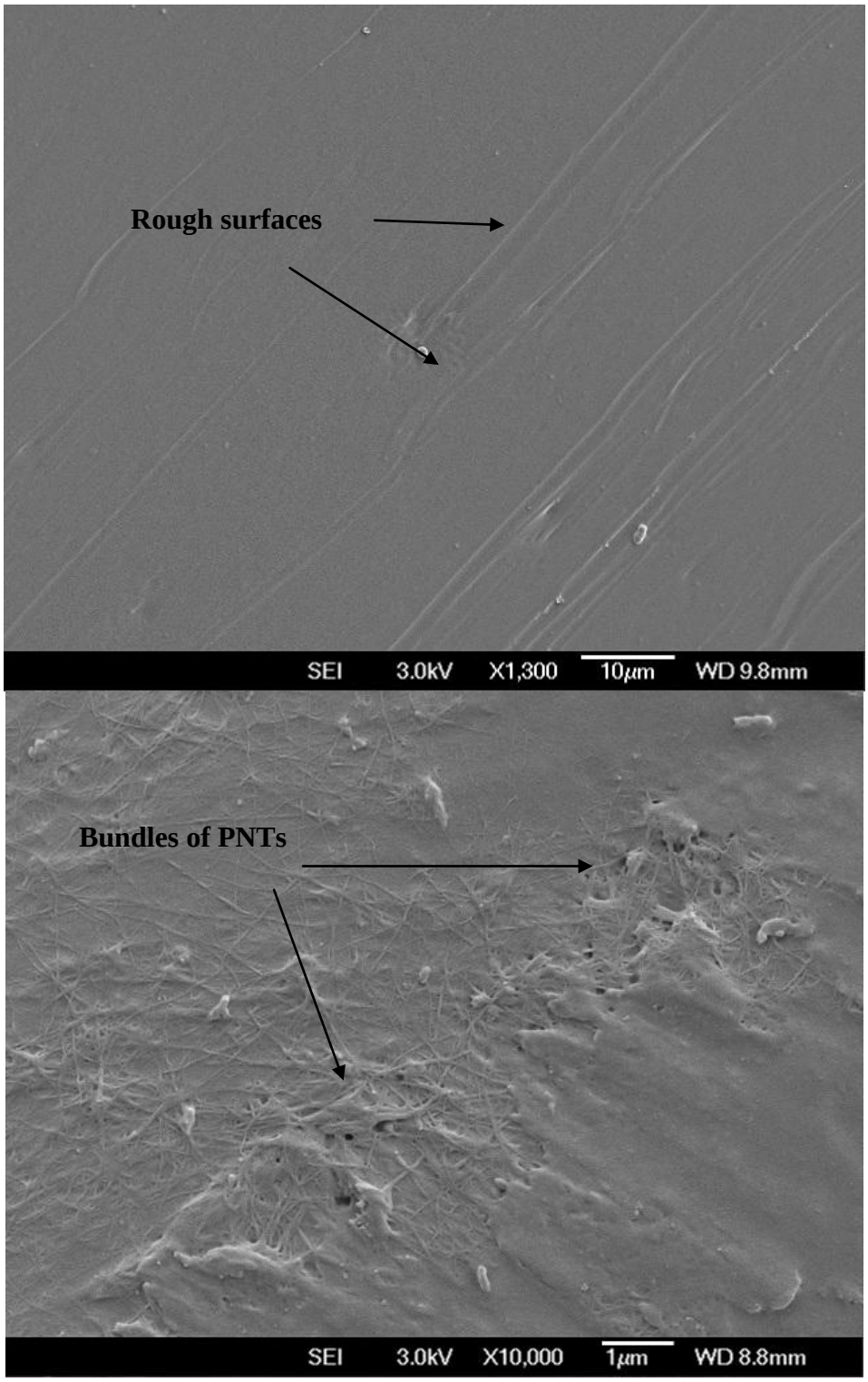

Figure 3-29: SEM images showing a blank polypropylene pellets (A) and a polypropylene pellet with PNTs stick on surface (B).

These SEM images were performed by Clement Roux.

3.4.3.2 Trial #5 - 500 mL volume with ISA scale-up

With the successful results from the 100 mL scale-up volume with ISA taken into account, the aim for trial #5 was to scale-up the volume further to 500 mL. The calculated ISA required for 500 mL scale up volume is 2,730 cm^2. The polypropylene pieces were cut in the mechanical workshop, where each individual piece was cut into the same dimension, trimmed and cleaned with ethanol before used in the scale-up experiment.

TEM images of 500 mL volume scale-up with ISA at low and high magnifications (14,000x and 89,000x respectively)

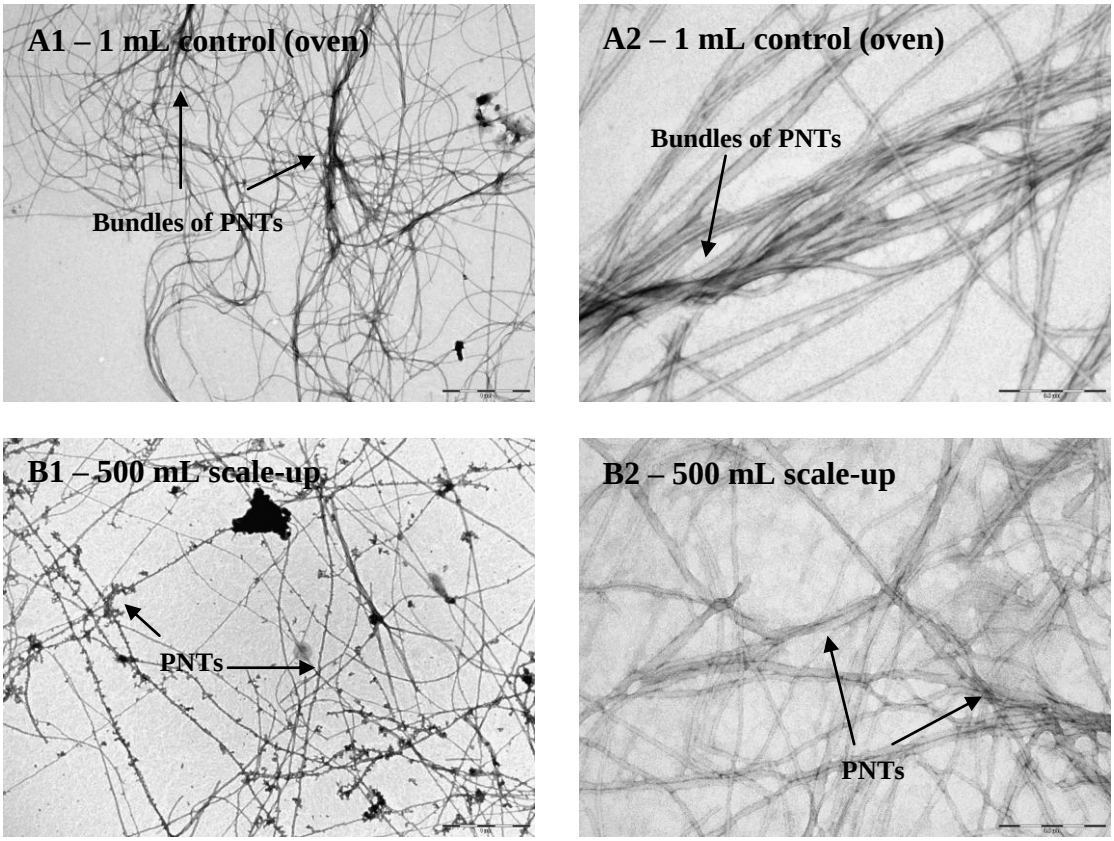

Figure 3-30: Scale-up of 500 mL volume with ISA.

Based on **Figure 3-30**, the formation of protein nanofibres was found in both the control samples and the 500 mL volume. The same results were observed with the repeated TEM

grids prepared using the same sample. Based on the results, it was concluded that the scale-up volume of 500 mL was successful.

3.4.3.3 Trial #6 - Polypropylene beads for ISA

Based on the last trial results (3, 4 and 5) of using ISA for scale-up, consuming more convenient form of high surface area polypropylene was sought. In this trial, small polypropylene beads were used to substitute for the cut polypropylene pieces for 10 mL volume **Figure 3-31**. The total ISA of the polypropylene beads required for 10 mL volume was calculated and matched with the exact ISA that was tabulated in **Table 8**. The ISA calculations of the polypropylene beads are shown in the section below.

Figure 3-31: Polypropylene beads used to substitute the pellets for convenience for larger scale-up volume.

A total of 3.8 g of polypropylene beads were used to match the required ISA needed for 10 mL volume scale-up. Detailed calculations for polypropylene beads' surface area can be found in Appendix A5. The original polypropylene pellets were used as a control and performed in 10 mL volume instead of 1 mL.

TEM images of 10 mL volume with polypropylene beads at low and high magnifications (14,000x and 89,000x respectively)

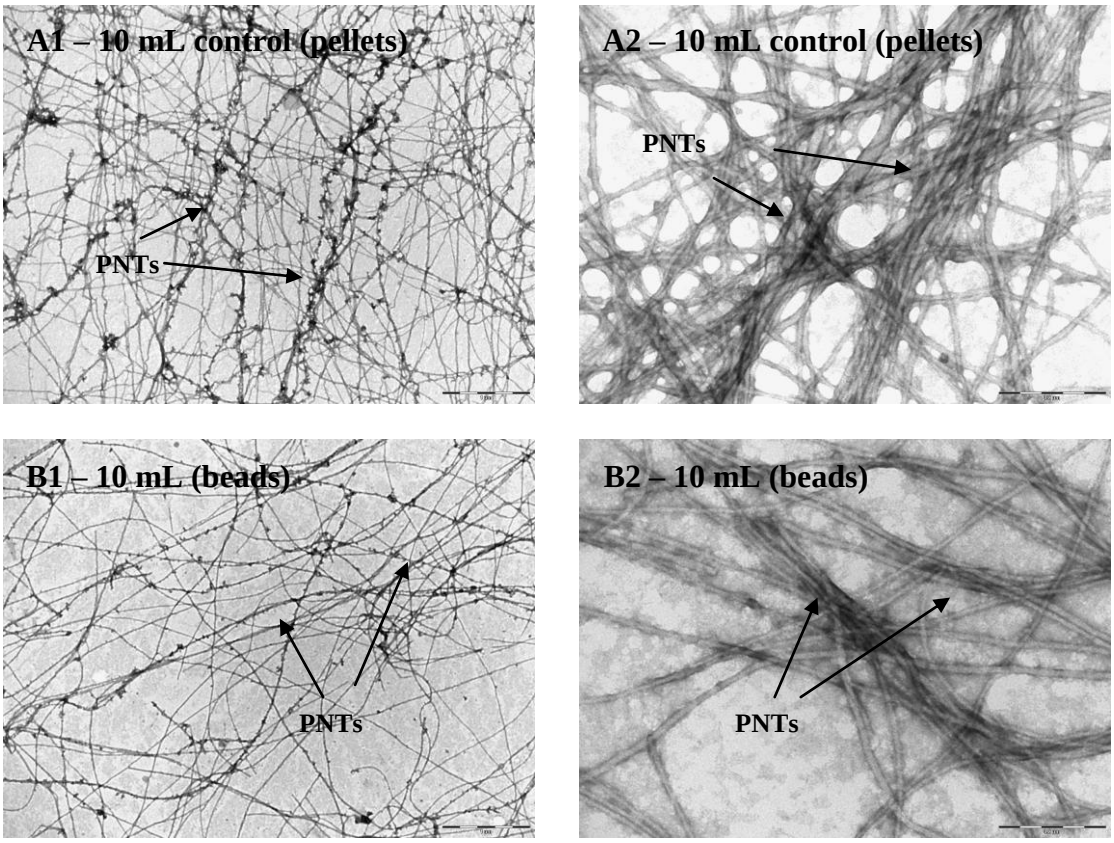

Figure 3-32: Comparison between polypropylene pellets and beads for 10 mL volume scale-up with ISA.

By replacing the ISA materials with polypropylene beads from polypropylene pieces, bundles of protein nanofibres were observed under the TEM for both control and the 10 mL volume **Figure 3-32 A2, B2**. The problem that was encountered in this trial was the submerging of all the beads into the solution to achieve the required ISA. It was found that not all the beads were submerged into the solution because the density of the beads was lighter than the solution. However, bundles of protein nanofibres can still be found under the TEM because the majority of the beads (approximately 75%) were submerged into the solution which contributes sufficient ISA for the scale-up volume. However, due to the submerging issue of

using polypropylene beads to contribute ISA, therefore, polypropylene pellets were used for the final 1 L volume scale-up.

3.4.3.4 Trial #7 - 1 L volume scale-up

The target scale-up volume for the thesis is 1 L. Polypropylene pellets were used instead of beads due to the problem with beads floating on the top of the solution. The scale-up process flow is illustrated in method Section 2.3.2.

TEM images of 1 L volume scale-up with ISA at low and high magnifications (14,000x and 89,000x respectively)

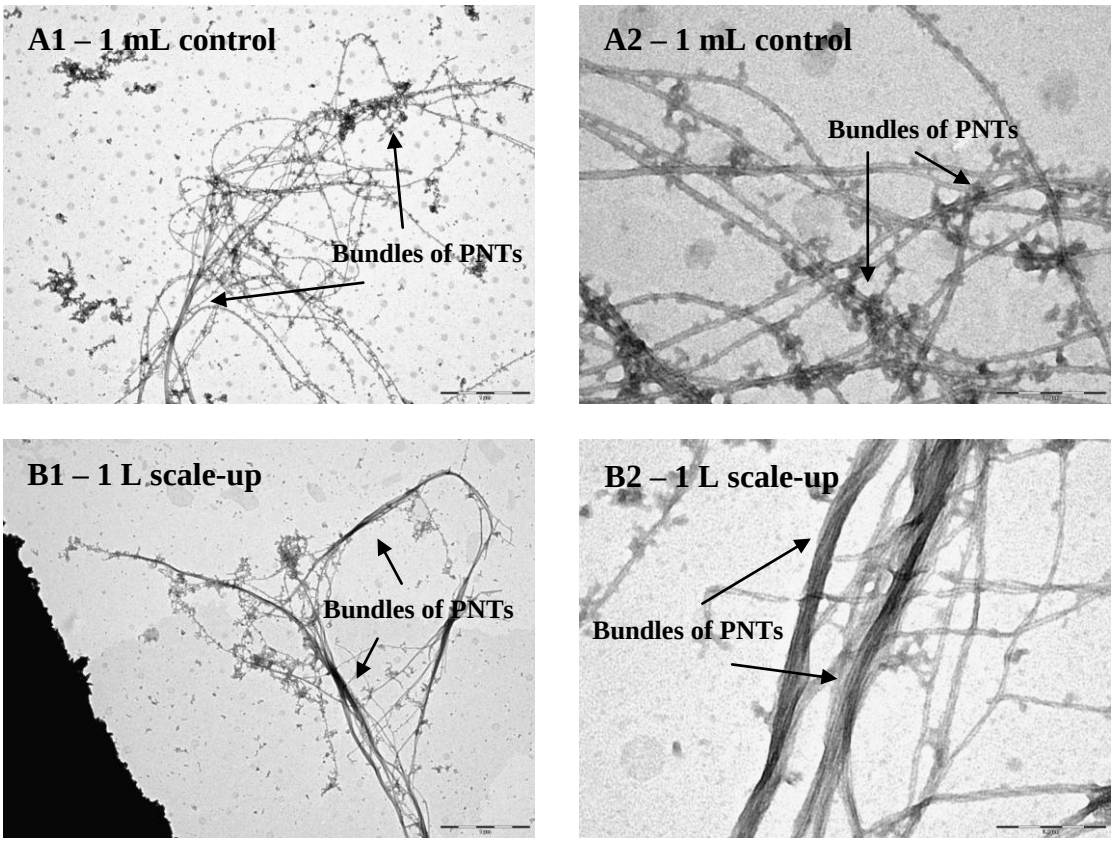

Figure 3-33: The scale-up volume of 1 L with ISA.

Based on the **Figure 3-33**, both the control samples (1 mL) and the 1 L scale-up volume yielded protein nanofibre bundles of high quality. The TEM grids were repeated and the results were confirmed. Thus it was concluded that the 1 L scale-up was successful.

3.4.4 Different types of fish lens combined

As the scale-up volume increases, large quantities of fish lenses would be required (i.e. 200 fish lenses for 1 L scale-up volume). Additionally, due to the unpredictable nature of the seafood industry, different species of fish may supplied throughout the year. It would be difficult to control and use the same species of fish lens for the raw material all the time. Hence, different types of fish lenses were combined, homogenised and used in the experiment to determine if the protein nanofibres can be manufactured using the same process. The combined fish lenses were barracuda, groper and deep sea perch, all classified as deep sea fish.

TEM images showing PNTs made from using mixed fish lenses at low and high magnifications (14,000x and 89,000x respectively)

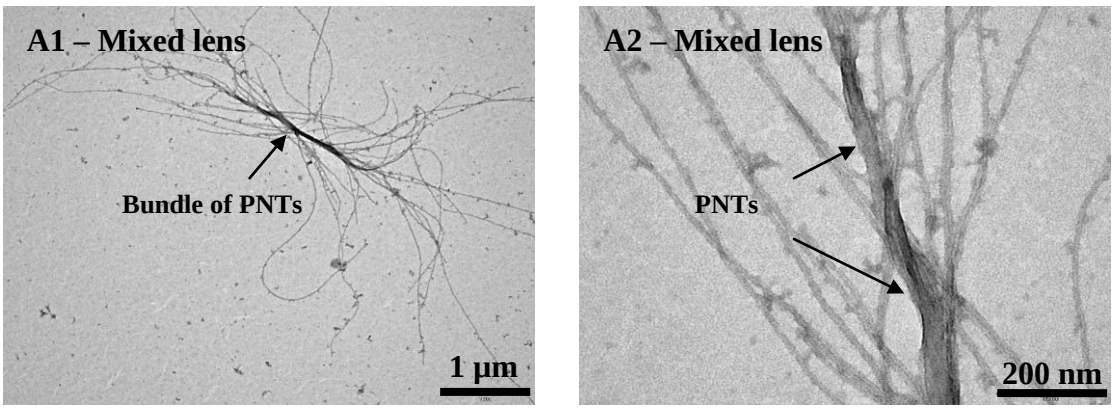

Figure 3-34: Three different types of fish lenses were homogenized and used for protein nanofibres synthesis.

Based on **Figure 3-34**, bundles of protein nanofibres can be manufactured regardless of which types of fish lenses were used as the starting material for the process. However, only the different types of fish from the deep sea zone were tested. Based on this finding, not only will this significantly reduce the preparation time before production but it also shows flexibility regarding raw materials selection from the seafood industry.

3.4.5 Scale-up cost

The ISA required for any scale-up volume can be calculated using $x = volume \times 5.46$. The volume has a unit of mL and the calculated value has a unit of cm^2, this value will determine the ISA needed for large volume scale-up. Large-scale process can be very different compared to the small-scale experiments carried out in the laboratory. Simple tasks such as buffer preparation, pH adjustment, sample application and the transfer of materials become complicated as well as time consuming and can have an impact on the process itself. The timeline required for batch production of 1 L was calculated to be 49.5 hours as illustrated in **Table 9**. The only difference between the small scale (i.e. 1 mL) and large scale (i.e. 1 L) is 1 hour, with manufacturing times of 48.5 and 49.5 hours respectively. However, the throughput is 1000 times more than the bench scale volume.

Table 9: Timeline of production for protein nanofibres for 1 L volume.

Task name	Duration	Timeline
	Hours	1 2 3 7 8 9 10 11 12 13 14 15 16 17 18 19 20 21 22 23 24 25 26 27 28 29 33 34 35 36 37 38 39 40 41 42 43 44 45 46 47 48 49 50
Fish lens extraction	1	
Pre-heating	0.25	
Heat incubation	24	
Centrifugation	0.25	
Storage	24	
Total	49.5	

The manufacturing cost was calculated with all the resources needed in the process of manufacture protein nanofibres. It was estimated that the manufacturing cost will be $0.28

per mL of the product and the yield is estimated to be 7% ~ 12%. This cost only includes the cost of manufacturing and does not include the capital cost (i.e. equipment). To date, there has been no current market value set for protein nanofibres.

Table 10: Production cost for 1 L volume.

Materials Cost	Quatity	Volume (ml)	Duration (hrs)	Cost	
Raw material (fish lenses)	26	-	-	$ -	
Extraction buffer	-	40	-	$ 20.00	
Polypropylene pieces	58	-	-	$ 40.60	
1 L volume polypropylene container	1	-	-	$ 60.00	
10% v/v TFE	-	100	-	$ 70.00	
Operating Cost					
Pre-heating	-	-	3	$ 0.18	
Heat incubation	-	-	24	$ 1.44	
Centrifugation	-	-	0.17	$ 0.017	
Bench storage	-	-	24	$ -	
Labour Cost					
Labour	6	-	-	$ 90.00	
Total				$282.24	(per litre)

3.4.6 Fragmenting the protein nanofibres

Fragmenting protein nanofibres is a process of breaking up the long protein nanofibres into shorter fragments. Examples of the applications were mentioned in Section 1.5 of using short fragments of nanofibres. Sonicating protein nanofibres into smaller fragments can also be used for seeding, as mentioned in Section 1.5.4. Some researchers have also suggested that by adding some of the fragmented nanofibres into a solution with protein nanofibres can enhance the speed of self-assembly process, which can significantly reduce the manufacturing time. Using the sonication method described in the Section 2.5, the experiment was conducted on samples contained high quality of protein nanofibres and TEM grids were prepared before and after the sonication process of the same sample.

TEM images showing PNTs before/after sonication at low and high magnifications (14,000x and 89,000x respectively)

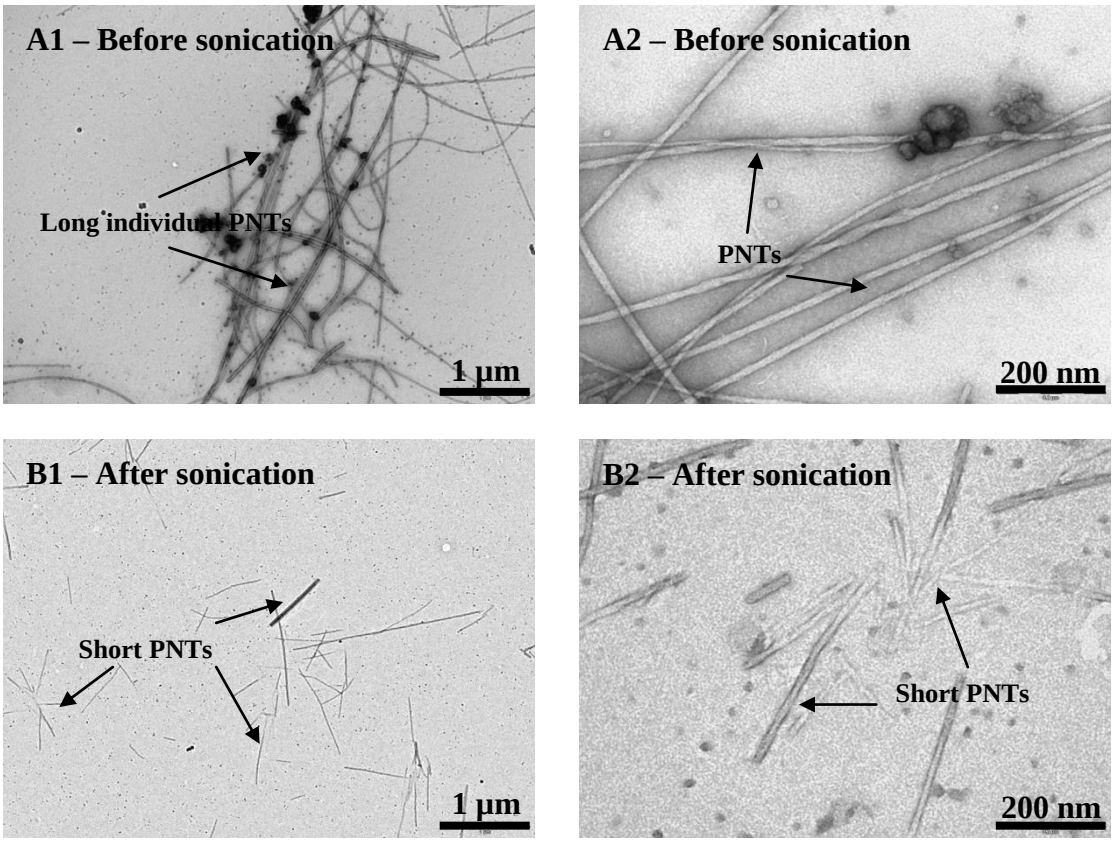

Figure 3-35: TEM images showing the effect of sonication on protein nanofibres.

After sonication, all the long protein nanofibres were broken into shorter fragments **Figure 3-35 A1, B1**. TEM images were prepared before the sonication and after the sonication process using the same sample for consistency. The lengths of the nanofibres were recorded before and after the sonication process, and the average length was calculated and the TEM images can be found in Appendix A4. The average length of the nanofibres before the sonication was recorded to be 4.2 µm, becoming 0.9 µm after sonication **Table 11**.

Table 11: Comparison before and after sonications of PNTs.

Samples	Before sonication (μm)	After sonication (μm)
1	4.0	1.5
2	3.5	1.0
3	5+	0.5
4	4.5	0.8
5	4.0	0.5
6	5+	1.0
7	4.5	1.0
8	5+	0.5
9	5+	2.0
10	4.5	0.5
Average	4.2	0.9

3.4.6.1 Seeding using fragmented nanofibres

The purpose of seeding is to reduce the manufacturing time for self-assembly of protein nanofibres as mentioned in Section 1.5.4. The experimental results were compared based on the number of protein nanofibres bundles for before and after the seeding process. The counting of the number of bundles for before and after of seeding is illustrated in **Figure 3-36**. The sample was added with 10% v/v of the fragmented nanofibres solution before the 24 hours of heat incubation at 80^{o}C and then left for another 24 hours at room temperature storage for self-assemble process. TEM grids were prepared before the addition for seeding and prepared again after 24 hours at room temperature storage for comparison. Based on **Table 12**, the average number of bundles increased from 1 to 3 for before and after seeding respectively. Based on this result, this clearly indicates that seeding can reduce the manufacturing time for the process. However, the reduced time for manufacturing was not calculated, as the objective was to yield the highest quality of protein nanofibres.

TEM images showing PNTs before/after seeding at low magnifications (14,000x)

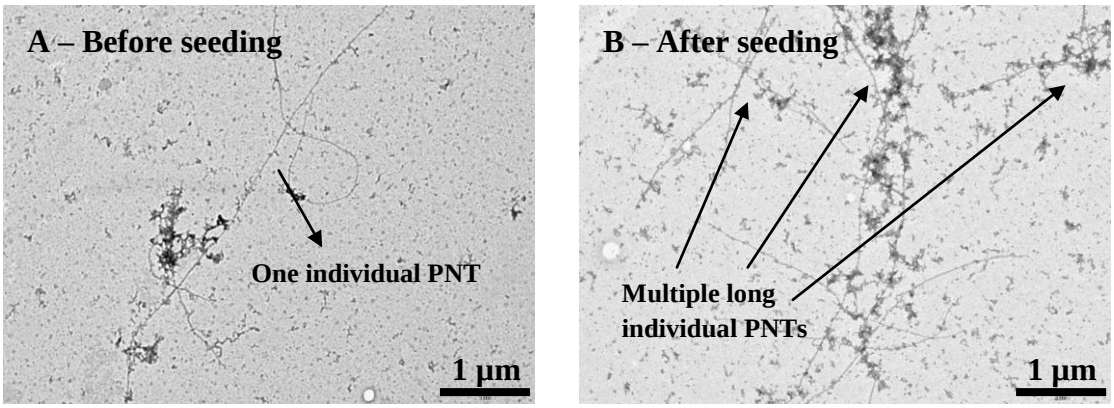

Figure 3-36: Seeding using sonicated protein nanofibres.

Table 12: Comparison between before and after seeding using fragmented PNTs

Samples	Before Seeding	After Seeding
1	2	1
2	2	3
3	1	2
4	1	3
5	1	5
6	1	2
7	1	2
8	0	4
9	2	5
10	1	2
Average	1	3

3.5 Thioflavin T fluorescence

ThT fluorescence measurements were conducted on low, medium and the high quality samples, and the results are tabulated in **Table 13**. The low quality of nanofibre without any centrifugation step showed an increase in ThT fluorescence after it was incubated for the first 15 minutes (from 67 to 8001 in ThT), and a further increase to 8164 after 24 hours of heat incubation at 80^{o}C. Medium quality nanofibre was centrifuged after 15 minutes of heat incubation and then heat incubated for 24 hours. The sample was centrifuged after the first

15 minutes of heat incubation, an approximately 90% reduction in ThT was recorded (from 8176 to 841 in ThT). After 24 hours of continuous heating, the final ThT reading was recorded at 2731. Finally, with the high quality of nanofibre, the sample was centrifuged after 24 hours of heat incubation and the ThT measurements were recorded from 8088 to 1418.

Table 13: ThT measurements and protein concentrations for all three different qualities of nanofibres developed.

Quality of nanofibres	ThT measurements	Protein Concentrations (mg/mL)
Low	8164	2.5 ~ 3.5
Medium	2731	1.5 ~ 2.0
High	1418	0.7 ~ 1.2

Both low and medium quality of nanofibres produced high ThT fluorescence measurements. The resulting of high reading from ThT assay was due to the high content of beta sheets structures in the crystallin proteins. In contrast, high quality of nanofibres produced low ThT readings, even though well-defined structures of nanofibres were confirmed under the TEM (**Figure 3-6 C**). Many researchers have suggested that ThT is a specific dyes for binding nanofibres and it is more sensitive than CR, as discussed in the Section 1.6.3. However, in this case, the results from the ThT test showed only a subtle increase in fluorescence reading when the high quality of nanofibres were produced compared to the low and medium quality nanofibre samples.

Based on these results, two possibilities can be suggested. First, the slight increase of fluorescence test could have resulted from the background reading of the native beta sheets structures that was remained in solution. The sample containing high quality nanofibres could be too dilute for ThT measurement, as protein nanofibres could potentially bind to the

amorphous aggregates and these aggregates were removed through centrifugation, which may be a reason for the low ThT readings. Similar results were seen with protein concentrations. Protein concentrations for three different qualities of nanofibres were measured using the Nanodrop. Interestingly, as the quality of nanofibres increased, the protein concentration decreased **Table 13**. Again, this could suggest that some of the protein nanofibres were lost during centrifugation, which may have decreased the protein concentrations. In addition, it has also been reported that there has been some debate as to the efficacy of ThT for the study of amyloid formation in crystallin systems (Meehan *et al.,* 2004). Overall, ThT measurements can be problematic due to the high degree of β-sheet structures in the native crystallins. Thus, ThT dye binding to native crystallins gave a high background reading even before the formation of fibrils.

3.6 X-Ray fibre diffraction

The samples used for X-ray examination were prepared from the 500 mL scaled-up sample in Section 3.4.3.2. X-ray fibre diffraction examines the spacing of the isotropic reflections in the nanofibre structures. As discussed in Section 1.4.1, native crystallin proteins have a high proportion of β-sheets, which resulted in a high fluorescence measurement of ThT that could lead to misleading results. Hence instead of relying completely on ThT binding to confirm amyloid fibril formation, X-ray fibre diffraction was carried out.

The diffraction pattern obtained showed isotropic reflections at 0.46 nm and 1.03 nm **Figure 3-37 A**, which corresponds to the spacing between hydrogen bonded β-strands within a β-sheet and the spacing between two β-sheets, as mentioned in Section 1.6.1, a characteristic of amyloid fibrils. However, as the samples were prepared by pelleting the fibril bundles, no oriented samples of fibrils could be prepared and the relative orientation of the hydrogen

bonds and the fibril axis could not be determined from these images. TEM was therefore used to confirm that the only material contributing to the diffraction was the amyloid fibrils. TEM images were taken of samples from the same resuspended pellet as used for preparation of the X-ray fibre diffraction sample. Based on **Figure 3-37 B**, fibrils were present with no visible un-fibrilised protein. This means that the observed diffraction pattern can be confidently attributed to the presence of amyloid fibrils, in agreement with other results reported in the literature (Groenning *et al.*, 2007).

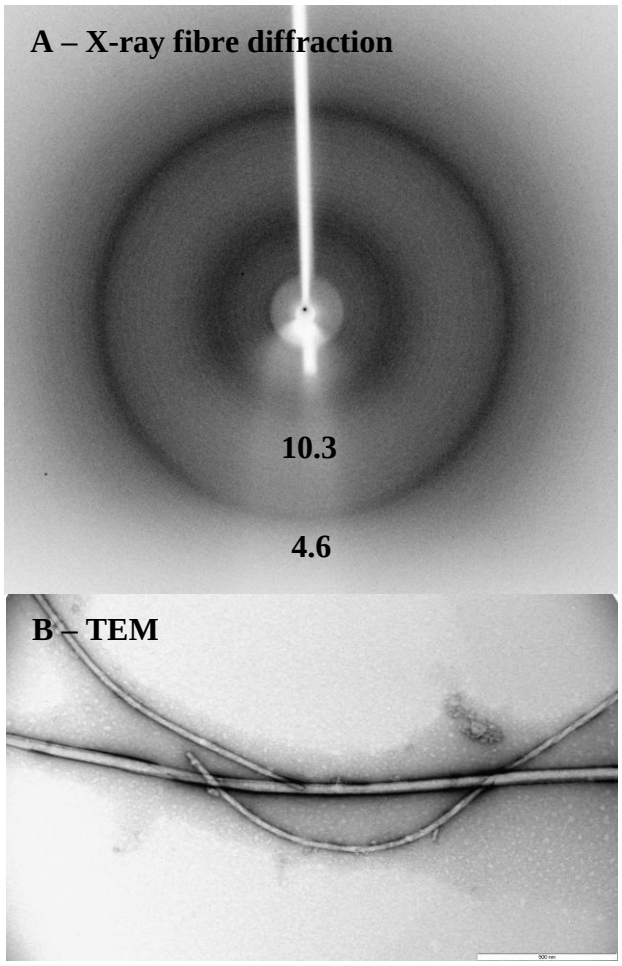

Figure 3-37: X-ray fibre diffraction on protein nanofibres.

A: X-ray diffraction results show two distinctive ring consistent with the spacings diagnostic for amyloid fibrils, and B: TEM images for the same sample which was used for X-ray diffraction experiment.

3.7 Scanning electron microscopy

Usually, protein nanofibres are imaged using TEM or AFM, as their size limits their suitability for imaging under a SEM. Based on the results in Section 3.3.4, incubation at high temperature 80^{o}C and above, higher order structures of crystallin nanofibres that existed as bundles were produced and the samples were analysed using SEM. The images obtained from SEM of the higher ordered structures showed structures similar to those observed using TEM. In addition, the diameter of the nanofibre bundles measured by TEM was similar to that measured under the SEM for the same sample. Based on **Figure 3-39**, the thickness of the protein nanofibres bundle measured was approximately 100 nm in diameter, which is similar to those measured by SEM.

The higher ordered structures of crystallin nanofibres formed at 85^{o}C and 90^{o}C were vacuum filtered on a 0.2 µm nitrocellulose filter, dried overnight, gold coated, and then imaged using SEM. Based on the SEM images, the diameter of the bundle nanofibres formed from individual nanofibres coming together in an intertwining fashion could be clearly seen in these SEM images **Figure 3-38 A, B**. The filters did not have a uniform coating of protein nanofibres but there were some patches where the protein nanofibres were densely packed **Figure 3-38 C, D**, while patches were less densely packed. It was expected that some of the individual nanofibres that are not part of a bundle, will be lost in the filter, where protein nanofibres could be seen wrapped around the edges of the pores. To confirm the presence of protein nanofibres, the image was compared to a control filter that was filtered with just buffer. Based on **Figure 3-38 E, F**, clearly protein nanofibres were observed and none in the blank filter. Furthermore, the diameter of the bundle nanofibres were measured and compared between the SEM and the TEM images to confirm the results. Based on the TEM

images, the diameter of the bundle nanofibres was measured as approximately 100 nm and similar diameter was also measured using the SEM images **Figure 3-39 A, B**.

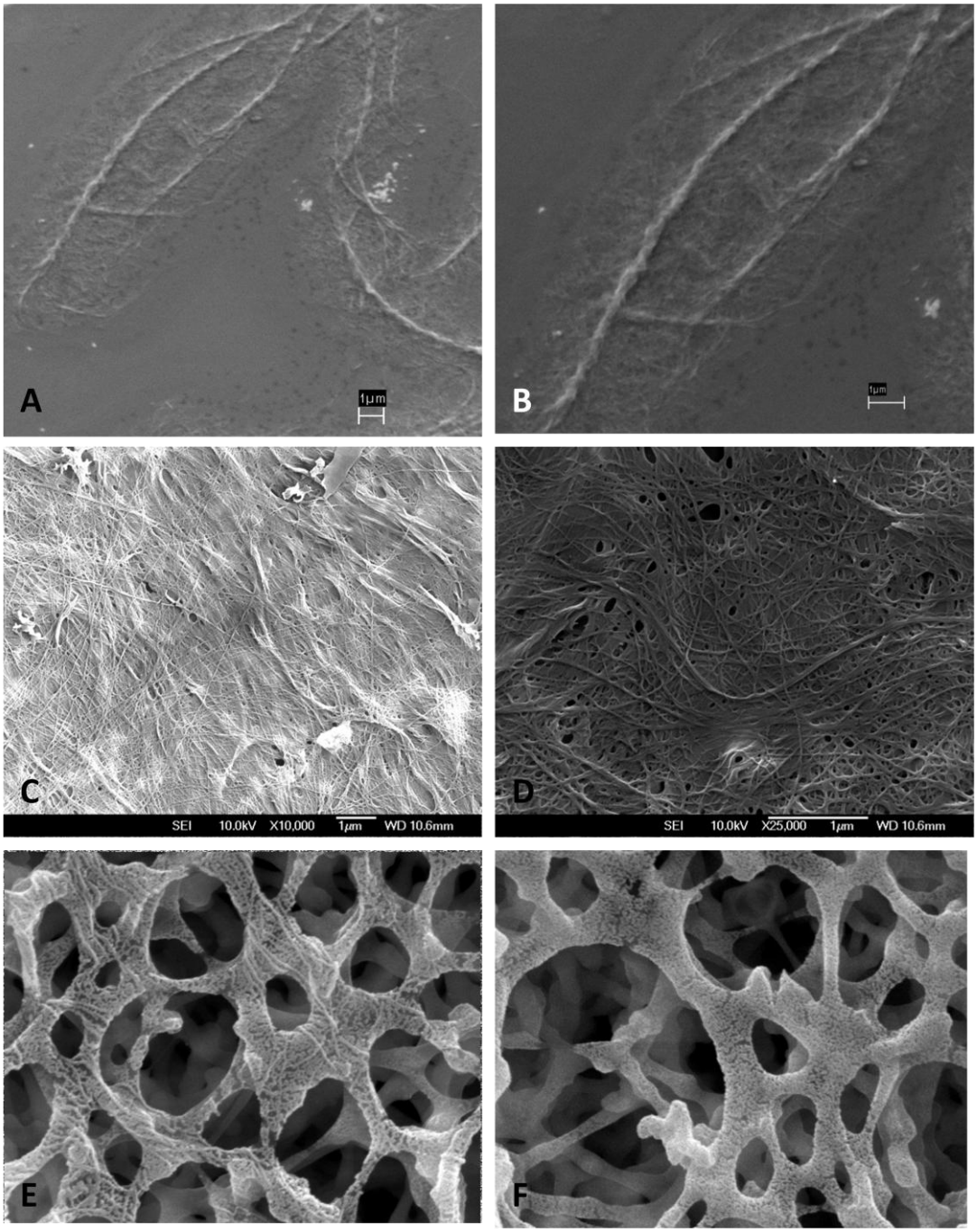

Figure 3-38: SEM images of protein nanofibres formed from crude barracuda lens crystallins.

A & B: SEM image showing bigger bundles of fibrils formed at 85^{o}C, C & D: A high density patch of protein nanofibres on a 0.2µm nitrocellulose filter, 10,000x and 25,000x respectively, E: SEM image low density patch of protein nanofibres showing individual fibres wrapped around the pores of 0.2µm nitrocellulose filter and F: 0.2µm nitrocellulose filter with just buffer (blank). These SEM images were performed by Clement Roux.

The size correlation between the TEM and the SEM images on bundles of protein nanofibres

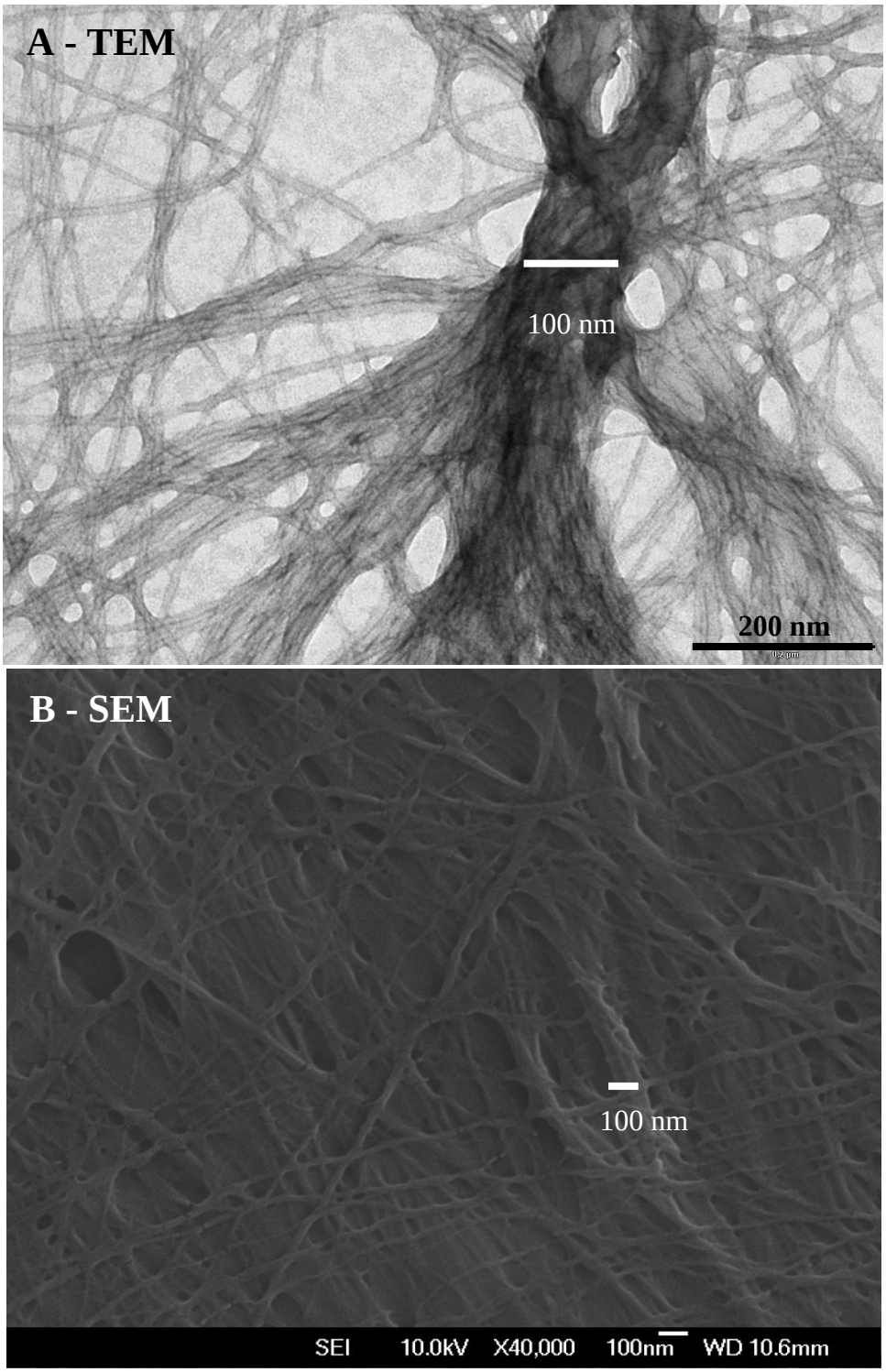

Figure 3-39: Protein nanofibres diameter comparison between TEM and SEM of the same sample.

4 CONCLUSIONS

Several key conclusions can be drawn from this study on scaling up the production of protein nanofibres. In addition, an evaluation has been made of the success in meeting the central project objectives (Section 1.7).

Researchers around the world are working towards overcoming the challenges of translating advantages of protein nanofibres and related bionanomaterials into useful applications. However, along with these challenges exists another challenge of identifying a cheap raw material source and optimizing a method for inexpensive manufacture of protein nanofibres. In this study, protein nanofibres production was successfully scaled from a 1 mL batch size to a 1 L batch size. In conjunction, bundles of nanofibres can be manufactured using an inexpensive crude mixture of fish eye lens crystallins, also classified as a form of waste from the seafood industry. Using waste materials as raw materials can significantly reduce the capital cost and increase the profit for the final product. This can also create a substantial opportunity to support environmental sustainability. By controlling the temperature, higher ordered structures and various morphologies of protein nanofibres, products can be obtained which can used in specific applications.

The summary of the optimized variables were:

1) 10% v/v of TFE at pH 3.8
2) 10 mg/ml starting protein concentrations
3) 80^{o}C heating temperature
4) 24 hours heat incubation
5) 24 hours storage time

The primary project objective to develop a scaled method for production of protein nanofibres from 1 mL to 1 L has been achieved. An optimized method for protein nanofibres production has been developed using an inexpensive crude mixture of fish eye lens crystallins. Traditionally, protein nanofibres/amyloid fibrils have been made using purified proteins, which be expensive for large scale applications. A series of recommendations to aid in future development of the 1 L scale production are presented in Chapter 5.

5 RECOMMENDATION

A number of recommendations for further study on scaling up the production of protein nanofibres developed in this project have been identified:

- Increase the internal surface area (greater than 5.46 cm^2) for 1 mL volume production and monitor the quality of protein nanofibres.
- To replace the use of TFE with an alternative chemicals to save on manufacturing cost (i.e. ethanol).
- To design different ways for the purified fibrils to be produced in preserved form that can be used for bionanotechnological applications.

6 REFERENCES

A. Aggeli, M. Bell, N. Boden, J. N. Keen, P. F. Knowles, T. C. McLeish, M. Pitkeathly and S. E. Radford (1997). "Responsive gels formed by the spontaneous self-assembly of peptides into polymeric beta-sheet tapes." Nature **386**(6622): 259-262.

A. Aggeli, I. A. Nyrkova, M. Bell, R. Harding, L. Carrick, T. C. B. McLeish, A. N. Semenov and N. Boden (2001). "Hierarchical self-assembly of chiral rod-like molecules as a model for peptide β-sheet tapes, ribbons, fibrils, and fibers." Proceedings of the National Academy of Sciences **98**(21): 11857-11862.

A. Ahmad, I. S. Millett, S. Doniach, V. N. Uversky and A. L. Fink (2003). "Partially folded intermediates in insulin fibrillation." Biochemistry **42**(39): 11404-11416.

C. B. Andersen, H. Yagi, M. Manno, V. Martorana, T. Ban, G. Christiansen, D. E. Otzen, Y. Goto and C. Rischel (2009). "Branching in amyloid fibril growth." Biophysical Journal **96**(4): 1529–1536.

C. Arnold (2008). "From diseases to devices." Chemical And Engineering News **86**(29): 44-50.

M. Balbirnie, R. Grothe and D. S. Eisenberg (2001). "An amyloid-forming peptide from the yeast prion Sup35 reveals a dehydrated β-sheet structure for amyloid." Proceedings of the National Academy of Sciences **98**: 2375-2380.

A. J. Baldwin, R. Bader, J. Christodoulou, C. E. MacPhee, C. M. Dobson and P. D. Barker (2006). "Cytochrome display on amyloid fibrils." Journal of the American Chemical Society **128**: 2162-2163.

T. Ban, D. Hamada, K. Hasegawa, H. Naiki and Y. Goto (2003). "Direct observation of amyloid fibril growth monitored by thioflavin T fluorescence." The Journal of Biological Chemistry **278**(19): 16462-16465.

U. Baxa, K. L. Taylor, J. S. Wall, M. N. Simon, N. Cheng, R. B. Wickner and A. C. Steven (2003). "Architecture of Ure2p prion filaments: the N-terminal domains form a central core fiber." The Journal of Biological Chemistry **278**.

M. Biancalana, K. Makabe, A. Koide and S. Koide (2009). "Molecular mechanism of Thioflavin T binding to the surface of beta-rich peptide self-assemblies. ." Journal of Molecular Biology **385**: 1052–1063.

S. E. Blondelle, B. Forood, R. A. Houghton and E. Pérez-Payá (1997). "Polyalanine-based peptides as models for self-associated β-pleated-sheet complexes." Biochemistry **36**: 8393-8400.

D. R. Booth, *et al.* (2007). "Instability, unfolding and aggregation of human lysozyme variants underlying amyloid fibrillogenesis." Nature **385**: 787-793.

M. Bouchard, J. Zurdo, E. J. Nettleton, C. M. Dobson and C. V. Robinson (2000). "Formation of insulin amyloid fibrils followed by FTIR simultaneously with CD and electron microscopy." Protein Science **9**(10): 1960–1967.

M. Calamai, F. Chiti and C. M. Dobson (2005). "Amyloid fibril formation can proceed from different conformations of a partially unfolded protein." Biophysical Journal **89**(6): 4201-4210.

R. Carrotta, J. Barthes, A. Longo, V. Martorana, M. Manno, G. Portale and P. L. S. Biagio (2007). "Large size fibrillar bundles of the Alzheimer amyloid beta-protein." European Biophysics Journal with Biophysics Letters **36**(7): 701-709.

C. Chai and K. W. Leong (2007). "Biomaterials approach to expand and direct differentiation of stem cells." Molecular Therapy **15**: 467-480.

H. Chanki and C. B. Park (2005). "Template-directed self-assembly and growth of insulin amyloid fibrils." Biotechnology and Bioengineering **90**(7): 848–855.

F. Chiti and C. M. Dobson (2006). "Protein misfolding, functional amyloid, and human disease." Annual Review of Biochemistry **75**: 333-366.

F. Chiti, N. Taddei, M. Bucciantini, P. White, G. Ramponi and C. M. Dobson (2000). "Mutational analysis of the propensity for amyloid formation by a globular protein." Nature **19**(7): 1441-1449.

F. Chiti, N. Taddei, M. Stefani, C. M. Dobson and G. Ramponi (2001). "Reduction of the amyloidogenicity of a protein by specific binding of ligands to the native conformation." Protein Science **10**(4): 879-886.

S. R. Collins, A. Douglass, R. D. Vale and J. S. Weissman (2004). "Mechanism of prion propagation: Amyloid growth occurs by monomer addition." PLoS Biology **2**(10): e321.

K. A. Conway, S. J. Lee, J. C. Rochet, T. T. Ding, R. E. Williamson and P. T. Lansbury (2000). "Acceleration of oligomerization, not fibrillization, is a shared property of both α-synuclein mutations linked to early-onset Parkinson's disease: implications for pathogenesis and therapy." Proceedings of the National Academy of Sciences **97**(2): 571-576.

M. J. Dalby, M. O. Riehle, D. S. Sutherland, H.Agheli and A.S.G.Curtis (2004). "Changes in fibroblast morphology in response to nano-columns produced by colloidal lithography." Biomaterials **25**(23): 5415-5422.

G. L. Devlin, T. P. J. Knowles, A. Squires, M. G. McCammon, S. L. Gras, M. R. Nilsson, C. V. Robinson, C. M. Dobson and C. E. MacPhee (2006). "The component polypeptide chains of bovine insulin nucleate or inhibit aggregation of the parent protein in a conformation-dependent manner." Journal of Molecular Biology **360**: 497-509.

A. L. Devries, A. J. Kiss and C. H. C. Cheng (2004). "Cold stable eye lens crystallins from the Antarctic nototheniid toothfish: A new model system to understand human cataracts." Integrative and Comparative Biology **44**(6): 713.

C. M. Dobson (2003). "Protein folding and misfolding." Nature **426**(6968): 884-890.

M. Dumoulin, *et al.* (2003). "A camelid antibody fragment inhibits amyloid fi bril formation by human lysozyme." Nature **424**: 783-788.

E. D. Eanes and G. Glenner (1968). "X-ray diffraction studies on amyloid filaments." Journal of Histochemistry and Cytochemistry **16**(11): 673-677.

H. Ecroyd and J. Carver (2009). "Crystallin proteins and amyloid fibrils." Cellular and Molecular Life Sciences **66**(1): 62-81.

M. Fandrich (2007). "On the structural definition of amyloid fibrils and other polypeptide aggregates." Cellular and Molecular Life Sciences **64**: 2066-2078.

B. Forood, E. Perez-Paya, R. A. Houghten and S. E. Blondelle (1995). "Formation of an extremely stable polyalanine β-sheet macromolecule." Biochemical and Biophysical Research Communications **211**: 7-15.

D. M. Fowler, A. V. Koulov, C. Alory-Jost, M. S. Marks, W. E. Balch and J. W. Kelly (2006). "Functional amyloid formation within mammalian tissue." PLoS Biology **4**(1): e6.

T. Fukuma, A. S. Mostaert and S. P. Jarvis (2006). "Explanation for the mechanical strength of amyloid fibrils." Tribology Letters **22**(3): 233-237.

M. Garvey, S. L. Gras, S. Meehan, S. J. Meade, J. A. Carver and J. A. Gerrard (2009). "Protein nanofibres of defined morphology prepared from mixtures of crude crystallins." International Journal of Nanotechnology **6**(3/4): 258-273.

K. Gast, A. Modler, H. Damaschun, R. Kröber, G. Lutsch, D. Zirwer, R. Golbik and G. Damaschu (2003). "Effect of environmental conditions on aggregation and fibril formation of barstar." European Biophysics Journal **32**(8): 710-723.

E. Gazit (2010). "Bioinspired chemistry: Diversity for self-assembly." Nature Chemistry **2**: 1010-1011.

T. A. Giorgadze, N. Shiina, Z. W. Baloch, J. E. Tomaszewski and P. K. Gupta (2004). "Improved detection of amyloid in fat pad aspiration: an evaluation of Congo red stain by fluorescent microscopy." Diagnostic Cytopathology **31**: 300-306.

S. L. Gras (2007). "Amyloid fibrils: From disease to design. New biomaterial applications for self-assembling cross-β fibrils." Australian Journal of Chemistry **60**(5): 333–342.

M. Groenning (2009). "Binding mode of Thioflavin T and other molecular probes in the context of amyloid fibrils-current status." The Journal of Biological Chemistry **3**(1): 1-18.

M. Groenning, M. Norrman, J. M. Flink, M. v. d. Weert, J. T. Bukrinsky, G. Schluckebier and S. Frokjaer (2007). "Binding mode of Thioflavin T in insulin amyloid fibrils." Journal of Structural Biology **159**: 483–497.

H. L. Grothe, M. R. Little, A. S. Cho, A. J. W. Huang and C. Yuan (2009). "Denaturation and solvent effect on the conformation and fibril formation of TGFBIp." Molecular Vision **15**: 2617-2626.

J. I. Guijarro, M. Sunde, J. A. Jones, I. D. Campbell and C. M. Dobson (1998). "Amyloid fibril formation by an SH3 domain." Proceedings of the National Academy of Sciences **95**: 4224-4228.

R. A. Guirado-Lopez and M. E. Rincon (2006). "Structural and optical properties of highly hydroxylated fullerenes: stability of molecular domains on the C_60 surface." Journal of Chemical Physics **125**(15): 154312.

M. Hamedi, A. Herland, R. H. Karlsson and O. Inganäs (2008). "Electrochemical devices made from conducting nanowire networks self-assembled from amyloid fibrils and alkoxysulfonate PEDOT." Nano letters **8**(6): 1736-1740.

N. K. Holm, *et al.* (2007). "Aggregation and fibrillation of bovine serum albumin." Biochimica et Biophysica Acta **1774**(9): 1128–1138.

J. Horwitz (1992). "Alpha-crystallin can function as a molecular chaperone." Proceedings of the National Academy of Sciences **89**(21): 10449-10453.

J. Horwitz (2003). "Alpha-crystallin." Exp eye res **76**(2): 145-153.

A. J. Howie and D. B. Brewer (2009). "Optical properties of amyloid stained by Congo red: history and mechanisms." Micron **40**(3): 285-301.

M. R. Hurle, L. R. Helms, L. Li, W. Chan and R. Wetzel (1994). "A role for destabilizing amino acid replacements in light-chain amyloidosis." Proceedings of the National Academy of Sciences **91**(12).

Y. Inoue, S. Kawai-Noma, A. Koike-Takeshita, H. Taguchi and M. Yoshida (2011). "Yeast prion protein New1 can break Sup35 amyloid fibrils into fragments in an ATP-dependent manner." Molecular Biology Society of Japan **16**(5): 545-556.

Y. Inoue, A. Kishimoto, J. Hirao, M. Yoshida and H. Taguchi (2001). "Strong growth polarity of yeast prion fiber revealed by single fiber imaging." The Journal of Biological Chemistry **276**: 35227-35230.

T. R. Jahn and S. E. Radford (2005). "The Yin and Yang of protein folding." The FEBS Journal **272**(23): 5962-5970.

X. Jiang, C. S. Smith, H. M. Petrassi, P. Hammarström, J. T. White, J. C. Sacchettini and J. W. Kelly (2001). "An engineered transthyretin monomer that is nonamyloidogenic, unless it is partially denatured." Biochemistry **40**(38): 11442-11452.

J. L. Jime´nez, E. J. Nettleton, M. Bouchard, C. V. Robinson, C. M. Dobson and H. R. Saibil (2002). "The protofilament structure of insulin amyloid fibrils." Proceedings of the National Academy of Sciences **99**(14): 9196-9201

J.-M. Jung and R. Mezzenga (2010). "Liquid crystalline phase behavior of protein fibers in water: Experiments versus theory." Langmuir **26**(1): 504-514.

E. Katz and I. Willner (2004). "Biomolecule-functionalized carbon nanotubes: Applications in nanobioelectronics." ChemPhysChem **5**(8): 1084-1104.

R. Khurana, J. R. Gillespie, A. Talapatra, L. J. Minert, C. Ionescu-Zanetti, I. Millett and A. L. Fink (2001). "Partially folded intermediates as critical precursors of light chain amyloid fibrils and amorphous aggregates." Biochemistry **40**(12): 3525-3535.

Y. S. Kim, T. W. Randolph, M. C. Manning, F. J. Stevens and J. F. Carpenter (2003). "Congo red populates partially unfolded states of an amyloidogenic protein to enhance aggregation and amyloid fibril formation." The Journal of Biological Chemistry **278**(12): 10842-10850.

A. J. Kiss, A. Y. Mirarefi, S. Ramakrishnan, C. F. Zukoski, A. L. Devries and C. H. Cheng (2004). "Cold-stable eye lens crystallins of the Antarctic nototheniid toothfish Dissostichus mawsoni Norman." Journal of Experimental Biology **207**(26): 4633-4649.

W. E. Klunk, R. F. Jacob and R. P. Mason (1999). "Quantifying amyloid β-peptide (Aβ) aggregation using the Congo red-Aβ (CR-aβ) spectrophotometric assay." Analytical Biochemistry **266**: 66–76.

W. E. Klunk, J. W. Pettegrew and D. J. Abraham (1989). "Two simple methods for quantifying low-affinity dye-substrate binding." Journal of Histochemistry and Cytochemistry **37**(8): 1293-1297.

T. P. Knowles, J. F. Smith, A. Craig, C. M. Dobson and M. E. Welland (2006). "Spatial persistence of angular correlations in amyloid fibrils." Physical Review Letters **96**(23): 238301.

R. Kodali and R. Wetzel (2007). "Polymorphism in the intermediates and products of amyloid assembly." Current Opinion in Structural Biology **1**: 48-57.

T. Koga, M. Matsuoka and N. Higashi (2005). "Structural control of self-assembled nanofibers by artificial beta-sheet peptides composed of D- or L-isomer." Journal of the American Chemical Society **127**(50): 17596-17597.

T. Konno (2001). "Multistep nucleus formation and a separate subunit contribution of the amyloidgenesis of heat-denatured monellin." Protein Science **10**: 2093-2101.

T. Kowalewski and D. M. Holtzman (1999). "In situ atomic force microscopy study of Alzheimer's β-amyloid peptide on different substrates: New insights into mechanism of β-sheet formation." Proceedings of the National Academy of Sciences **96**(7): 3688-3693

L. Kreplak and U. Aebi (2006). "From the polymorphism of amyloid fibrils to their assembly mechanism and cytotoxicity." Advances in Protein Chemistry **73**: 217-233.

C. H. Lee, H. J. Shin, I. H. Cho, Y.-M. Kang, I. A. Kim, K.-D. Park and J.-W. Shin (2005). "Nanofiber alignment and direction of mechanical strain affect the ECM production of human ACL fibroblast." Biomaterials **26**(11): 1261-1270.

H. LeVine (1993). "Thioflavine T interaction with synthetic Alzheimer's disease β-amyloid peptides: Detection of amyloid aggregation in solution." Protein Science **2**: 404-410.

H. Levine (1997). "Stopped-Flow Kinetics Reveal Multiple Phases of Thioflavin T Binding to Alzheimer β(1-40) Amyloid Fibrils." Archives of Biochemistry and Biophysics **342**(2): 306-316

H. LeVine (1999). "Quantification of β-sheet amyloid fibril structures with Thioflavin T." Methods in Enzymology **309**: 274-284.

M. Lindgren, K. Sörgjerd and P. Hammarström (2005). "Detection and characterization of aggregates, prefibrillar amyloidogenic oligomers and protofibrils using fluorescence spectroscopy." Biophysical Journal **88**: 4200-4212.

S. M. Loveday, X. L. Wanga, M. A. Raob, S. G. Anemac, L. K. Creamera and H. Singh (2010). "Tuning the properties of β-lactoglobulin nanofibrils with pH, NaCl and CaCl2." International Dairy Journal **20**(9): 571-579.

C. E. MacPhee and C. M. Dobson (2000). "Formation of Mixed Fibrils Demonstrates the Generic Nature and Potential Utility of Amyloid Nanostructures." Journal of the American Chemical Society **122**(51): 12707–12713.

S. K. Maji, *et al.* (2009). "Functional amyloids as natural storage of peptide hormones in pituitary secretory granules." Science **325**(5938): 328-332.

S. K. Maji, D. Schubert, C. Rivier, S. Lee, J. E. Rivier and R. Riek (2008). "Amyloid as a depot for the formulation of long-acting drugs." PLoS Biology **6**(2).

S. K. Maji, L. Wang, J. Greenwald and R. Rie (2009). "Structure–activity relationship of amyloid fibril." FEBS Letters **583**: 2610-2617.

O. S. Makin and L. C. Serpell (2005). "X-ray diffraction studies of amyloid structure." Methods in Molecular Biology **299**: 67-80.

J. E. Meegan, A. Aggeli, N. Boden, R. Brydson, A. P. Brown, L. Carrick, A. R. Brough, A. Hussain and R. J. Ansell (2004). "Designed self-assembled beta-sheet peptide fibrils as templates for silica nanotubes." Advanced Functional Materials **14**: 31-37.

S. Meehan, Y. Berry, B. Luisi, C. M. Dobson, J. A. Carver and C. E. MacPheea (2004). "Amyloid fibril formation by lens crystallin proteins and Its implications for cataract formation." The Journal of Biological Chemistry **279**: 3413-3419.

P. Mesquida, D. L. Ammann, C. E. MacPhee and R. A. McKendry (2005). "Microarrays of peptide fibrils created by electrostatically controlled deposition." Advanced Materials **17**(7): 893–897.

D. Moreira and P. Lopez-Garcia (2002). "The molecular ecology of microbial eukaryotes unveils a hidden world." Trends in Microbiology **10**(1): 31–38.

A. S. Mostaert and S. P. Jarvis (2007). "Beneficial characteristics of mechanically functional amyloid fibrils evolutionarily preserved in natural adhesives." Nanotechnology **18**(4).

H. Naiki, K. Higuchi, M. Hosokawa and T. Takeda (1989). "Fluorometric determination of amyloid fibrils in vitro using the fluorescent dye, Thioflavin T." Analytical Biochemistry **177**: 244–249.

R. Nelson, M. R. Sawaya, M. Balbirnie, A. Ø. Madsen, C. Riekel, R. Grothe and D. Eisenberg (2006). "Structure of the cross-β spine of amyloid-like fibrils." Nature **435**(7043): 773–778.

M. Nomura, H. Uda-Tochio, K. Murai, N. Mori and Y. Nishimura (2005). "The neural repressor NRSF/REST binds the PAH1 domain of the SIN3 corepressor by using its distinct short hydrophobic helix." Journal of Molecular Biology **354**(4): 903-915

T. Oppenheim, T. P. Knowles, S. P. Lacour and M. E. Welland (2009). "Fabrication and characterisation of protein fibril-elastomer composites." Acta Biomaterialia **6**(4): 1337-1341.

D. Otzena and P. H. Nielsen (2008). "We find them here, we find them there: Functional bacterial amyloid." Cellular and Molecular Life Sciences **65**(6): 910-927.

F. G. Pearce, S. H. Mackintosh and J. A. Gerrard (2007). "Formation of amyloid-like fibrils by ovalbumin and related proteins under conditions relevant to food processing." Journal of Agricultural and Food Chemistry **55**: 318-322.

A. T. Petkova, R. D. Leapman, Z. Guo, W.-M. Yau, M. P. Mattson and R. Tycko (2005). "Self-propagating, molecular-level polymorphism in alzheimer's β-amyloid fibrils." Science **307**(5707): 262-265

T. Pettersson and Y. T. Konttinen (2009). Semin arthritis rheum. Press.

S. M. Pilkington, S. J. Roberts, S. J. Meade and J. A. Gerrard (2010). "Amyloid fibrils as a nanoscaffold for enzyme immobilization." Biotechnology Progress **26**(1): 93-100.

Y. Porat, A. Abramowitz and E. Gazit (2006). "Inhibition of amyloid fibril formation by polyphenols: Structural similarity and aromatic interactions as a common inhibition mechanism." Chemical Biology & Drug Design **67**: 27–37.

M. Ramírez-Alvarado, J. S. Merkel and L. Regan (2000). "A systematic exploration of the influence of the protein stability on amyloid fibril formation in vitro." Proceedings of the National Academy of Sciences **97**(16): 8979-8984.

R. Sabate and S. J. Saupe (2007). "Thioflavin T fluorescence anisotropy: An alternative technique for the study of amyloid aggregation." Biochemical and Biophysical Research Communications **360**(1): 135–138.

S. M. Saeed and G. Fine (1967). "Thioflavin T for amyloid detection." American Journal of Clinical Pathology **47**(5): 588–593.

T. Scheibel, R. Parthasarathy, G. Sawicki, X.-M. Lin, H. Jaeger and S. L. Lindquist (2003). "Conducting nanowires built by controlled self-assembly of amyloid fibers and selective metal deposition." Proceedings of the National Academy of Sciences **100**(8): 4527-4532.

N. Schönbrunner, J. Wey, J. Engels, H. Georg and T. Kiefhaber (1996). "Native-like beta-structure in a trifluoroethanol-induced partially folded state of the all-beta-sheet protein tendamistat." Journal of Molecular Biology **260**(3): 432-445.

S. Sen and G. Başdemir (2003). "Diagnosis of renal amyloidosis using Congo red fluorescence." Pathology International **53**: 534-538

H. Şengül, T. Theis and S. Ghosh (2008). "Towards sustainable nanoproducts: An overview of nanomanufacturing methods." Journal of Industrial Ecology **12**(3): 329-359.

L. Serpell, P. Fraser and M. Sunde (1999). "X-ray fiber diffraction of amyloid fibrils." Methods in Enzymology **309**(526-536).

L. C. Serpell and J. M. Smith (2000). "Direct visualisation of the β-sheet structure of synthetic Alzheimer's amyloid." Journal of Molecular Biology **299**(1): 225-231.

V. Sluzky, J. A. Tamada, A. M. Klibanov and R. Langer (1991). "Kinetics of insulin aggregation in aqueous solutions upon agitation in the presence of hydrophobic surfaces." Proceedings of the National Academy of Sciences **88**(21): 9377-9381.

A. V. Smith and C. K. Hall (2001). "Protein refolding versus aggregation: Computer simulations on an intermediate-resolution protein model." Journal of Molecular Biology **312**(1): 187-202.

D. P. Smith, S. Jones, L. C. Serpell, M. Sunde and S. E. Radford (2003). "A systematic investigation into the effect of protein destabilisation on beta 2-microglobulin amyloid formation." Journal of Molecular Biology **330**: 943-954.

J. F. Smith, T. P. J. Knowles, C. M. Dobson, C. E. MacPhee and M. E. Welland (2006). "Characterization of the nanoscale properties of individual amyloid fibrils." Proceedings of the National Academy of Sciences **103**(43): 15806-15811.

A. M. Squires, G. L. Devlin, S. L. Gras, A. K. Tickler, C. E. MacPhee and C. M. Dobson (2006). "X-ray scattering study of the effect of hydration on the cross-beta spine of amyloid fibrils." Journal of the American Chemical Society **128**(36): 11738-11739.

S. Srisailam, H. M. Wang, T. K. Kumar, D. Rajalingam, V. Sivaraja, H. S. Sheu, Y. C. Chang and C. Yu (2002). "Amyloid-like fibril formation in an all beta-barrel protein involves the formation of partially structured intermediate(s)." The Journal of Biological Chemistry **277**(21): 19027-19036.

M. M. Stevens and J. H. George (2005). "Exploring and engineering the cell surface interface." Science **310**(5751): 1135-1138.

P. Taboada, S. Barbosa, E. Castro and V. Mosquera (2006). "Amyloid fibril formation and other aggregate species formed by human serum albumin association." Journal of Physical Chemistry **110**(42): 20733–20736.

Y. Takahashi and H. Mihara (2004). "Construction of a chemically and conformationally self-replicating system of amyloid-like fibrils." Bioorganic & Medicinal Chemistry Letters **12**(4): 693-699.

A. I. Teixeira, G. A. Abrams, P. J. Bertics, C. J. Murphy and P. F. Nealey (2003). "Epithelial contact guidance on well-defined micro- and nanostructured substrates." Journal of Cell Science **116**: 1881-1892

D. C. Thorn, S. Meehan, M. Sunde, A. Rekas, S. L. Gras, C. E. MacPhee, C. M. Dobson, M. R. Wilson and J. A. Carver (2005). "Amyloid fibril formation by bovine milk kappa-casein and its inhibition by the molecular chaperones alphaS- and beta-casein." Biochemistry **44**(51): 17027-17036.

W. G. Turnell and J. T. Finch (1992). "Binding of the dye congo red to the amyloid protein pig insulin reveals a novel homology amongst amyloid-forming peptide sequences." Journal of Molecular Biology **227**(4): 1205–1223.

P. S. Vassar and C. F. Culling (1959). "Fluorescent stains, with special reference to amyloid and connective tissues." Archives of Pathology **68**: 487–494.

R. Virchow (1854). "Weitere Mittheilungen u¨ber das Vorkommen der pflanzlichen Cellulose beim Menschen." Virchows Arch **6**: 268-271.

S. H. Waterhouse and J. A. Gerrard (2004). "Amyloid fibrils in bionanotechnology." Australian Journal of Chemistry **57**(6): 519-523.

G. M. Whitesides and B. Grzybowsk (2002). "Self-assembly at all scale." Science **295**(5564): 2418-2421.

C. Wu, Z. Wang, H. Lei, Y. Duan, M. T. Bowers and J.-E. Shea (2008). "The binding of Thioflavin T and its neutral analog BTA-1 to protofibrils of the Alzheimer's disease Aβ16–22 peptide probed by molecular dynamics simulations." Journal of Molecular Biology **384**(3): 718-729

M. Xie and R. L. Schowen (1999). "Secondary structure and protein deamidation." Journal of Pharmaceutical Sciences **88**(1): 8-13.

C. Y. Xu, R. Inai, M. Kotaki and S. Ramakrishna (2004). "Electrospun nanofiber fabrication as synthetic extra cellular matrix and its potential for vascular tissue engineering." Tissue Engineering **10**(7): 1160-1168.

W. F. Xue, A. L. Hellewell, W. S. Gosal, S. W. Homans, E. W. Hewitt and S. E. Radford (2009). "Fibril fragmentation enhances amyloid cytotoxicity." The Journal of Biological Chemistry **284**(49): 34272-34282.

K. Yamaguchi, H. Naiki and Y. Goto (2006). "Mechanism by which the amyloid-like fibrils of a beta 2-microglobulin fragment are induced by fluorine-substituted alcohols." Journal of Molecular Biology **363**(1): 279-288.

E. K. F. Yim and K. W. Leong (2005). "Significance of synthetic nanostructures in dictating cellular response." Nanomedicine **1**(1): 10-21.

E. K. F. Yim, R. M. Reano, S. W. Pang, A. F. Yee, C. S. Chen and K. W. Leong (2005). "Nanopattern-induced changes in morphology and motility of smooth muscle cells." Biomaterials **26**(26): 5405–5413.

M. Zhu, P. O. Souillac, C. Ionescu-Zanetti, S. A. Carter and A. L. Fink (2002). "Surface-catalyzed amyloid fibril formation." The Journal of Biological Chemistry **277**: 50914-50922.

J. Zurdo, J. I. Guijarro and C. M. Dobson (2001). "Preparation and characterization of purified amyloid fibrils." Journal of the American Chemical Society **123**(33): 8141-8142.

7 APPENDIX A

A.1 Protein concentration calculations

Starting protein concentration preparation:

Assume the crude protein concentration from the extraction step is 300 mg/mL using Nanodrop spectrometer.

$$\frac{Protein\ concentration}{Final\ protein\ concentration} = \frac{300\frac{mg}{ml}}{5.8\frac{mg}{ml}} = 52\ \times$$

For volume = 1 mL or 1000 µl

$$\frac{1000\ \mu l}{52\ \times} = 19\ \mu l$$

In 1 mL volume, 19 µl of the extracted protein solution was mixed together with 981 µl of the 10% TFE to have a final protein concentration 5.8 mg/mL.

A.2 5 L scale-up preparation calculations

Pre-calculations for 5 L scale-up

Total volume for scale-up = 5 L

From all the previous fish lenses extraction trials, the average protein concentration yield was approximately 300 mg/mL using Nanodrop. Therefore, assume the crude extracted protein concentration is 300 mg/mL. The starting protein concentrations in 5 L volume need to be prepared to 10 mg/mL based on process optimization results in Section 3.3.3.

Based on the assumption:

$$\frac{Protein\ concentration}{Final\ protein\ concentration} = \frac{300\,\frac{mg}{ml}}{10\,\frac{mg}{ml}} = 30\ \times$$

$$\frac{5000\ ml}{30\ \times} = 166.7\ ml$$

Based on the pre-calculations above, a total of 166.7 mL of protein solution is required for the 5 L scale-up to achieve 10 mg/mL of protein concentration. Additionally, from all the previous fish lenses extraction trials, there was an average of 20% increase in liquid volume at the end of the extraction process because lenses contained water and other membrane fluids.

Based on the 20% increased in volume after extraction:

$$166.7\ ml - (20\% \times 166.7\ ml) = 133.4\ ml$$

During the preparation of fish lenses extraction, one mL of the extraction buffer was required for one gram of fish lenses weighed. 133.4 mL is the volume of the extraction buffer that is

required. Therefore, at least 133.4 grams of fish lenses is needed for the scale-up. Deep sea peach (DSP) lens weigh an average 0.76 gram per lens.

$$\frac{133.4\ g}{0.76\ g} = 176\ lenses$$

A.3 Internal surface area calculations for 1 mL volume

1.5 mL Eppendorf with blue screw cap (with 1 mL of fluids)

Total height to the fluid level is 30 mm

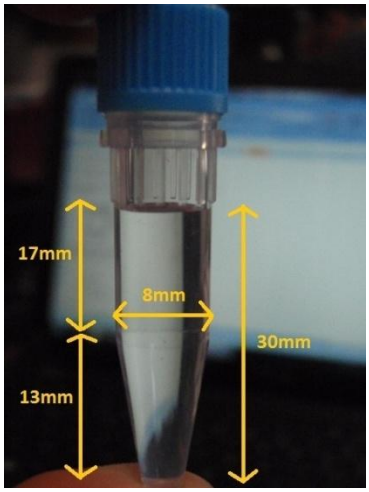

The Eppendorf can be separated into two sections; Section A (the cylinder) and Section B (the cone)

Surface Area of a Cylinder:

Section A = $2\pi rh$

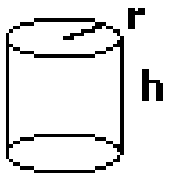

Lateral surface area of a cone:

Section B = $\pi rs = \pi r\sqrt{(r2 + h2)}$

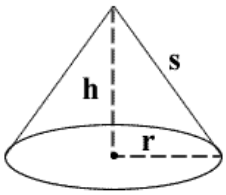

Section A:

h = 13 mm

r = 4mm

Surface area of the cylinder is 327 mm^2

Section B:

h = 17 mm

r = 4mm

Lateral surface area of a cone is 219 mm^2

So the total internal surface area of the eppendorf with 1mL of fluid is ***546 mm^2 or 5.46 cm^2*.**

A.4 TEM images of fragmented protein nanofibres

Before sonication

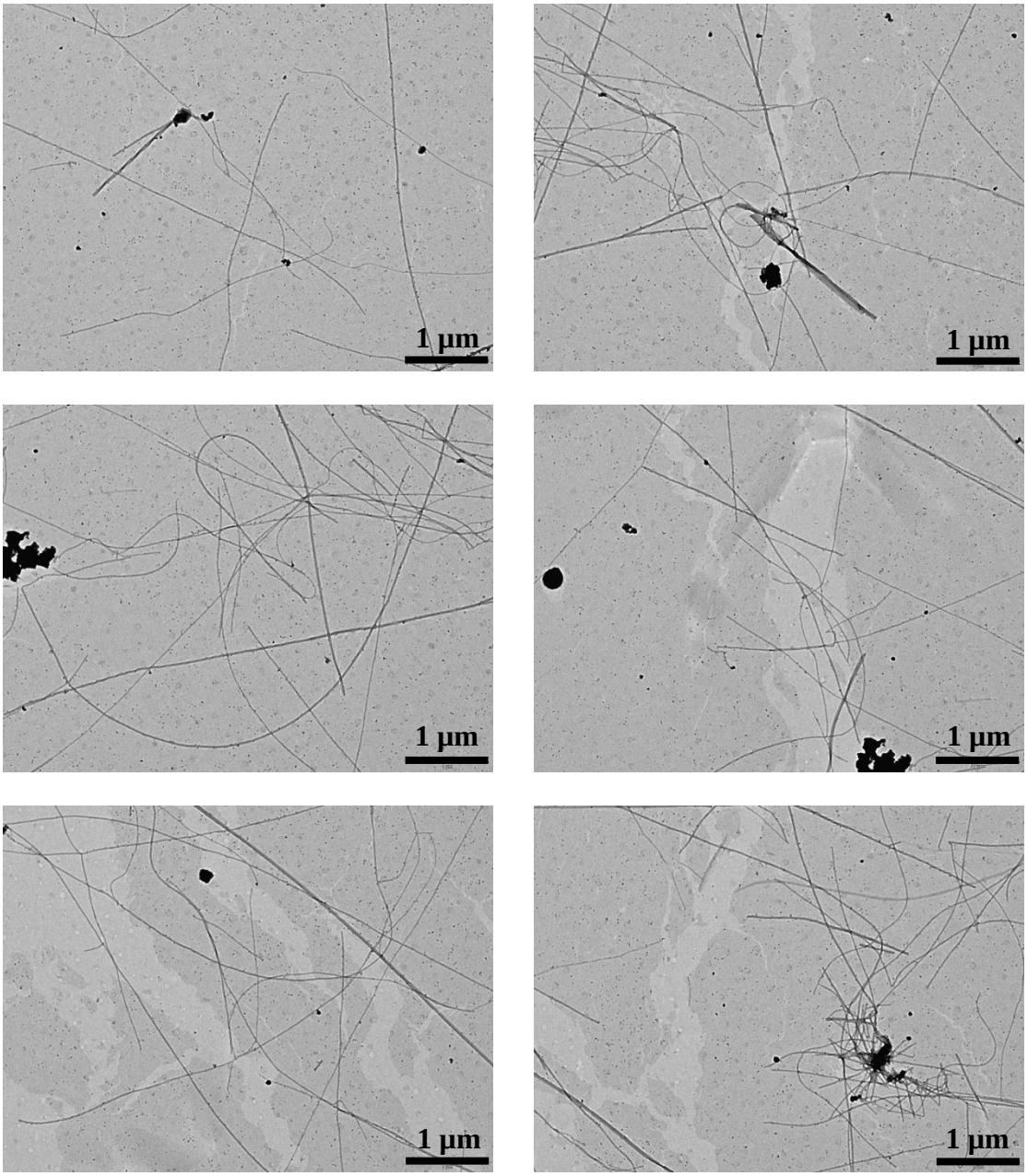

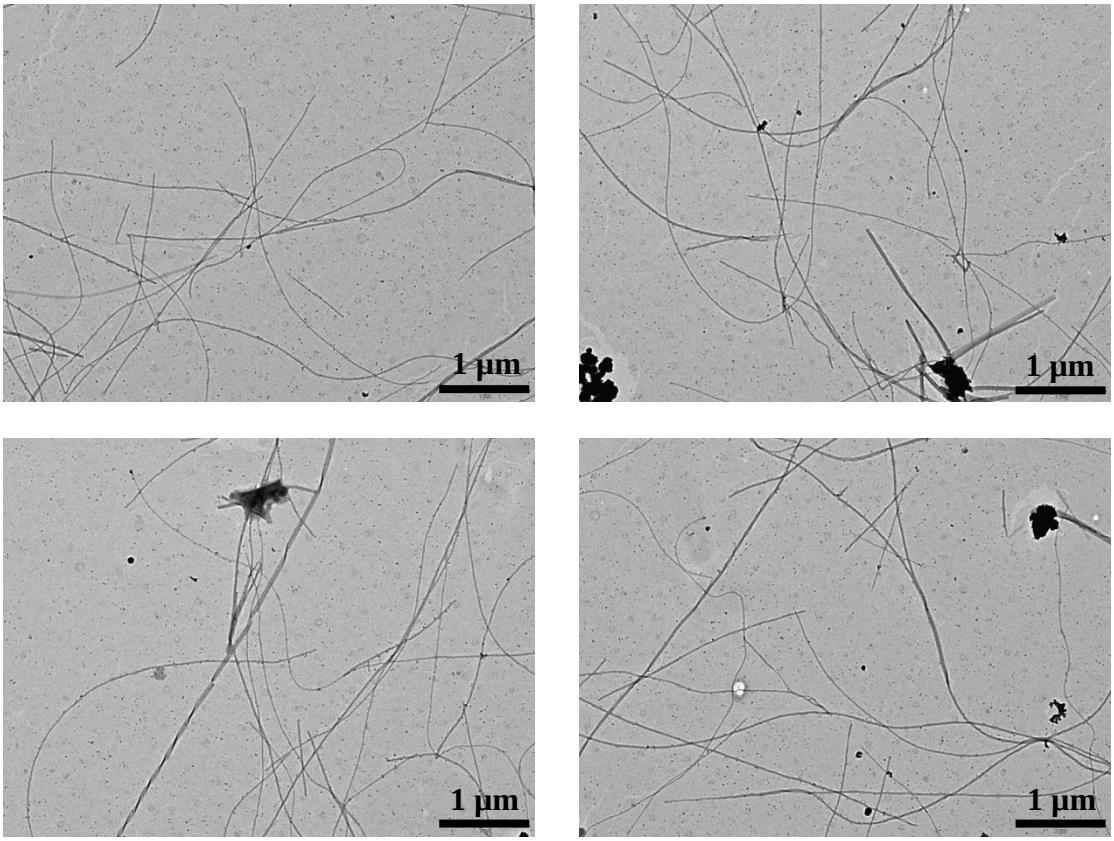

After sonication

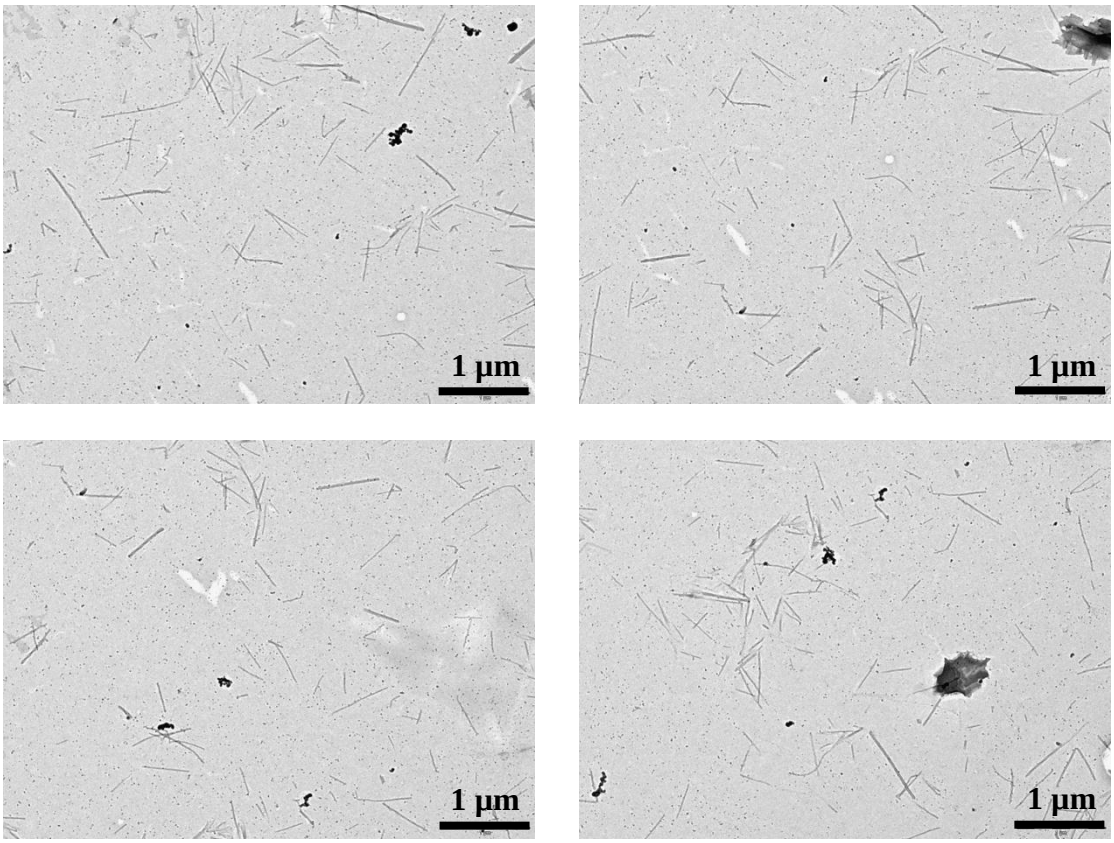

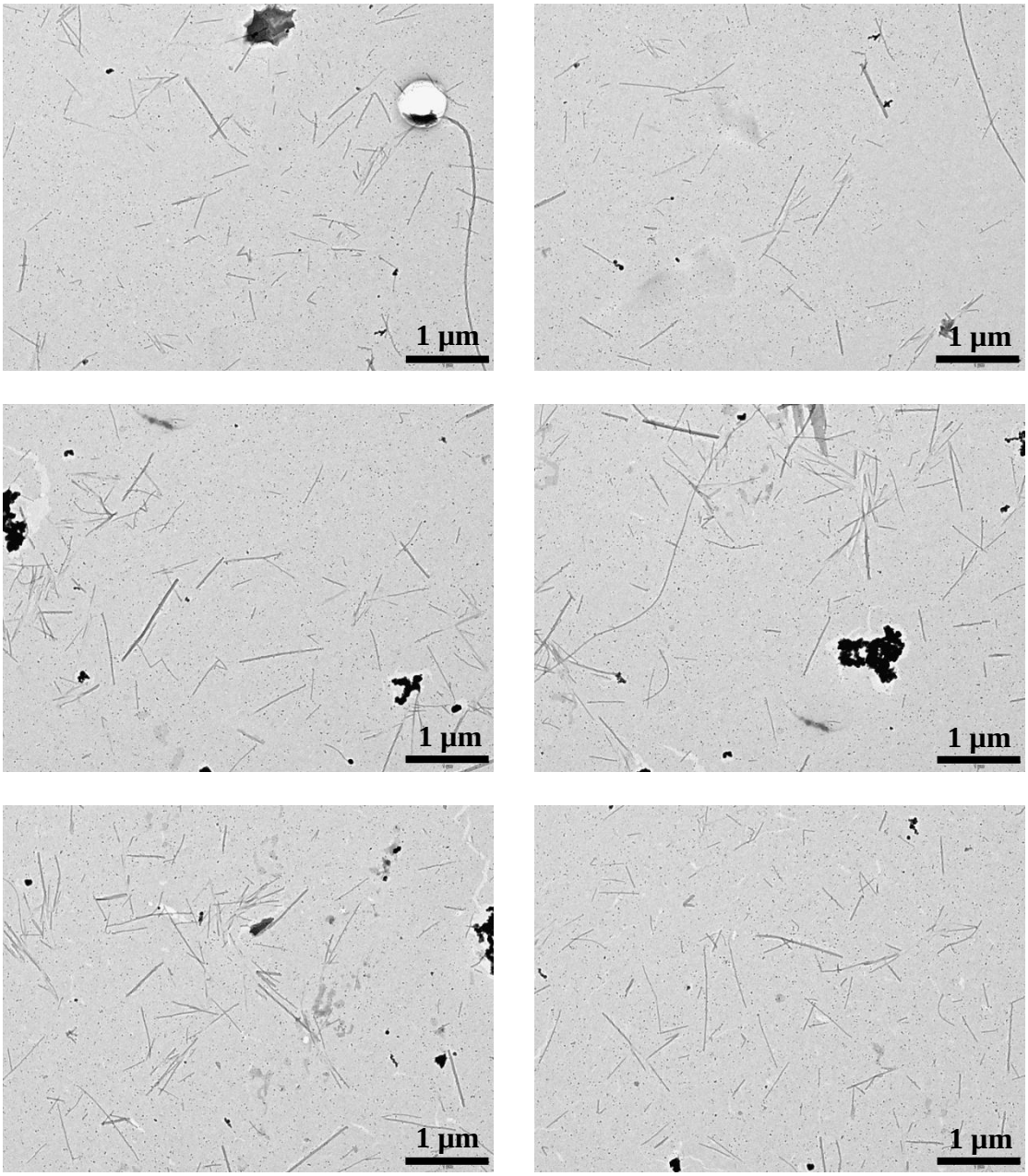
1 µm
1 µm
1 µm
1 µm
1 µm
1 µm

A.5 Polypropylene beads surface area calculations

Pre-calculations:

All the beads were assumed to be cylinders and the surface area was measured using a mirco caliper in mm^2.

Average width (d) = 4mm

Average height (h) = 1.5mm

Surface area (SA) $= 2\pi r^2 + \pi * d * h$

$= 2*\pi(4) + \pi(4)(1.5)$

$= 43.98 mm^2$

Target scale-up volume = 10 mL

Total internal surface area required = 10 x 546 mm^2

Beads needed to match Falcon tube surface area = $5460 mm^2 / 43.98 mm^2$

= 124.15 beads rounded to 125

Average weight of 1 bead = 0.03g

Weight of 125 beads = 0.03g x 125

= 3.75g

Actual weight of beads used = 3.752g